SCUOLA DI DOTTORATO
UNIVERSITÀ DEGLI STUDI DI MILANO-BICOCCA

Department of Material Sciences

PhD program in Chemical, Geological and Environmental Sciences Cycle XXX
Curriculum in Chemical Sciences

POLY(3,4-ETHYLENDIOXYTHIOPHENE) (PEDOT) BASED MATERIALS FOR THERMOELECTRIC APPLICATIONS

Surname: Galliani Name: Daniela

Registration number: 726530

Tutor: Professor Dario Narducci

Coordinator: Professor Maria Luce Frezzotti

ACADEMIC YEAR 2016/2017

"There is a theory which states that if ever anyone discovers exactly what the Universe is for and why it is here, it will instantly disappear and be replaced by something even more bizarre and inexplicable. There is another theory which states that this has already happened."

Douglas Adams – The Hitchhiker's Guide to the Galaxy

Abstract

Intrinsically conductive polymers (ICPs) are a class of organic materials characterized by unique features. They are lightweight, flexible and easy to process and print, as expected from polymers, but, also, they can conduct electricity up to metallic conductivities. Such an exceptional pairing of characteristics enables the development of flexible and printed electronic devices, which are of a particularly appealing for portable electronic devices, even integrated in the human body (e.g. implantable biosensors) or worn (e.g. smartwatches).

Even thermoelectric (TE) application of ICPs recently gained a lot of attention. An organic TE generator (OTEG) can convert heat into electrical energy by means of the Seebeck effect. This technology aims to recover heat produced as low-grade side-product of energy consumption and to transform it into exploitable energy.

Even though ICPs showed promising TE properties, their use is still hindered by low TE efficiencies, which cannot compete with the inorganic benchmark (i.e. tellurides).

The design of better ICPs for TE application must start from a deep knowledge of which techniques and treatments impact the charge transport features. The intrinsic complexity of ICP systems, however, often makes this task difficult, preventing a full comprehension of the phenomena involved.

This PhD project focused on the impact of different parameters on TE properties of ICPs, aiming at the needed deeper understanding on how charge transport is affected.

The specific ICP poly(3,4-ethylendioxythiophene) -PEDOT- was investigated modifying different parameters at three different levels of system perturbation. First, the role of polymerization conditions and post-polymerization treatments was studied. Different polymerization techniques, oxidants and solvents have been used for the same ICP, and the occurring changes have been investigated. Moreover, PEDOT oxidation level was tuned to optimize TE efficiency.

At a second level, the monomer molecular structure was modified to prepare a PEDOT-based copolymer. The copolymer included conjugated (i.e. conductive) and not conjugated (i.e. not conductive) portions, which deeply impacted the charge transport behaviour. The results show the versatility of this strategy, still barely explored in TE field, and how final transport properties can be finely tuned by means of molecular modifications.

Finally, at a third level, PEDOT macroscopic features were tuned by embedding inorganic nanostructure. Such a strategy is usually exploited to improve TE efficiency by means of nanostructuration beneficial effects already known in inorganic materials. Nanoparticles of two different metal oxides (CuO and Mn_3O_4) of different size and shape were dispersed in PEDOT matrix. Evaluation of humidity and oxidation level effects on charge transport features allowed to obtain novel insights into transport properties in nanocomposites.

Riassunto

I polimeri intrinsecamente conduttori sono una classe di materiali con caratteristiche uniche. In quanto materiali polimerici, infatti, sono leggeri e flessibili, e possono essere facilmente processati e stampati. Al contempo, però, possono condurre corrente elettrica, raggiungendo anche conducibilità tipiche di metalli. Questa combinazione eccezionale ha consentito lo sviluppo di dispositivi elettronici stampati e flessibili, i quali risultano estremamente interessanti nell'ambito dei dispositivi elettronici portabili, sia integrati nel corpo umano (ad esempio, biosensori impiantabili) sia indossabili (come, ad esempio, gli smartwatch).

Anche l'applicazione termoelettrica di questi polimeri conduttori ha recentemente guadagnato un certo rilievo in campo scientifico. Un dispositivo termoelettrico, in questo caso organico, può convertire il calore in energia elettrica grazie allo sfruttamento dell'effetto Seebeck. Grazie a questo processo, il dispositivo può recuperare il calore di scarto dissipato in tutti i processi che coinvolgono il consumo di energia e trasformarlo in energia utilizzabile.

Anche se i polimeri intrinsecamente conduttori hanno già mostrato interessanti proprietà termoelettriche, il loro utilizzo in questo campo è ancora molto limitato per via delle basse efficienze di conversione termoelettrica raggiunte finora, che impediscono a questi materiali di essere competitivi con i più diffusi materiali inorganici per questa applicazione, ovvero i tellururi.

Il design di un polimero conduttore che abbia elevate prestazioni termoelettriche parte necessariamente da una conoscenza approfondita di quali tecniche e trattamenti influenzino le proprietà finali di trasporto di carica. La complessità intrinseca di questi sistemi, tuttavia, rende spesso difficoltoso ottenere queste informazioni, impedendo una comprensione accurata dei fenomeni coinvolti nella variazione delle proprietà di trasporto.

Questo progetto di dottorato ha riguardato lo studio dell'impatto di diversi parametri sulle proprietà termoelettriche dei polimeri conduttori, con lo scopo di raggiungere una comprensione approfondita di come il trasporto di carica ne venga influenzato.

Nello specifico, lo studio ha riguardato il poli(3,4-etilendiossitiofene) -PEDOT-, il quale è stato studiato modificando diversi parametri a tre livelli di perturbazione del sistema.

In primo luogo, un'indagine è stata svolta sul ruolo delle condizioni di polimerizzazione e su quello dei trattamenti effettuati dopo la polimerizzazione. In particolare, è stata studiata l'influenza di diverse tecniche di polimerizzazione, diversi ossidanti e diversi solventi sulla

qualità finale del film polimerico. Inoltre, il livello di ossidazione del PEDOT è stato modificato dopo la polimerizzazione, ottenendo un'ottimizzazione della sua efficienza termoelettrica.

Ad un secondo livello di perturbazione, la struttura molecolare del monomero è stata modificata per preparare un copolimero. Il copolimero includeva una porzione centrale coniugata (e quindi, conduttiva) e due porzioni laterali non coniugate (isolanti), che hanno comportato una modifica sostanziale delle proprietà di trasporto del materiale finale. I risultati ottenuti sulla nuova struttura mostrano la versatilità di questa strategia, ancora poco esplorata nel campo termoelettrico, e come le proprietà di trasporto possano essere finemente modificate grazie all'introduzione di modifiche della struttura molecolare.

Infine, al terzo livello, le proprietà macroscopiche del PEDOT sono state modificate grazie all'introduzione di nanostrutture di natura inorganica. Questa strategia è solitamente utilizzata per migliorare l'efficienza termoelettrica dei materiali inorganici, grazie alla generazione di effetti benefici dovuti alla nanostrutturazione. Due tipologie diverse di nanoparticelle di ossidi metallici (CuO e Mn_3O_4) sono state sintetizzate in diverse forme e dimensioni e introdotte nella matrice di PEDOT in diverse concentrazioni. Grazie allo studio dell'effetto dell'umidità sulle proprietà di trasporto ed allo studio sulla variazione dello stato di ossidazione è stato possibile ottenere nuove informazioni sul comportamento elettrico dei nanocompositi.

Contents

List of Figures

Chapter 1

Chapter 2

Chapter 4

Chapter 5

Page

Chapter 6

Page

Introduction

1.1 Organic electronics

When we talk about polymers, the first idea that pops up in our mind is "plastics". Then, we may start to think about how largely and deeply plastic invention impacted and still impacts our everyday life, starting with the packaging of our food, going to our furniture and maybe ending up with the tires of our cars. Already in 1967, in the popular comedy-drama "The Graduate", Mr McGuire advised a young Dustin Hoffman about the future with just one word "Plastics", adding that there was a great future in it.

The common feature of this kind of polymers, that we think about as "plastics", is that they are structural material. We use them for their specific mechanical properties. They are lightweight, but strong. Tuning their composition allows to obtain rigid or elastic material, can make them adhesive or perfect waterproof coatings.

Another plastic common feature is its insulating behaviour. We could not think about plastics as an active material for circuits in our laptop or as electrical wires in our house walls, could we?

That is true for almost all plastics. In 1977 Alan G. MacDiarmid, Alan J. Heeger, Hideki Shirakawa and co-workers developed a polymeric material, polyacetylene, which, after being oxidize with halogens, could reach the electrical conductivity of a metal[1].

This discovery, celebrated with a Nobel Prize in Chemistry in 2000, is considered the birth of organic based electronics. A novel purpose was found for polymers, no more as structural material, but as active ones inside electronic devices. Still, these materials could preserve structural features that make them unique, such as lightweight, strength and flexibility. This was a great chance for novel technologies to be developed in completely new ways.

The great opportunity represented by this class of material guaranteed to them popularity over the last few decades, with an outburst in efforts put in their development and improvement by the scientific community.

Figure 1.1 shows the different roadmaps for organic electronic applications, which shows the current state of the technological development (bottom) and the expected future development (top).

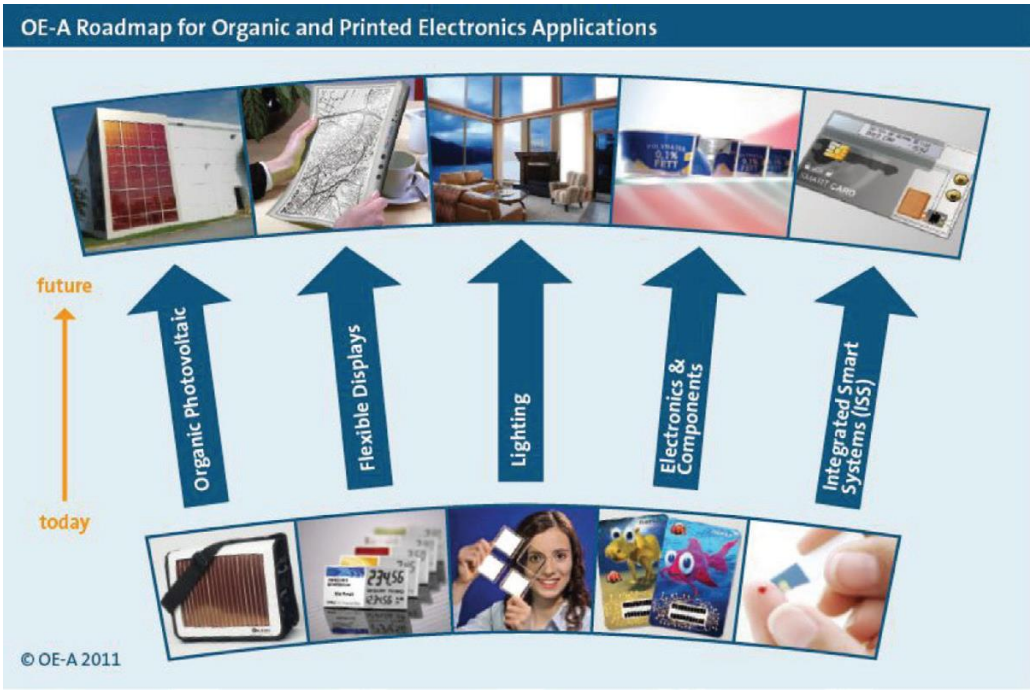

FIGURE 1.1: COMPREHENSIVE ROADMAP FOR ALL THE MOST STUDIED ORGANIC ELECTRONICS APPLICATIONS. SOURCE ORGANIC AND PRINTED ELECTRONICS ASSOCIATION (OE-A)[2].

Over the last few decades, the application in three devices led the development and the improvement of organic materials[3]: organic photovoltaic cells[4] (OPVCs), organic light-emitting diodes[5] (OLEDs) and organic thin-film transistors[6] (OTFTs). Other applications have been also developed, such as sensors[7], batteries and supercapacitors[8], which can be considered within the two last categories shown by Figure 1.1.

Although the large scientific production on the topic, there has been little to show for the much-heralded organic electronics revolution into the market.

The only exception is represented by OLED, which has become a market worth over $10 billion, largely driven by high-resolution colour mobile displays on glass. The other applications are still facing the first steps to reach market relevance. A lot can be learnt on this issue from the history of OLED technology development.

A 32-year long path led OLED from the first publication of the bilayer OLED device in 1981[9] to the $10 billion market size milestone in 2013[3].

Early OLEDs suffered from many issues, including very short lifetime (of the order of minutes), poor efficiency, and poor colour reproduction. Process tools for vacuum deposition and patterning of OLED layers uniformly and rapidly over large areas of glass did not exist. Over the next 20 years, enormous resources were used to understand and overcome the causes of degradation and to develop novel organic materials that could provide better efficiency and

increased lifetime. Moreover, process tools for mass manufacture were developed and technical challenges were overcome. All this has taken a lot of time and efforts and well exemplifies the common theme of organic electronics: lifetime and performance are the main issues, which can be usually addressed by material development over years and specialization of manufacturing techniques over organic material specific features. Nevertheless, we see from the pioneering organic electronics technology of OLED that enormous improvements are possible and that consumer electronics products based on the technology can be advantaged in the marketplace.

Given the very long time it took for OLED to move from laboratory to market, it was possible for significant improvements to occur in the other organic based technologies, if they are going to follow the same path.

Among these technologies, an application of organic electronics is still lingering at first steps of material and device development, organic thermoelectric generators (OTEG). Even though numerous studies on different materials have been done for this specific application[10–14], together with various proof-of-concept devices[15–17], several issues must still be faced to overcome development step and reach the market. An insight in technology features is necessary to better understand the potentialities of organic materials in this field and the issues that still need to be overcome.

1.2 Organic Thermoelectric Generators (OTEG)

A dedicated paragraph on specific physical explanation on thermoelectric phenomena can be found in Chapter 2, but a general description of thermoelectric generators will be herein provided.

If we consider two bars of semiconductors, as shown in Figure 1.2a, and we apply to them a temperature difference, charge carriers move from the hot side to the cold one. The resulting charge gathering in one side of the bar originates a potential difference (ΔV), due to the so-called Seebeck effect.

Electrically connecting the two bars (so-called legs, in thermoelectric devices) as shown in Figure 1.2b allows to create a circuit in which charge carriers, moving by means of thermal gradient, can flow in an electric current (black arrows).

A thermoelectric module is made up by several of these leg couples connected in series, as represented in Figure 1.2 c.

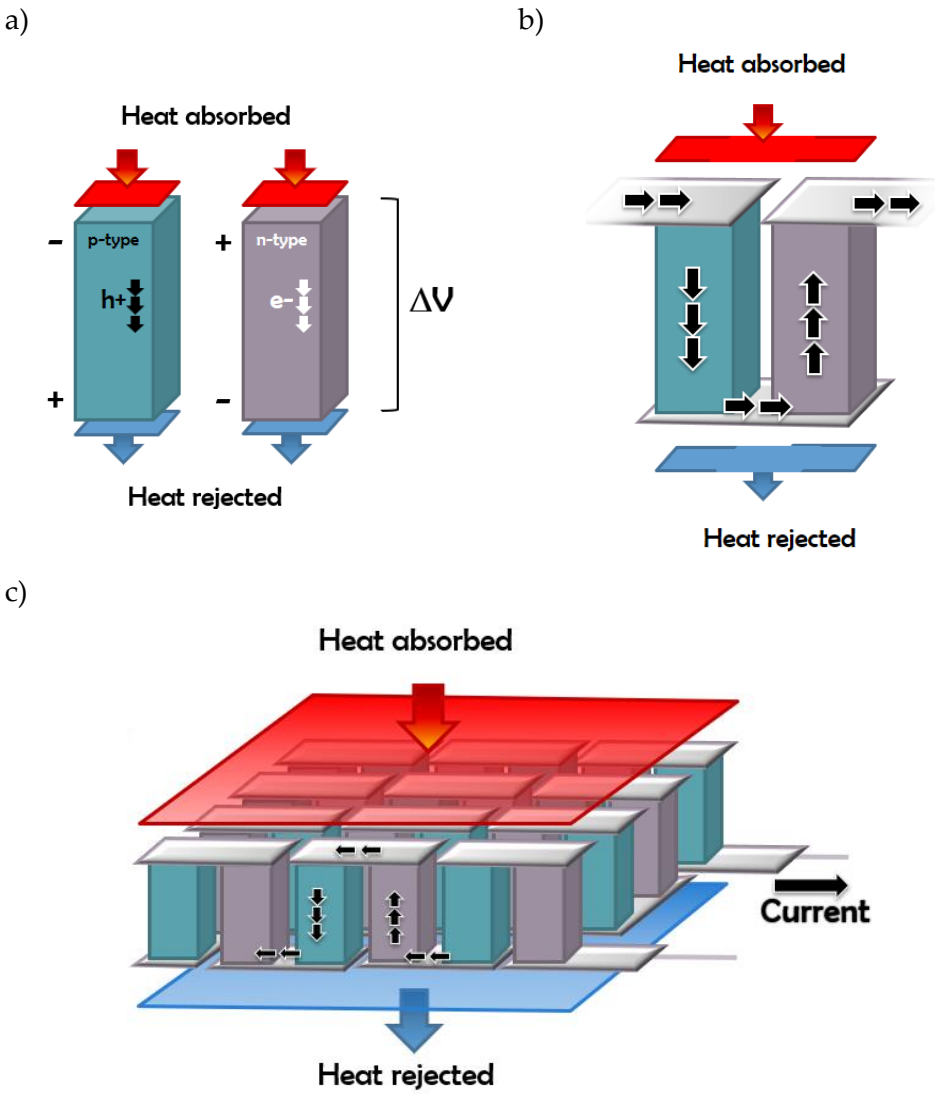

FIGURE 1.2: A) SKETCH OF THERMOVOLTAGE GENERATION IN TWO BARS OF SEMICONDUCTOR N-TYPE AND P-TYPE; B) ELECTRICALLY CONNECTING THE TWO BARS (LEGS) IN A PROPER WAY IT IS POSSIBLE TO EXPLOIT THERMOVOLTAGE TO GENERATE CURRENT; C) CONNECTING SEVERAL COUPLES OF LEGS IN SERIE IT IS POSSIBLE TO INCREASE THE CURRENT OUTPUT. THE RESULT IS A SO-CALLED THERMOELECTRIC MODULE.

The description of this technology makes clear how it can be an alternative and environmentally friendly way for harvesting and recovering heat which is directly converted into electrical energy. A key aspect for TEGs is, quite obviously, the efficiency of heat-electrical energy conversion, which is strongly dependent upon the materials used for legs.

Thermoelectric efficiency of a specific material can be evaluated by means of its thermoelectric figure of merit zT value, which is defined as:

$$z\bar{T} = \frac{\alpha^2 \sigma}{k} \bar{T} \tag{1.1}$$

where α is the Seebeck coefficient ($\alpha = \frac{\Delta V}{\Delta T}$), σ is the electrical conductivity and k is the thermal conductivity. The term $\bar{T} = \frac{T_H + T_C}{2}$ is the mean operating temperature, since T_H and T_C are the temperatures of the hot and cold sinks. Eq. 1.1 will be derived in Chapter 2.

According to this relation, a good thermoelectric efficiency is owed to both high electrical conductivity σ and high Seebeck coefficient α, but is also linked to a low thermal conductivity k. Moreover, since these quantities depend upon temperature, the material can be evaluated as a good thermoelectric material candidate only in a specific range of operating temperatures. Figure 1.3[18] well represents this temperature dependence of zT.

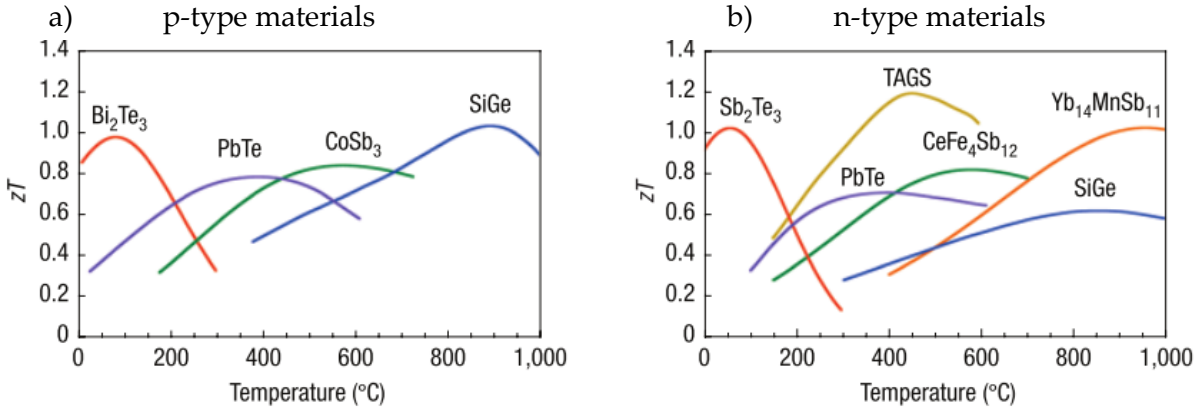

FIGURE 1.3: FIGURE-OF-MERIT ZT OF STATE-OF-THE-ART COMMERCIAL MATERIALS AND THOSE USED OR BEING DEVELOPED BY NASA FOR THERMOELECTRIC POWER GENERATION. A) P-TYPE AND B) N-TYPE. REPRODUCED FROM REF. [18].

Even though thermopower measurements were already performed on intrinsically conductive polymers (ICPs)[19,20], the first studies that actually investigated the possibility to use them as thermoelectric material can be dated back to late 90s[21,22] and to the beginning of this century[23–25]. It was immediately clear that operating temperature range for ICP would have been room temperature, due to their poor stability at high temperatures. So, reference inorganic benchmarks were bismuth telluride (Bi_2Te_3) for p-type doping and antimony telluride (Sb_2Te_3) for n-type doping (Figure 1.3).

Studies on ICPs revealed low thermal conductivity values, (a through-plane value of 0.15 $WK^{-1}m^{-1}$ and an in-plane value of 0.8 $WK^{-1}m^{-1}$ were measured[26]), which make them appealing for this application. Unfortunately, such values were usually paired with low electrical conductivities and low Seebeck coefficients.

Therefore, in the last 15 years, research efforts focused on the simultaneous increase of the Seebeck coefficient and of the electrical conductivity, with a variety of different techniques[16,27–31]. Equivalently, we can say that the focus has been on thermoelectric power factor (PF) enhancement, where PF is defined as:

$$PF = \alpha^2 \sigma \qquad (1.2)$$

Reported telluride zT at room temperature reach a top value of 1.4[32], and a record value of 2.4 has been reported for p-type BiTe/SbTe superlattice device[17]. In comparison, most recent zT values obtained for the most widely used ICP, poly(3,4-ethylenedioxythiophene) (PEDOT), appeared quite poor: top records are 0.31[16] and 0.42[31]. Such values tell us that low thermal conductivities do not compensate low PF, which is the main issue that should be addressed in this field.

The second issue is the difficulty to obtain n-type organic materials that are as efficient as p-type. Doping process allows to obtain an excess of positive charges (p-type) or negative charges (n-type) into semiconductors, and even for ICPs it is fundamental to obtain a conductive material. Such a process will be described more in detail in Chapter 2.

In principle, it is possible to dope ICPs in both ways. Several classes of ICPs can be easily p-doped and used for thermoelectric application, such as polyanilines[21] (PANI), polythiophenes (PTH), polypyrroles[22,23] (PPY), polycarbazoles[33] (PC) and polyphenylenevinylene (PPV). The n-doped form of most ICPs, though, is highly unstable and cannot be used for practical purposes. Thus, the available n-type ICPs are specific structures synthetized to stably bear negative charges.

Among the few n-type ICPs developed, the best performances were obtained for P(NDIOD-T2)[34a], perylene diimide[35] based polymers and BDPPV[b] based structures[36]. The power factors recorded for these polymers span from 10^{-1} to a few tens of $\mu WK^{-2}m^{-1}$, still one order of magnitude lower than best performing p-type ICPs.

The low efficiency for materials that should operate around room temperature, i.e. over small temperature differences, together with the absence of a good n-type doped counterpart, may lead to wonder why one should put so much effort in trying to use these materials for thermoelectrics.

The answer lies in the specific organic polymer features. Unlike their inorganic counterpart, i.e. tellurides, they are made of earth-abundant elements (carbon, hydrogen, oxygen, sulphur and nitrogen), they are easy to process via solution, which enable cheap printing techniques. Moreover, they are easily integrable in flexible substrate, lightweight and biocompatible[37].

All the ICP features listed are particularly interesting for wearable thermoelectric generator application, which is a technology still at its early development steps, but extremely appealing for nowadays market.

---

[a]Poly{N,N2-bis(2-octyl-dodecyl)-1,4,5,8-napthalenedicarboximide-2,6-diyl]-alt-5,52-(2,22-dithiophene)} doped with dihydro-1H-benzoimidazol-2-yl (N-DBI) derivatives.

[b]Poly benzodifurandione-based p-phenylene vinylene (PPV) doped with N-DMBI ((4-(1,3-dimethyl-2,3-dihydro-1Hbenzoimidazol-2-yl)phenyl)dimethylamine).

1.2.1 Wearable Thermoelectric Generators

A human body constantly generates heat. Only a part of this heat is dissipated into the ambient as a heat flow and infrared radiation, the rest of it is rejected in a form of water vapor. Furthermore, only a small fraction of the heat flow can be used in a wearer's friendly and unobtrusive device (i.e., a person might easily wear a wristwatch-like device, while a device covering a larger body area is too uncomfortable to be worn).

Nevertheless, body heat harvesting for powering wearable sensors and electronics is extremely interesting as it would enable harnessing uninterrupted energy from body heat, without the necessity to recharge or even change any battery. In harsh environments and in emergency situations, the wearable TEG could be constantly used as an energy source.

This major problem that is faced when integrating a TEG into clothing or wearable technology is that the efficiency of the device is related to various factors such as: device structure, air speed with respect to the person and placement on the human body. Nevertheless, three main problems can be identified in designing a wearable TEG. First, human body is not a good heat source, due to its high thermal resistance. Dissipated heat has been estimated to be about 3–5 $mWcm^{-2}$ on average, considering an indoor environment[38]. Moreover, in such an ambient, a temperature difference lower than 10 K is expected to be sustained by a TEG.

Furthermore, if we consider that a device should cover a small skin area (40 cm^2, the typical wristband area), clearly the used thermoelectric material must reach high efficiencies. So, thermoelectric efficiency of the chosen material is the first concern to meet the 10–30 μWcm^{-2} electrical power requirement[38] needed for sensor powering.

The second crucial aspect is the thermal contact among the device and the skin. Human skin is a challenging substrate for a device, since it is neither rigid or flat. Even though mechanical contact resistances are rather unpredictable, resistances in excess of $10^2\ cm^2K/W$ are expected[39]. A large thermal resistance can cause a significant drop of the temperature difference exploitable by the TEG. So, even using a high-performing thermoelectric material, the power output would be dramatically decreased.

A third, but not less important aspect, is material safety. Since the device would be in direct contact with the human skin, a toxic material inside it is less than desirable.

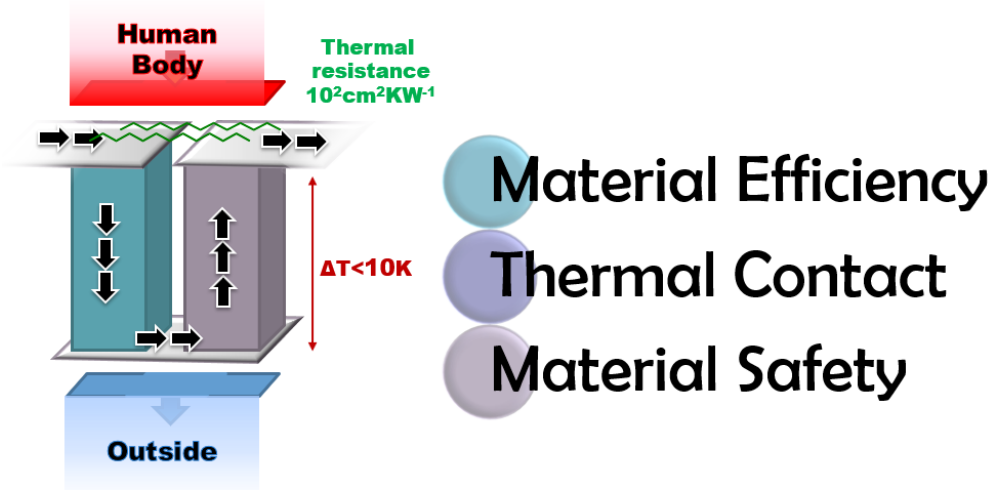

FIGURE 1.4: SKETCH SUMMARIZING THE CRITICAL ASPECTS OF WEARABLE TEGS.

Wearable thermoelectric harvester prototypes developed up to now adopted different strategies to match human skin flexibility and to lessen thermal interface resistance, including use of fabrics as device support[40–43] or thin plastic sheets[44,45]. Since a high performing material is required, all the developed devices have exploited tellurides. Unfortunately, these material are toxic[46], which makes them poor candidates for a safe device in direct contact with human skin. Moreover, telluride production is a high-cost process with a high-environmental impact[47].

ICPs would perfectly match requirements of safety and low costs. They can be easily integrated on flexible substrates and are biocompatible. Moreover, all the other features already listed, such lightweight and low cost, seem to perfectly fit this application.

The main issue, which still must be overcome, is their poor efficiency. In spite of the huge steps forward of the last few years, starting from a thermoelectric PFs around 1 $\mu WK^{-2}m^{-1}$ in early 00s[23] to a record value of 1270 $\mu WK^{-2}m^{-1}$ in 2013[16], this is not enough. A breakthrough is still needed to eventually meet wearable thermoelectrics efficiency demand.

1.3 ICP Thermoelectric Efficiency

As already stated, the increase of ICP thermoelectric efficiency mainly focus on PF increase, since thermal conductivity k is considered to be very low in most cases[26,48]. Since ICPs, as semiconductors, can be doped to increase charge carrier concentration and, therefore, electrical conductivity σ, one might think this could be a good strategy to obtain an efficiency enhancement. Unfortunately, Seebeck coefficient has an opposite dependence on charge carrier concentration, meaning that this strategy is not useful to obtain a major PF increase. Nevertheless, an optimization of the doping level allows to reach a maximum trade-off value[28].

Another possibility is to increase charge carrier mobility, which causes an increase of electrical conductivity, without any detrimental impact on Seebeck coefficients. This strategy requires a good knowledge of charge carrier transport mechanism, to understand which is the determining step of charge transport. For ICP this is not a trivial task. As it will be explained

more in detail in Chapter 2, ICPs are heterogeneously disordered systems with both crystalline and amorphous domains, in which charge carrier can move by different mechanisms. Figure 1.5 describes the possible paths of charge carriers. It is commonly accepted[49–52] that in crystalline domains the better π-π stacking allows a more efficient charge carrier hopping, while charge carrier transport in the amorphous regions is impeded.

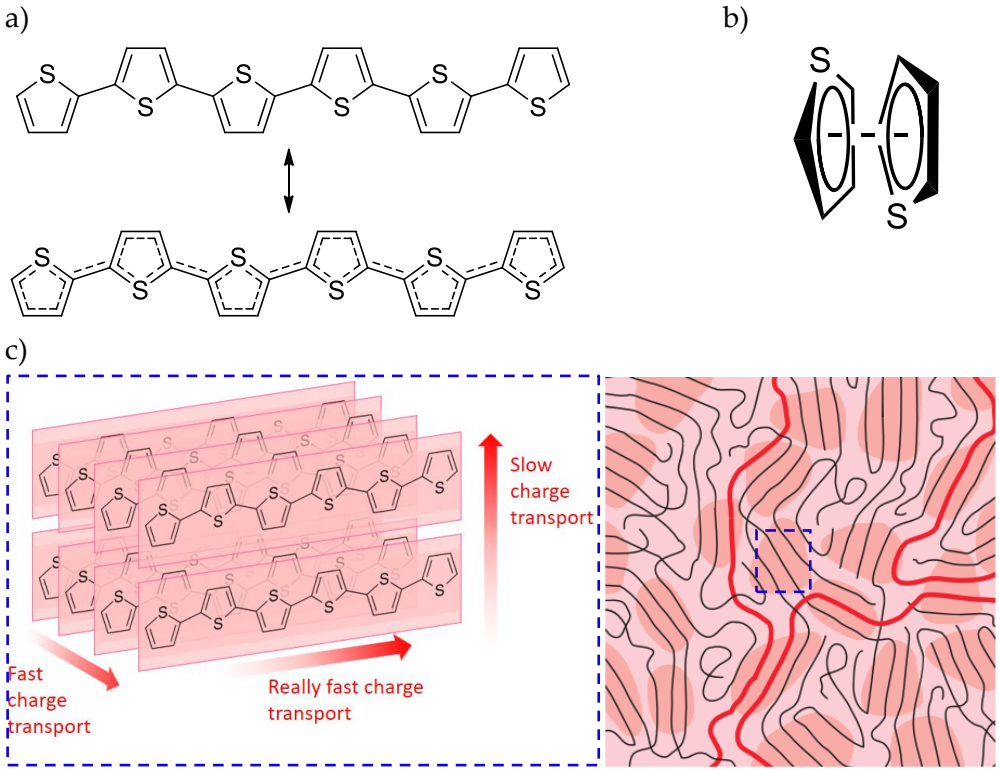

FIGURE 1.5: A) MOLECULAR STRUCTURE OF POLYTHIOPHENE HEXAMER, AN HETEROAROMATIC ICP. THE RESONANCE STRUCTURES SHOW THE COMPLETE DELOCALIZATION OF Π ORBITAL ALL OVER THE CHAIN. SUCH A DELOCALIZATION ALLOWS CHARGE CARRIER MOVEMENT ALONG THE CHAINS. B) AROMATIC SYSTEMS, SUCH AS THIOPHENE, INTERMOLECULARLY INTERACT THROUGH Π-Π STACKING, AS DEPICTED. THIS INTERACTION IS CRYSTALLISATION DRIVING FORCE IN ICPS. C) CRYSTALLITES ARE FORMED BY PACKING OF CHAIN PORTIONS (*LEFT*). CHARGE TRANSPORT CAN HAPPEN ALONG THE CHAIN (REALLY FAST), THROUGH FACING CHAINS (FAST) DUE Π-Π STACKING OR EVEN THROUGH CLOSE CHAINS (SLOW). THE LAST MECHANISM CHARACTERIZES ALSO AMORPHOUS REGIONS, WHICH ARE PRESENT TOGETHER WITH CRYSTALLINE ONES IN ICP SAMPLES (*RIGHT*)(REPRODUCED FROM REF. [51]).

Therefore, mainly adopted strategies focus on enhancing ICP crystallinity, which can be reached through many different paths. These strategies can be split in two main categories. On one side, the strategies that involve addition of specific chemicals which influences the polymerization reaction. On the other, treatments that can be performed on the polymerized films, i.e. after the polymerization. The most popular strategies are listed for the two categories in Table 1.1.

Before/During Polymerization Treatments		
	Description	**Ref.**
Polymerization Technique	The use of a more controlled polymerization technique can lead to more crystalline films.	53,54
Inhibitor	The introduction of a weak base (such as imidazole or pyridine) or polyglycoles can slow down polymerization rate. A slower reaction lessens the conjugation defects along the growing chains and gives more time to the macromolecules to organize.	54–56
Solvent/Co-solvent	The use of specific solvent or co-solvent in polymerization environment influences final chain order.	57,58
Counterion	Since the final polymer is charged, counterions will be present within the structure. Introducing a source of smaller counterions during polymerization allows a better chain packing.	59
After Polymerization		
Secondary dopants	A secondary dopant is a polar solvent (e.g. ethylene glycol or N-methyl pyrrolidone) in which the film is immersed. The solvent straightens up ICP chains, increasing crystalline domain extension.	16,60
Acid treatments	Treating ICP with strong acid provides a counterion exchange within the polymer. The counterion provided by the acid (such as SO_4^-) is smaller than the one originated by polymerization reaction.	56,61
Stretching	Film stretching forces polymer lamellar fibres to slide along each other, leading to a microstructural order enhancement.	62

TABLE 1.1: LIST OF THE MOST POPULAR STRATEGIES FOR ENHANCING ICP PERFORMANCE, INCLUDING A BRIEF DESCRIPTION. FEW REFERENCES ARE LISTED FOR EACH STRATEGY TO GIVE SOME PRACTICAL EXAMPLE OF ITS APPLICATION, RATHER THAN GIVE A FULL ACCOUNT ON THE WORK DONE FOR EACH STRATEGY, WHICH IS BEYOND THE PURPOSE OF THIS TABLE.

Another strategy to improve PF value is to take advantage of the unique chance given by organic structures. Organic synthesis allows to modify the molecular structure of the monomer, tuning moieties according to the necessities. Including a specific moiety, which might be either electron-rich or electron-poor or changing a heteroatom, deeply affects the final properties of the polymer.

Monomer modification affects intermolecular interactions, causing a strong impact on charge carrier transport. For instance, alternated copolymerization of a donor (i.e. electron-rich) monomer and an acceptor (i.e. electron-poor) one, gives rise to dipolar intermolecular interactions between chains which can support π-π stacking[63], leading to an optimized charge

transfer. A more detailed account on all the possibilities contemplated by this strategy will be given in Chapter 5.

A more recent strategy to enhance performances took inspiration from the inorganic semiconductor design for thermoelectric application. One of the most popular strategy to obtain a performing material is the nanostructuration. Theoretically hypothesized in early Nineties[64], nowadays nanoscale effects on charge transport have been experimentally studied in different inorganic semiconductors and their extremely beneficial impact on thermoelectric properties has been widely reported[18,65–67].

Application of nanostructuration concept to ICPs led to the development of the so-called nanocomposites. In these novel materials, nanostructured inorganic materials are embedded into an ICP matrix, giving rise to interfacial effects that can push the material PF value beyond those of the two components[27,68,69]. A detailed analysis of nanocomposite features, along with the description of nanoscale effects, will be given in Chapter 6.

1.4 Concluding Remarks

The given description of all the strategies that may be implemented to increase material performances provided clues about the many possibilities open to improve thermoelectric ICPs. Moreover, possible combinations among different strategies widen even more the range of paths that can be pursued.

In this scenario, the avenues already explored appear to be only a fraction of this range. Furthermore, the precise effect of some material modifications are not fully understood yet, also due to the physical models used to describe ICP based systems, which sometimes are insufficient[70].

An effort in this direction has been done in the experimental work carried out in this thesis, as it will be better described in Chapter 3. The object of our analysis has been one of the most studied ICPs, poly(3,4-ethylendioxythiophene) or PEDOT. The effects of different strategies, and even their combination, were studied, characterizing charge transport features. Moreover, different interpretation models have been implemented to obtain some insights on which could be the final effects of chemicals, treatments, molecular modifications and nanostructure embedding.

Truth to be told, ICP use as thermoelectric material in wearable devices is still at the beginning of its history, and the path to success seems to be long, tortuous, and arduous. Someone might even think that such an idea is science-fiction flavoured. But even a plastic that can conduct electricity should have seemed science fiction at the beginning, should not have it?

1.5 References

1 C. K. Chiang, C. R. Fincher, Y. W. Park, A. J. Heeger, H. Shirakawa, E. J. Louis, S. C. Gau and A. G. MacDiarmid, *Phys. Rev. Lett.*, 1977, **39**, 1098–1101.

2 Organic and Printed Electronics Association- OEA, http://www.oe-org.

3 D. Lupo, W. Clemens and S. Breitung, *Organic and Printed Electronics: Fundamentals and Applications*, CRC Press, 2016.

4 L. Dou, J. You, Z. Hong, Z. Xu, G. Li, R. A. Street and Y. Yang, *Adv. Mater.*, 2013, **25**, 6642–6671.

5 S. Reineke, M. Thomschke, B. Lüssem and K. Leo, *Rev. Mod. Phys.*, 2013, **85**, 1245–1293.

6 H. Sirringhaus, *Adv. Mater.*, 2014, **26**, 1319–1335.

7 R. Shinar and J. Shinar, *Organic Electronics in Sensors and Biotechnology*, The McGraw-Hill Companies, Inc., 2009.

8 C. Liu, F. Li, L.-P. Ma and H.-M. Cheng, *Adv. Mater.*, 2010, **22**, E28–E62.

9 US 4281053 A, 1981.

10 B. Russ, A. Glaudell, J. J. Urban, M. L. Chabinyc and R. A. Segalman, *Nat. Rev. Mater.*, 2016, **1**, 16050.

11 B. T. McGrail, A. Sehirlioglu and E. Pentzer, *Angew. Chem. Int. Ed. Engl.*, 2015, **54**, 1710–23.

12 M. Culebras, C. M. Gomez and A. Cantarero, *Materials (Basel).*, 2014, **6**, 6701–6732.

13 Q. Zhang, Y. Sun, W. Xu and D. Zhu, *Adv. Mater.*, 2014, **26**, 6829–6851.

14 L. M. Cowen, J. Atoyo, M. J. Carnie, D. Baran and B. C. Schroeder, *ECS J. Solid State Sci. Technol.*, 2017, **6**, N3080–N3088.

15 R. Buchner, K. Froehner, C. Sosna, W. Benecke and W. Lang, *J. Microelectromechanical Syst.*, 2008, **17**, 1114–1119.

16 T. Park, C. Park, B. Kim, H. Shin and E. Kim, *Energy Environ. Sci.*, 2013, **6**, 788.

17 R. Venkatasubramanian, E. Siivola, T. Colpitts and B. O'Quinn, *Nature*, 2001, **413**, 597–602.

18 G. J. Snyder and E. S. Toberer, *Nat. Mater.*, 2008, **7**, 105–114.

19 Y. Nogami, H. Kaneko, T. Ishiguro, A. Takahashi, J. Tsukamoto and N. Hosoito, *Solid State Commun.*, 1990, **76**, 583–586.

20 W. Park, H. Choi and H. Shirakawa, 1984, **30**.

21 N. Mateeva, H. Niculescu, J. Schlenoff and L. R. Testardi, *J. Appl. Phys.*, 1998, **83**, 3111.

22 N. T. Kemp, A. B. Kaiser, C. J. Liu, B. Chapman, O. Mercier, A. M. Carr, H. J. Trodahl,

R. G. Buckley, A. C. Partridge, J. Y. Lee, C. Y. Kim, A. Bartl, L. Dunsch, W. T. Smith and J. S. Shapiro, *J. Polym. Sci. Part B Polym. Phys.*, 1999, **37**, 953–960.

23 H. Yan, T. Ishida and N. Toshima, *Proc. ICT 2001, 20th Int. Conf. Thermoelectr.*, 2001, 310–313.

24 H. Yan, N. Sada and N. Toshima, *J. Therm. Anal. Calorim.*, 2002, **69**, 881–887.

25 Y. Shinohara, K. Ohara, Y. Imai, Y. Isoda and H. Nakanishi, *Int. Conf. Thermoelectr. ICT, Proc.*, 2003, **2003–Janua**, 298–300.

26 Q. Wei, M. Mukaida, K. Kirihara, Y. Naitoh and T. Ishida, *Materials (Basel).*, 2015, **8**, 732–750.

27 S. K. Yee, N. E. Coates, A. Majumdar, J. J. Urban and R. A. Segalman, *Phys. Chem. Chem. Phys.*, 2013, **15**, 4024–4032.

28 O. Bubnova, Z. U. Khan, A. Malti, S. Braun, M. Fahlman, M. Berggren and X. Crispin, *Nat. Mater.*, 2011, **10**, 429–33.

29 M. Culebras, C. M. Gómez and A. Cantarero, *J. Mater. Chem. A*, 2014, **2**, 10109.

30 A. M. Glaudell, J. E. Cochran, S. N. Patel and M. L. Chabinyc, *Adv. Energy Mater.*, 2015, **5**.

31 G.-H. Kim, L. Shao, K. Zhang and K. P. Pipe, *Nat Mater*, 2013, **12**, 719–723.

32 H. J. Goldsmid, *Materials (Basel).*, 2014, **7**, 2577–2592.

33 I. Lévesque, P.-O. Bertrand, N. Blouin, M. Leclerc, S. Zecchin, G. Zotti, C. I. Ratcliffe, D. D. Klug, X. Gao, F. Gao and J. S. Tse, *Chem. Mater.*, 2007, **19**, 2128–2138.

34 R. A. Schlitz, F. G. Brunetti, A. M. Glaudell, P. L. Miller, M. A. Brady, C. J. Takacs, C. J. Hawker and M. L. Chabinyc, *Adv. Mater.*, 2014, **26**, 2825–2830.

35 B. Russ, M. J. Robb, F. G. Brunetti, P. L. Miller, E. E. Perry, S. N. Patel, V. Ho, W. B. Chang, J. J. Urban, M. L. Chabinyc, C. J. Hawker and R. A. Segalman, *Adv. Mater.*, 2014, **26**, 3473–3477.

36 K. Shi, F. Zhang, C. A. Di, T. W. Yan, Y. Zou, X. Zhou, D. Zhu, J. Y. Wang and J. Pei, *J. Am. Chem. Soc.*, 2015, **137**, 6979–6982.

37 R. Balint, N. J. Cassidy and S. H. Cartmell, *Acta Biomater.*, 2014, **10**, 2341–2353.

38 V. Leonov and R. J. M. Vullers, *J. Renew. Sustain. Energy*, 2009, **1**, 62701.

39 E. Gmelin, M. Asen-Palmer, M. Reuther and R. Villar, *J. Phys. D. Appl. Phys.*, 1999, **32**, R19–R43.

40 M.-K. Kim, M.-S. Kim, S. Lee, C. Kim and Y.-J. Kim, *Smart Mater. Struct.*, 2014, **23**, 105002.

41 S. J. Kim, J. H. We and B. J. Cho, *Energy Environ. Sci.*, 2014, **7**, 1959.

42 Z. Lu, H. Zhang, C. Mao and C. M. Li, *Appl. Energy*, 2016, **164**, 57–63.

43 M. Thielen, L. Sigrist, M. Magno, C. Hierold and L. Benini, *Energy Convers. Manag.*, 2017,

131, 44–54.

44 W. Glatz, E. Schwyter, L. Durrer, C. Hierold and S. Member, 2009, **18**, 763–772.

45 L. Francioso, C. De Pascali, I. Farella, C. Martucci, P. Cretì, P. Siciliano and a. Perrone, *J. Power Sources*, 2011, **196**, 3239–3243.

46 Stanford Advance Materials, *http://www.samaterials.com*, 2012.

47 S. Leblanc, S. K. Yee, M. L. Scullin, C. Dames and K. E. Goodson, *Renew. Sustain. Energy Rev.*, 2014, **32**, 313–327.

48 A. Weathers, Z. U. Khan, R. Brooke, D. Evans, M. T. Pettes, J. W. Andreasen, X. Crispin and L. Shi, *Adv. Mater.*, 2015, **27**, 2101–2106.

49 A. B. Kaiser, *Adv. Mater.*, 2001, **13**, 927–941.

50 V. I. Arkhipov, I. I. Fishchuk, A. Kadashchuk and H. Bassler, in *Photophysics of Molecular Materials*, ed. G. Lanzani, Wiley, 2006, pp. 262–366.

51 R. Noriega, J. Rivnay, K. Vandewal, F. P. V Koch, N. Stingelin, P. Smith, M. F. Toney and A. Salleo, *Nat. Mater.*, 2013, **12**, 1038–44.

52 S. A. Mollinger, B. A. Krajina, R. Noriega, A. Salleo and A. J. Spakowitz, *ACS Macro Lett.*, 2015, **4**, 708–712.

53 D. Evans, M. Fabretto, M. Mueller, K. Zuber, R. Short and P. Murphy, *J. Mater. Chem.*, 2012, **22**, 14889.

54 M. Mueller, M. Fabretto, D. Evans, P. Hojati-Talemi, C. Gruber and P. Murphy, *Polymer (Guildf).*, 2012, **53**, 2146–2151.

55 B. Winther-Jensen, D. W. Breiby and K. West, *Synth. Met.*, 2005, **152**, 1–4.

56 Z. U. Khan, O. Bubnova, M. J. Jafari, R. Brooke, X. Liu, R. Gabrielsson, T. Ederth, D. R. Evans, J. W. Andreasen, M. Fahlman and X. Crispin, *J. Mater. Chem. C*, 2015, **3**, 10616–10623.

57 M. Yamashita, C. Otani, M. Shimizu and H. Okuzaki, *Appl. Phys. Lett.*, 2011, **99**, 143307.

58 M. N. Gueye, A. Carella, N. Massonnet, E. Yvenou, S. Brenet, J. Faure-Vincent, S. Pouget, F. Rieutord, H. Okuno, A. Benayad, R. Demadrille and J. P. Simonato, *Chem. Mater.*, 2016, **28**, 3462–3468.

59 S. a. Spanninga, D. C. Martin and Z. Chen, *J. Phys. Chem. C*, 2010, **114**, 14992–14997.

60 H. Wang, U. Ail, R. Gabrielsson, M. Berggren and X. Crispin, *Adv. Energy Mater.*, 2015, **5**, 1–6.

61 N. Massonnet, A. Carella, A. de Geyer, J. Faure-Vincent and J.-P. Simonato, *Chem. Sci.*, 2015, **6**, 412–417.

62 Y. Hiroshige, M. Ookawa and N. Toshima, *Synth. Met.*, 2006, **156**, 1341–1347.

63 K. Müllen and W. Pisula, *J. Am. Chem. Soc.*, 2015, **137**, 9503–9505.

64 L. D. Hicks and M. S. Dresselhaus, *Phys. Rev. B*, 1993, **47**, 727–731.

65 A. Majumdar, *Science*, 2004, **303**, 777–8.

66 P. Pichanusakorn and P. Bandaru, *Mater. Sci. Eng. R Reports*, 2010, **67**, 19–63.

67 K. Nielsch, J. Bachmann, J. Kimling and H. Böttner, *Adv. Energy Mater.*, 2011, **1**, 713–731.

68 M. He, J. Ge, Z. Lin, X. Feng, X. Wang, H. Lu, Y. Yang and F. Qiu, *Energy Environ. Sci.*, 2012, **5**, 8351.

69 G. H. Kim, D. H. Hwang and S. I. Woo, *Phys. Chem. Chem. Phys.*, 2012, **14**, 3530.

70 J. J. Urban, *Nat. Mater.*, 2016, **16**, 157–159.

Theoretical Background

2.1 Thermoelectric Power Conversion

Hunger for energy is becoming a compelling problem in modern society. To make such a need compatible with environment preservation, a strong effort is required to exploit mostly renewable sources of energy and to make the energy production as efficient as possible. Among the strategies studied to pursue this ambitious aim, one is to take advantage of thermoelectric effect to recover wasted heat.

As already pointed out in the previous chapter, the use of conjugated polymers as active material for such application represents a great chance, but also a difficult challenge. In the first part of the present chapter, a description of thermoelectricity physics will be provided, while in the second part will focus on charge carrier transport in conjugated polymers.

2.1.1 A Brief History of Thermoelectrics

The first reported observation of thermoelectric phenomena can be dated back to 1794. The Italian scientist Alessandro Volta was studying electricity-related effects on frog bodies, when he put the legs and the back spine of one of them in two glasses containing the same solution at different temperatures (as reported in Figure 2.1). He observed that, sinking the extremities of a metallic arc in the two solutions, frog legs contracted. He was generating an electromotive force and correctly imputed it to the difference of temperature between the two solutions.

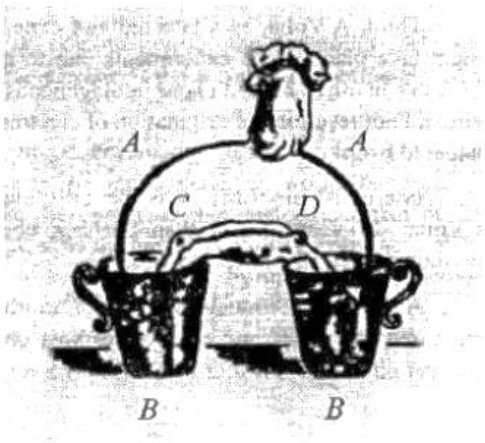

FIGURE 2.1: REPRESENTATION OF ALESSANDRO VOLTA'S EXPERIMENTAL SETUP. A IS A METALLIC ARC, C ARE FROG LEGS, WHILE D IS THE SPINE OF THE FROG. B ARE THE TWO GLASSES CONTAINING THE SAME SOLUTION AT DIFFERENT TEMPERATURES.

Years later, in 1821, the Estonian physicist Thomas Johann Seebeck found out that a circuit made from two dissimilar metals with junctions at different temperatures could deflect a compass magnet. Moreover, he observed that the angle of deflection depended on the value of the temperature difference between the junctions of the circuit. He imputed such behaviour to a magnetic field generated by temperature difference, and called the observed phenomenon "thermomagnetism".

Only four years later, in 1825, Hans Christian Oersted, who already proved that electrical currents induce magnetic fields, corrected Seebeck's hypothesis. Oersted understood that the effect observed by Seebeck was a consequence of an electrical current flowing due to the temperature difference, which ultimately deflected the magnet by Ampere's law. More exactly, the temperature difference could produce an electric potential which drives an electric current in a closed circuit. The phenomenon was then called by Oersted "thermoelectric effect" or "Seebeck effect".

In 1834, the French watchmaker Jean Charles Peltier carried out another discovery on physical effects originated by the interaction of temperature gradient and electrical phenomena. He observed that if a current is passing through the junction of dissimilar metals, the junction is heated or cooled depending on the direction of the current.

It took few years to assess that this effect was not correlated with Joule effect, but was a distinct effect, thus named "Peltier effect".

Later, in 1854, William Thomson, known as Lord Kelvin, eventually proposed a comprehensive explanation for both Seebeck and Peltier effects. Thanks to his studies on thermodynamics, he understood that Seebeck and Peltier effects were interrelated by a simple mathematical equation, since the Peltier coefficient is equal to the Seebeck coefficient times the absolute temperature (as it will be explained more in detail in the Sect. 2.1.2.2). Moreover, he predicted a third thermoelectric effect. He observed that in the presence of a temperature gradient, the current flow in a material generates the adsorption or the release of heat. Also, such heat resulted to be proportional to both the electric current and the temperature gradient. The proportionality constant is known as the Thomson coefficient.

Since this coefficient is related to Seebeck coefficient (Sect. 2.1.2.3), Thomson discovery had completed the picture on thermoelectric effects and their reciprocal relations.

The discoveries triggered the development of a new field of physics, the thermoelectricity, which studies the processes of thermal energy conversion into electrical power and vice versa.

Devices which convert heat into electricity are called thermoelectric generators (TEG), while devices which use electricity to heat or cool the environment are called Peltier cells, or simply thermoelectric coolers.

2.1.2 Thermoelectricity from a Macroscopic Point of View: Linear Thermodynamics

During the first half of the twentieth century, Lars Onsager[1] and Hendrik Casimir[2] gave a thermodynamic interpretation of thermoelectric processes, later further developed by Sybren De Groot. They were studying thermodynamics of dissipative system, taking advantage of an interpretation of links between out-of-equilibrium coupled processes. The fundamental assumption to describe out-of-equilibrium phenomena is that the system evolution is driven by a minimal production of entropy where each fluctuation of any thermodynamic potential undergoes a restoring force to equilibrium. So, even if the system is not steady, in this condition it is possible to define all the thermodynamic potentials involved, assuming a time-by-time stationary situation. In other words, all the different parameters of the process are defined at each time and location during the evolution of the system, so that we can consider the process itself as "quasi-static".

This implies that the intrinsic local time constants are much shorter than the time evolution of the macroscopic system itself. Consequently, the classical quasi-static relation:

$$dS = \frac{dQ_{qs}}{T} \tag{2.1}$$

between the heat (dQ) and the entropy variation (dS) can be extended in the following flux form expression,

$$\vec{J}_s = \frac{\vec{J}_q}{T} \tag{2.2}$$

where $\vec{J}_s$ is the entropy flux, $\vec{J}_q$ is the heat flux and T is the absolute temperature.

According to this description of the system, one can define the complete energy flux, using the first principle of thermodynamics, as:

$$\vec{J}_E = \vec{J}_q + \tilde{\mu}_e \vec{J}_N \tag{2.3}$$

where the energy flux $\vec{J}_E$ is equal to the heat flux $\vec{J}_q$ plus the energetic contribute of each particle, represented by particle flux $\vec{J}_N$ times the average electrochemical potential of each charge carrier $\tilde{\mu}_e$.
The electrochemical potential can be defined as:

$$\tilde{\mu}_e = \mu_e + eV \tag{2.4}$$

where μ_e is the chemical potential of the charge carrier, e is the fundamental charge and V is the electrical potential applied.
According to the interpretation of non-equilibrium thermodynamics, another thermodynamic field variable can be considered conjugated to each thermodynamic flux, namely the thermodynamic forces, which act as the driving force of a non-equilibrium process. Therefore, two thermodynamic forces can be paired to fluxes in Eq. 2.3, one originated by chemical potential gradient:

$$\vec{F}_N = \vec{\nabla}\left(-\frac{\tilde{\mu}_e}{T}\right) \tag{2.5}$$

and another one generated by temperature gradient:

$$\vec{F}_E = \vec{\nabla}\left(\frac{1}{T}\right) \tag{2.6}$$

If we now write down the linear coupling of forces and fluxes we get that the transport of energy and particles is given by a linear set of coupled equation:

$$\begin{bmatrix}\vec{J}_N \\ \vec{J}_E\end{bmatrix} = \begin{bmatrix}L_{NN} & L_{EN} \\ L_{NE} & L_{EE}\end{bmatrix}\begin{bmatrix}\vec{\nabla}\left(-\frac{\tilde{\mu}_e}{T}\right) \\ \vec{\nabla}\left(\frac{1}{T}\right)\end{bmatrix} \tag{2.7}$$

where L terms are the linear coefficients that correlate fluxes to forces, called phenomenological coefficients. The expression can be rearranged to use heat flux $\vec{J}_q$ instead of energy flux $\vec{J}_E$:

$$\begin{bmatrix}\vec{J}_N \\ \vec{J}_q\end{bmatrix} = \begin{bmatrix}L_{11} & L_{21} \\ L_{12} & L_{22}\end{bmatrix}\begin{bmatrix}-\frac{1}{T}\vec{\nabla}\tilde{\mu}_e \\ \vec{\nabla}\left(\frac{1}{T}\right)\end{bmatrix} \tag{2.8}$$

Relation between phenomenological coefficients in 2.7 and in 2.8 are reported in Appendix A. Using Eq. 2.8 is possible to derive expressions of laws that rule charge carrier transport phenomena inside materials, simply decoupling forces and fluxes. In other words, if we consider boundary conditions which set to zero one force or one flux, we can derive for each case a different relation. Such derivation allows also to understand the physical meaning of phenomenological coefficients.

For instance, if we consider an isothermal system, in which $\vec{\nabla}\left(\frac{1}{T}\right) = 0$, we obtain from Eq. 2.8:

$$\vec{J} = e\vec{J}_N = -\frac{eL_{11}}{T}\vec{\nabla}\tilde{\mu}_e \tag{2.9}$$

Considering the definition in Eq. 2.4, we can state that:

$$-\frac{\left(\vec{\nabla}\tilde{\mu}_e\right)}{e} = -\vec{\nabla}V = \vec{\varepsilon} \tag{2.10}$$

where $\vec{\varepsilon}$ is the electric field. Including such definition in Eq. 2.9, we can write the following expression of Ohm's law:

$$\vec{J} = \sigma_T\vec{\varepsilon} \tag{2.11}$$

where σ_T is the isothermal electrical conductivity, defined as:

$$\sigma_T = \frac{e^2L_{11}}{T} \tag{2.12}$$

Therefore, the phenomenological coefficient that correlates the charge carrier flux to the force represented by electrochemical potential gradient can be expressed as:

$$L_{11} = \frac{\sigma_T T}{e^2} \tag{2.13}$$

A second law can be derived considering another boundary condition. If we state that, in an open circuit (oc), there is no current flux, so that $\vec{J} = \vec{J}_N = 0$, Eq. 2.8 becomes:

$$\vec{J}_{q\ oc} = \frac{1}{T^2}\left(\frac{L_{21}L_{12} - L_{11}L_{22}}{L_{11}}\right)\vec{\nabla}T \tag{2.14}$$

We can obtain the following form of the Fourier's law:

$$\vec{j}_{q\,oc} = k_{oc}\vec{\nabla}T \tag{2.15}$$

if we set the thermal conductivity in an open circuit k_{oc} as:

$$k_{oc} = \frac{1}{T^2}\left(\frac{L_{21}L_{12} - L_{11}L_{22}}{L_{11}}\right) \tag{2.16}$$

In a similar way, if we consider a closed circuit (cc), boundary conditions include $\nabla\tilde{\mu}_e = 0$, since no electrochemical potential gradient is present in such system. In such circumstances, Eq. 2.8 becomes:

$$\vec{j}_{q\,cc} = \frac{L_{22}}{T^2}\vec{\nabla}T \tag{2.17}$$

Even in this case, we can define the thermal conductivity in a closed circuit k_{cc} as:

$$k_{cc} = \frac{L_{22}}{T^2} \tag{2.18}$$

We derived successfully two laws that correlate respectively current flux and electrochemical gradient and heat flux with thermal gradient. Such laws included the diagonal terms of phenomenological coefficient matrix (L_{11} and L_{22}) in constant definitions. Thermoelectric effects, though, imply the presence of a correlation between thermal forces with electrical fluxes and electrical forces with thermal fluxes.

2.1.2.1 Seebeck effect

Recalling the experimental setup used by Volta in his experiment, one can easily define it as an open circuit system in which no current flow was present, or $\vec{j} = \vec{j}_N = 0$, or, more specifically, considering Eq. 2.8

$$\vec{j} = -L_{11}\frac{\vec{\nabla}\tilde{\mu}_e}{T} + L_{12}\vec{\nabla}\left(\frac{1}{T}\right) = 0 \tag{2.19}$$

So, we can define the Seebeck coefficient α as:

$$-\frac{1}{e}\vec{\nabla}\tilde{\mu}_e = \alpha\vec{\nabla}\mathrm{T} \tag{2.20}$$

which becomes, considering Eq. 2.10, the macroscopic definition of Seebeck coefficient:

$$\alpha\vec{\nabla}\mathrm{T} = \vec{\varepsilon}_{oc} \tag{2.21}$$

meaning that the measured electric field in a material is equal to the temperature gradient applied times the Seebeck coefficient.

Moreover, considering phenomenological coefficients, Seebeck coefficient can be defined as:

$$\alpha = \frac{1}{eT}\frac{L_{12}}{L_{11}} \tag{2.22}$$

We observe that off-diagonal element L_{12} is included in the definition. This means that Seebeck effect is linked to the coupling of a current flux and a thermal gradient. Such phenomenological coefficient can be therefore expressed as:

$$L_{12} = \frac{\alpha \sigma_T T^2}{e} \tag{2.23}$$

Furthermore, it is possible to obtain a deeper comprehension of Seebeck coefficient physical meaning thanks to the Onsager-Casimir reciprocal relations. Considering that entropy flux can be defined as:

$$\vec{J}_s = \frac{\vec{J}_q}{T} \tag{2.24}$$

one can use this relation in Eq. 2.7 and Eq. 2.8 and obtain the following expression for entropy flux:

$$\vec{J}_s = \frac{L_{21}}{eTL_{11}}\vec{J} + \frac{L_{22}}{T}\vec{\nabla}\left(\frac{1}{T}\right) \tag{2.25}$$

Two terms build up entropy flux expression: the second term is standard and stands for the thermal contribute in $\vec{J}_s$. The first one accounts for the entropy current associated to the particle flux. If we consider the relation $\vec{J} = e\vec{J}_N$, we can define the expression of the "entropy per carrier" from the first term as:

$$\mathrm{S}_j = \frac{L_{21}}{TL_{11}} \tag{2.26}$$

Thus, if we consider Eq. 2.22,

$$\mathrm{S}_j = \mathrm{e}\alpha \tag{2.27}$$

Therefore, the Seebeck coefficient may be interpreted as the (average) contribution of carriers to the entropy current:

$$\vec{J}_s = \alpha\vec{J}_N - \frac{k_{\mathrm{oc}}\vec{\nabla}\mathrm{T}}{T} \tag{2.28}$$

2.1.2.2 Peltier effect

The derivation of an expression for Peltier coefficient can be obtained considering a closed-circuit isothermal system ($\vec{\nabla}\left(\frac{1}{T}\right) = 0$). For this boundary conditions, current flux can be expressed as in Eq. 2.9, while the heat flux can be expressed as:

$$\vec{J}_q = -\frac{L_{21}}{T}\vec{\nabla}\tilde{\mu}_e \tag{2.29}$$

Thus, considering 2.9, one can write the relation among the two fluxes as:

$$\vec{J}_q = \frac{L_{12}}{eL_{11}}\vec{\mathrm{j}} \tag{2.30}$$

Last equation describes exactly the Peltier effect, the generation of a heat flux due to the presence of a current flux. Therefore, we define Peltier coefficient as:

$$\vec{J}_q = \Pi\vec{\mathrm{j}} \tag{2.31}$$

or

$$\Pi = \frac{L_{12}}{eL_{11}} \tag{2.32}$$

If we compare this equation to Eq. 2.22, one can easily observe that the two thermoelectric effect coefficients (Peltier and Seebeck) are related to each other by the following direct proportionality:

$$\Pi = \alpha T \tag{2.33}$$

2.1.2.3 Thomson Effect

Let us consider a closed-circuit system composed of a single metal that has a temperature difference along its length. Now, in this circuit, we consider that a current flux is passing. The resulting heat exchanged in such a system would be composed by two contributions: Joule heat and Peltier heat, the second one generated by the non-zero Seebeck coefficient of the material.

This phenomenon is named as Thomson effect, for which the Thomson coefficient can be defined as:

$$\tau = T\frac{d\alpha}{dT} \tag{2.34}$$

As all the other transport coefficients, Thomson coefficient depends upon temperature.

The three thermoelectric effects (Seebeck, Peltier and Thomson) described have a different use in technological applications. In order to get an overview on differences among them, Figure 2.2 shows a comparison of schematic representations of thermoelectric effects described since now. Since this thesis work will focus on thermoelectric energy generation, a large part of the experimental work will concern Seebeck effect and its measurement. Therefore, it is important to highlight the boundary conditions in which it occurs and to set it apart of the other thermoelectric effects.

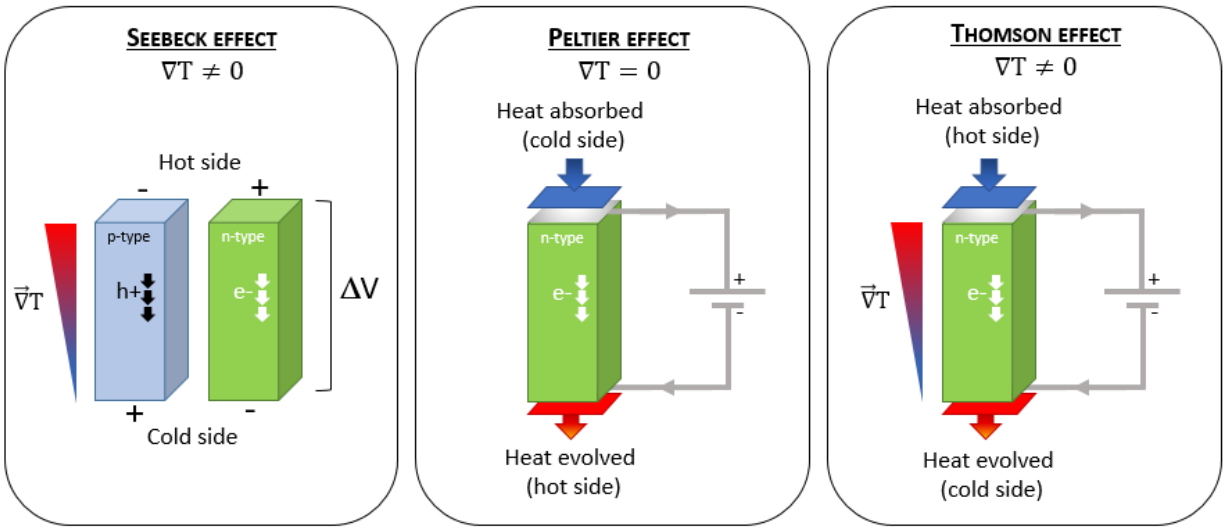

FIGURE 2.2: SEEBECK EFFECT (*LEFT*) IS REPRESENTED ON BOTH P-TYPE AND N-TYPE SEMICONDUCTOR BARS. THERMAL GRADIENT INDUCES THE MIGRATION OF CHARGES FROM THE HOT TO THE COLD SIDE, AND THE RESULTING POTENTIAL DIFFERENCE AMONG THE TWO SIDES. PELTIER EFFECT (*MIDDLE*) VERIFIES WHEN IN A CLOSED CIRCUIT, DUE TO A CURRENT FLOW, A HEAT FLOW IS PRODUCED FROM ONE JUNCTION (COLD SIDE IN THE PICTURE) TO THE OTHER (HOT SIDE). THOMSON EFFECT (*RIGHT*) COMBINES THE PRESENCE OF A CURRENT FLOW IN A CLOSED CIRCUIT TO THE ONE OF A THERMAL GRADIENT.

2.1.2.4 Efficiency of Thermoelectric Materials

As already stated, this thesis will concern thermoelectric energy generation. The efficiency of the conversion of the heat absorbed in electrical current is a key concept to obtain a performing device. Efficiency depends quite obviously on the active material that is used into the device, and, in particularly, on its transport properties.

We can consider the thermoelectric generator as a thermal engine, in which it is necessary to maximize the heat flow from the hot to the cold sink, but the thermal gradient between the two sides should be kept at its highest value. These two conditions can be related to the thermal conductivities of the material. On one side, the closed-circuit thermal conductivity k_{cc} rules the heat flow, which means that should be as high as possible, while on the other, the open-circuit thermal conductivity k_{oc} should be minimized, since it rules the temperature difference between the two sides.

Therefore, one can consider that the two thermal conductivities are related by the following (Eq. 2.16 and Eq. 2.18):

$$k_{cc} - k_{oc} = T\alpha^2\sigma_T \tag{2.35}$$

We obtain the optimal efficiency when the ratio k_{cc}/k_{oc} is maximized:

$$\frac{k_{cc}}{k_{oc}} = 1 + \frac{\alpha^2\sigma_T}{k_{oc}}T \tag{2.36}$$

More easily, we can refer to the quantity z, defined as:

$$z \equiv \frac{\alpha^2\sigma_T}{k_{oc}} \tag{2.37}$$

The quantity z times the working temperature T is defined as figure of merit zT, which is usually mentioned in scientific works on thermoelectric energy harvesting to evaluate the

thermoelectric performance of the material studied. In fact, such a quantity can be related to the conversion efficiency ξ by the following:

$$\xi = \frac{\Delta T}{T_h} \cdot \frac{\sqrt{1+zT}-1}{\sqrt{1+zT}+\frac{T_c}{T_h}} \tag{2.38}$$

where ΔT is the temperature difference among the hot side (T_h) and the cold side (T_c), while T is the average working temperature $(T_h + T_c)/2$.

An aspect should be stressed, the interdependence of the transport properties that contribute to z value. In fact, in semiconductors and metals (the classes of materials mainly used for this application) the Seebeck coefficient α, the electrical conductivity σ_T and the open-circuit thermal conductivity k_{oc} all depend upon the concentration of charge carriers (n) inside the materials through the following three relations:

$$\alpha = \frac{8\pi^2 k_b^2}{3eh^2}\, m^* T \left(\frac{\pi}{3\boldsymbol{n}}\right)^{2/3} \tag{2.39}$$

where k_b is the Boltzmann constant, h is the Plank constant, m^* is the effective mass of the charge carrier.

$$\sigma_T = \boldsymbol{n} e \mu_T \tag{2.40}$$

where μ_T is charge carrier mobility at the given temperature.

For the third relation, we should consider that k_{oc} is made up by two contributions: k_l, owed to the lattice thermal transport, i. e. phonon contribution, and k_e, owed to the charge carrier ability to transport heat. This second term is related to σ_T by the Wiedemann-Franz law:

$$k_e = L\sigma_T T = \boldsymbol{n} e \mu_T L T \tag{2.41}$$

where L is the Lorentz constant.

Figure 2.3 clarifies the issue generated by the dependence of all these three quantities on charge carrier concentration.

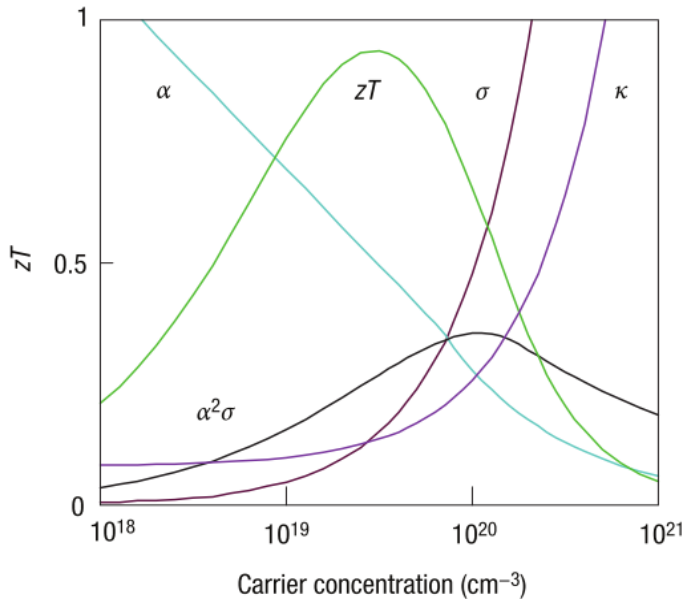

FIGURE 2.3: TRENDS OF SEEBECK COEFFICIENT $\boldsymbol{\alpha}$ (LIGHT BLUE LINE), ELECTRICAL CONDUCTIVITY $\boldsymbol{\sigma_T}$ (REPORTED AS $\boldsymbol{\sigma}$, BURGUNDY LINE) AND THERMAL CONDUCTIVITY $\boldsymbol{k_{oc}}$ (REPORTED AS $\boldsymbol{k}$, PURPLE LINE) ARE REPORTED VERSUS CARRIER CONCENTRATION. THE RESULTING VALUE OF ZT IS A PEAKED FUNCTION (GREEN LINE), AS WELL AS THE THERMOELECTRIC POWER FACTOR $\boldsymbol{\alpha^2\sigma}$ (BLACK LINE). REPRODUCED FROM REF[3].

The highest zT values are obtained for large thermoelectric power factor ($PF = \alpha^2\sigma_T$), which means high σ_T and high α, and low k_{oc}. Since the three quatities are intercorrelated it is not possible to tune one of them, without affecting the others. For instance, increasing electrical conductivity by enhancing the charge carrier concentration will lead both to an undesired decrease of Seebeck coefficient and to an undesired growth of thermal conductivity. In other words, a trade-off value of charge carrier concentration is needed to reach the maximum zT.

For many years, zT physical limit represented an insurmountable obstacle for thermoelectric technology development, since it strongly affected the device efficiency and, thus, restricted its applicability. A new field burst was possible thanks to the arrival of nanotechnology.

In fact, in nanosized structured material, it is possible for specific physical effects to provide a decoupled increasing/decreasing of one of the three transport properties, allowing in this way to overcome the trade-off value issue. Several effects have been reported in a number of different systems[3–5]. Their description is beyond the purpose of this theoretical introduction to thermoelectric effects. Nonetheless, some of these effects will be briefly presented in Chapter 6.

Thanks to the possibility given by nanostructures, research in thermoelectric field has flourished in the past two decades, with an increasing hunger for more complex and inedited materials to use, including organic based materials.

2.2 Intrinsically Conductive Polymers (ICPs)

The history of the class of these peculiar materials was already described in the previous chapter. This section will focus on chemical and physical characteristics of these systems, with a major attention to the interpretation of charge transport properties. Such an analysis aims to show the features that make ICPs interesting materials for thermoelectric application.

2.2.1 General description

In general, intrinsically conducting polymers (ICPs) include electronically conducting polymers and ionically conducting polymers[6], depending on which kind of charge carrier the conduction relies upon. Electronically conducting polymers can conduct electrons/holes, according to the doping type, while ionically conducting polymers conduct small ions. In this thesis, ICPs will designate only electronically conducting polymers.

The molecular feature that allows ICPs to be conductive is the extended π conjugation all over the chains. In regular saturated polymer (such as polyethylene), all carbon electrons are involved in covalent σ bond formation. So, each carbon atom forms four equivalent σ covalent bonds, due to sp^3 hybridization of its orbitals. In ICPs, the hybridization is sp^2, so carbon atoms can form three equivalent σ planar bonds. The unpaired electron in p_z orbital can interact with another unpaired electron on a next carbon atom, leading to the formation of a π molecular bond (Figure 2.4a).

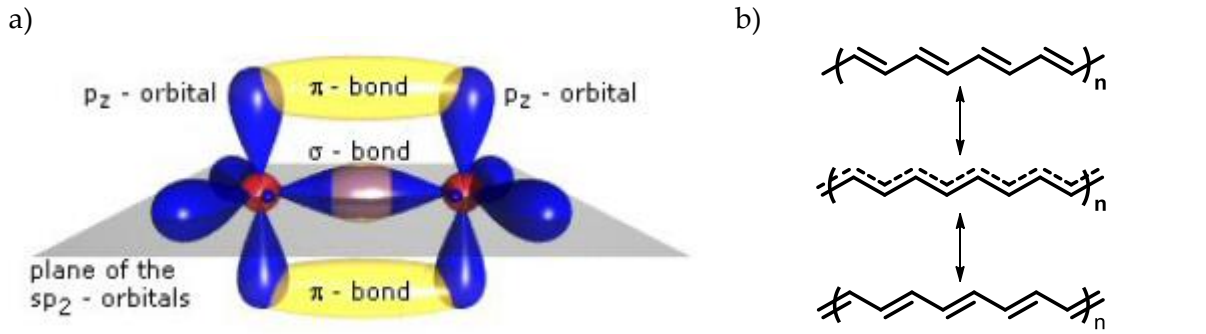

FIGURE 2.4: A) MOLECULAR BOND BETWEEN TWO SP2 HYBRIDIZED CARBON ATOMS. ONE OF THE THREE SP2 ORBITAL FOR EACH C ATOM GENERATES THE σ BOND, WHILE THE TWO PZ ORBITALS OVERLAP TO CREATE THE π BOND. B) CANONICAL STRUCTURES OF POLYACETYLENE (TOP AND BOTTOM) AND THE RESONANCE HYBRID (CENTRAL) WHICH SHOWS THE π DELOCALIZATION OF ALL OVER THE CHAIN.

When the sp^2 hybridization occurs for all the connected carbon atoms, we obtain a fully conjugated structure. The simplest example of linear conjugated chain is polyacetylene[7,8] (Figure 2.4b). In molecular structure representations of this species, alternating π bonds are usually depicted. This is just a simplification, since the conjugation is extended to all the sp^2 hybridized carbon atom, as shown by the resonant structures of polyacetylene (Figure 2.4b). The delocalization on all chain length of the π orbital means that π electrons are relatively free to move along the chain, which explains why, in the right conditions, ICPs can be conductive.

The inclusion of aromatic and heteroaromatic units into the chain increases ICP stability. Still, we can find the presence of alternating π bonds in all the structures reported in Figure 2.5, confirming that the fundamental feature of polyacetylene is retained.

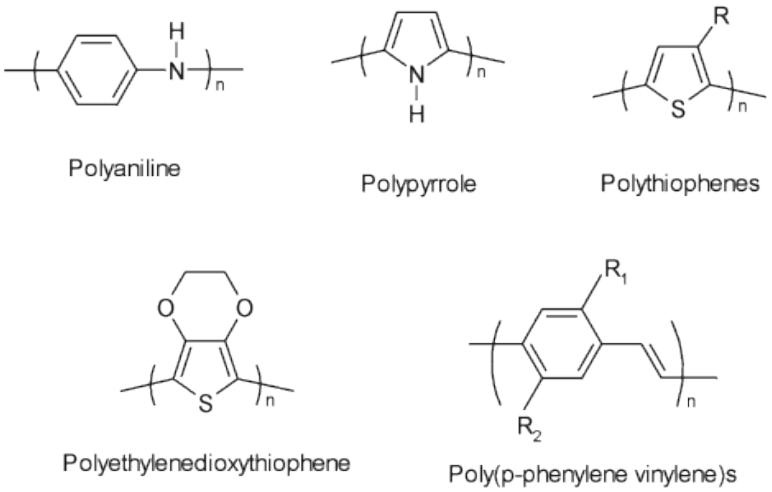

FIGURE 2.5: FIVE OF THE MOST STUDIED ICP STRUCTURES CONTAINING AROMATIC UNITS

Energetic diagram of molecular orbitals can help understand the source of ICP peculiar features. Figure 2.6 shows the diagrams for conjugated chains, with a progressive increase of carbon atom number. The π orbitals represent the frontier molecular orbitals (FMOs). In fact, bonding π orbital is the highest occupied molecular orbital (HOMO), while antibonding π* orbital is the lowest unoccupied molecular orbital (LUMO). When we extend the length of the chain, and, thus, the conjugation, we obtain a contraction of the energy gap between the two orbitals[9].

In a hypothetic infinite chain, the HOMO-LUMO diagram becomes like a semiconductor band structure, in which the HOMO contributes to the valence band while the LUMO contributes to the conduction band[10]. Still, in this condition, the energy gap is large, and the material is basically an insulator.

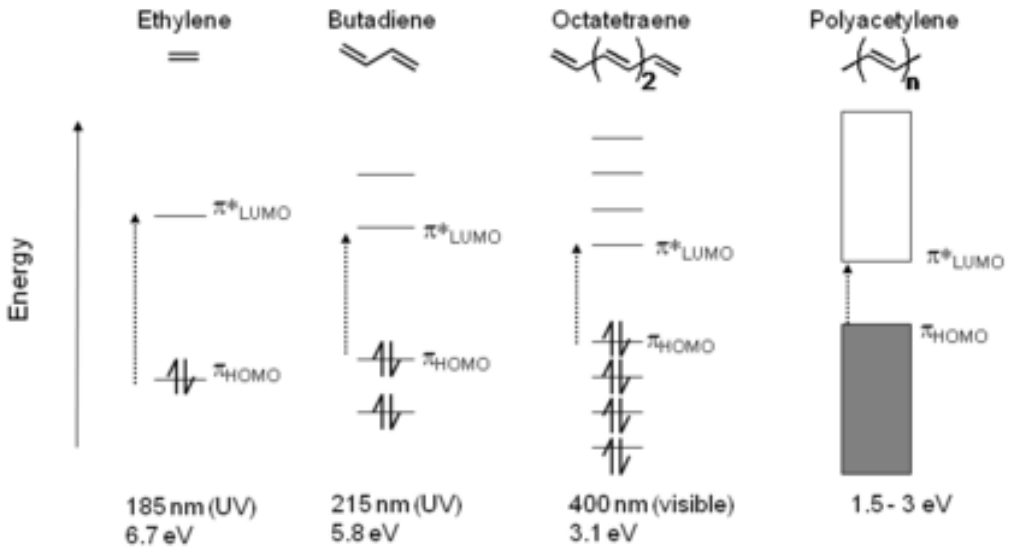

FIGURE 2.6: MOLECULAR ORBITALS OF CONJUGATED CARBON CHAIN WITH INCREASING LENGTH. THE ENERGY VALUES UNDERNEATH THE DIAGRAMS ARE THE GAPS BETWEEN HOMO AND LUMO, GROWING SMALLER DUE TO THE INCREASE OF CHAIN LENGTH.

ICPs can be transformed from insulators to conductive by the generation of extra charge carriers, in a process that is usually compared to doping in semiconductors.

Generation of charge carriers in organic materials is obtained through oxidation or reduction reactions[11]. In case of oxidation, the result is the removal of an electron from the HOMO (π orbital), which generates a mobile hole with a positive charge. Reduction will lead, instead, to the addition of an extra mobile electron to LUMO (π^* orbital). In this second case, the resulting negatively charged specie is highly instable for most ICPs, which rapidly re-oxidize. Therefore, the majority of ICPs (included poly(3,4-ethylenedioxythiophene), the polymer studied in this thesis) is doped through oxidation (Figure 2.7) and transports positive charge carriers.

It can be energetically favourable to localize the charges on the chain and to have, around them, a local distortion (relaxation) of the lattice. In ICP chains this usually corresponds to a change from a benzenoid structure to a quinoid structure[12]. Such a structural modification implies the energetical variation of the π and π^* orbitals: π increases in energy, while π^* decreases in energy. Thus, they both end up within the bandgap (Figure 2.7).

The positive charge coupled with the structural distortion that move along the chain has been defined polaron[13], in analogy to the polaron in inorganic semiconductors. If the oxidation goes further, a second electron might be extracted from π. In this case, a stronger structural distortion occurs, and the resulting double positive charge coupled to it is called bipolaron.

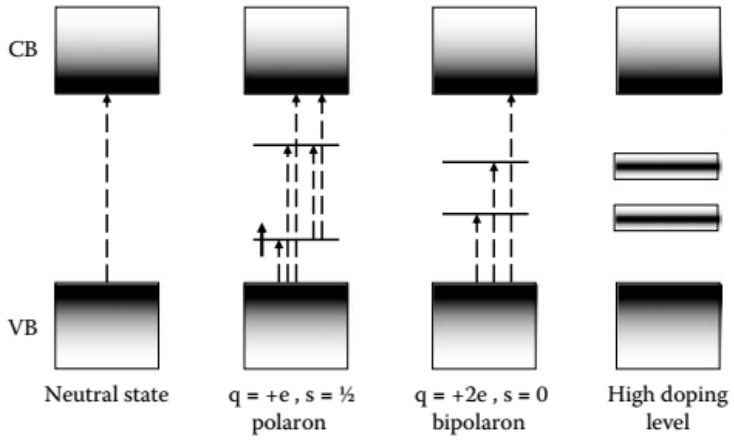

FIGURE 2.7: ENERGETIC BAND DIAGRAM OF ICP AT DIFFERENT OXIDATION LEVEL. IN NEUTRAL STATE, THE LARGE BAND GAP MAKES THE MATERIAL AN INSULANT. EXTRACTION OF AN ELECTRON BY OXIDATION CREATES A *POLARON*, A POSITIVE CHARGE CARRIER COUPLED WITH A LOCAL DISTORTION. THE REMOVAL OF THE SECOND ELECTRON GENERATES A FURTHER STRUCTURE DISTORTION DUE TO THE PRESENCE OF TWO POSITIVE CHARGES, A SO-CALLED BIPOLARON. GOING FURTHER WITH THE OXIDATION, INNER GAP STATES CAN BECOME DENSE ENOUGH TO CREATE BANDS, AS THE LAST DIAGRAM (RIGHT) REPORTS. REPRODUCED FROM REF.[14].

At high doping level, i.e. highly oxidized polymer, bipolaron density into the material generates two bands within the original bandgap. Such strong reduction of the bandgap results in a metallic behaviour of ICP in this condition.

The oxidation level of the ICP can be precisely estimated by XPS analysis[14]. Nonetheless, UV-vis absorption can roughly evaluate the oxidation thanks to the variation in electronic transition due to the oxidation level, as reported in Figure 2.8[15].

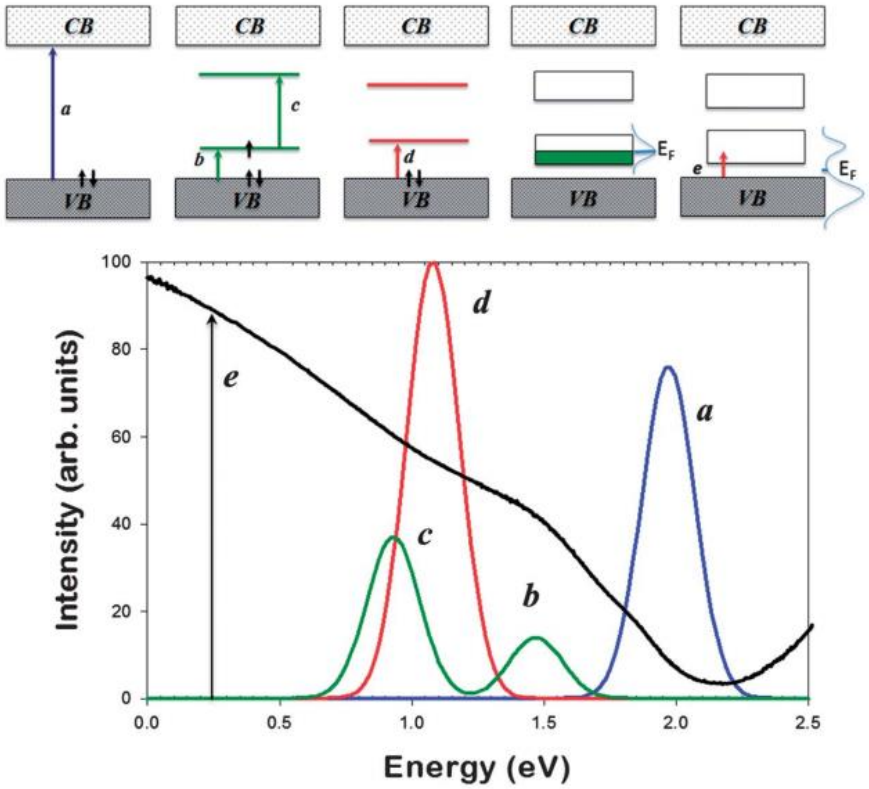

FIGURE 2.8: ICP ABSORBANCE SPECTRA RESULTING FROM DIFFERENT OXIDATION LEVELS. IN THE NEUTRAL FORM, ONLY THE TRANSITION **A** FROM THE VALENCE BAND TO THE CONDUCTION BAND TAKES PLACE AT HIGH ENERGY. THE EXTRACTION OF ONE ELECTRON DUE TO THE OXIDATION LEADS TO TWO POSSIBLE TRANSITION, **C** AND **B**. GOING FURTHER WITH THE OXIDATION, THE EXTRACTION OF THE SECOND ELECTRON IMPLIES THE PRESENCE OF TWO EMPTY STATES IN THE BAND GAP, WITH ONLY ONE POSSIBLE TRANSITION **D**, FROM THE VALENCE BAND TO THE π ORBITAL. A HIGH DENSITY OF POLARONIC AND BIPOLARONIC STATES CAUSES THE FORMATION OF TWO BANDS INTRA BAND GAP. THIS BROADENS THE ABSORPTION PEAK AND ALLOWS THE **E** TRANSITION AT LOW ENERGIES. REPRODUCED FROM REF.[15].

Once that energetic diagrams and charge carrier nature (polarons and bipolarons) have been addressed, we can consider how charge carriers are transported into the material. We already saw that ICPs span from insulators (neutral state) to semiconductor (oxidized) to metallic (highly oxidized). The understanding of transport properties in the oxidized state is thus crucial to figure out the possible use of for ICPs as thermoelectric materials.

2.2.1.1 Role of order

Before briefly describing the charge transport models that have been proposed until now, a preliminary general observation must be made. We already observed that π orbital allows the delocalization, and thus conduction, of charge carriers along polymer chain. Since the material is made up of several chains, carriers should also hop from one chain to the other. This is possible through the π-π stacking interaction among aromatic rings of different ICP chains, that can pack to each other thanks to this intermolecular force[16], as reported in Figure 2.9a. The result of this packing is the generation of lamellar crystallites, in which hopping among chains is highly favourable. The straightforward conclusion is that transport properties of ICP strongly depend upon their morphology[17,18].

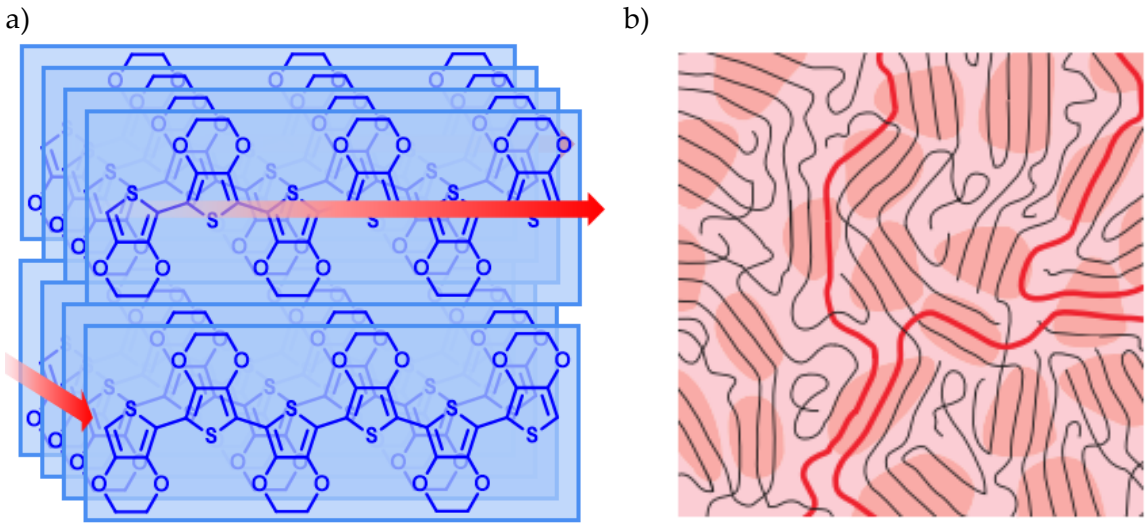

FIGURE 2.9: A) PACKING OF ICP (POLY(3,4-ETHYLENDIOXYTHIOPHENE)) CHAINS, RED ARROWS INDICATE CHARGE TRANSPORT POSSIBLE DIRECTION. B) TYPICAL SEMI-CRYSTALLINE STRUCTURE OF ICP: BLACK LINES ARE ICP CHAINS, DARK PINK AREAS MARK THE EXTENSION OF CRYSTALLINE DOMAINS, WHERE THE INTERMOLECULAR HOPPING IS MOST LIKELY. RED LINES REPRESENT CARRIER PERCOLATION PATHS INTO THE SAMPLE. REPRODUCED FROM REF.[18].

A possible morphology for ICP is represented in 2.9b. On the left side, there is the representation of highly crystalline material, in which large crystallites dominate on the amorphous phase.

The conduction between different crystallites is possible through the so-called tie chains, longer polymer chains that connect crystallites[18,19]. Charge carrier movement is expected to follow percolation paths depicted as red lines. It must be noticed that the longer the chain, the smaller the probability for it to maintain the rigid planarity for all its length. In a long chain, transport occurs by hopping between connected segments, rather than by delocalization.

2.2.2 Charge transport mechanism in ICPs

Most terms and interpretations used for describing ICPs have been borrowed from semiconductor solid state physics, as already noticed for energetic diagrams and for charge carrier description. The same happened also for charge carrier transport models.

Transport mechanism in ICPs strongly relies on both oxidation level and crystallinity[20]. This means that ICP behaviour ranges from insulating to semiconducting to metallic, making more difficult to propose a unified model that can fit all situations. These means that different models have been proposed according to the transport regime in which the studied ICP is[21]. Transition from insulating to metallic behaviour (the so-called Mott transition[22]) is usually described from an energetic point of view with the concept of mobility edge[23]. Considering a density of states shaped as reported in Figure 2.10, a tail of localised states (black area) is expected in disordered systems. Mobility edge separates such states from the extended ones (at higher energies). So, if the Fermi level lies below the mobility edge, an insulating behaviour is expected, while if it is located above the mobility edge, metallic transport takes place.

The Fermi level position is tuned by the oxidation of the ICP.

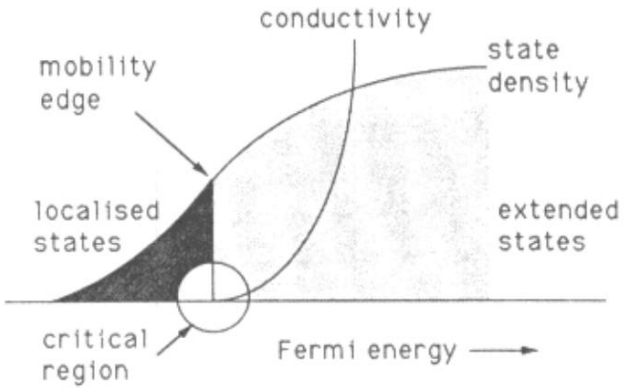

FIGURE 2.10: THE CONCEPT OF MOBILITY EDGE. ELECTRONIC STATES ABOVE AND BELOW MOBILITY EDGE ARE EXTENDED AND LOCALIZED, RESPECTIVELY.

From a macroscopic point of view, the estimation of polymer transport regime can be obtained by calculating the reduced activation energy as:

$$W = \frac{d(ln\sigma)}{d(lnT)} \tag{2.42}$$

A negative slope of W versus T indicates a semiconductor regime, a positive slope marks a metallic behaviour, while a weak dependence of the electrical conductivity on the temperature can be interpreted as a critical regime[24].

A full account on the models studied in this field is beyond the aim of this thesis, but the reader may refer to books and reviews covering the topic[25–27]. Nonetheless, a brief presentation of the various interpretations and a comparison among them provide useful information for a better understanding of the experiments.

2.2.2.1 Band structure model

Even though a band structure diagram is often used to describe electronic structure in ICPs (as it has been done in Sect. 2.2.1), it can be legitimately used only in case of largely crystalline and highly doped materials. This is not the case most of the times, since the presence of amorphous portions and, thereof, disorder, affects transport. Nonetheless, modifications of the band model (discussed in paragraphs 2.2.2.3) can be introduced to include disorder, thus giving a more realistic picture.

A qualitative description of band transport model can rely on Figure 2.10.

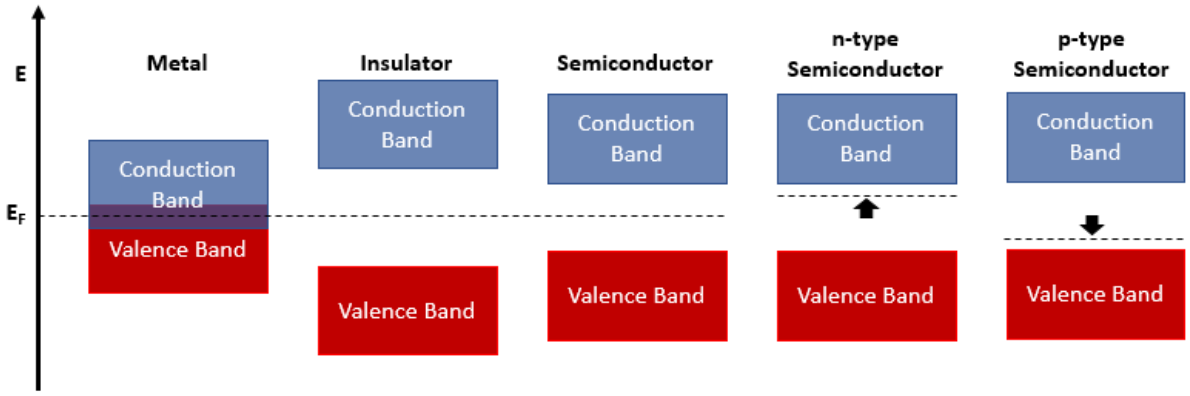

FIGURE 2.11: SIMPLIFIED SCHEME OF BAND STRUCTURE FOR DIFFERENT CLASSES OF MATERIALS. METALS, INSULATORS AND SEMICONDUCTORS DISTINGUISH AMONG THEMSELVES DUE TO THE ENERGY GAP WIDTH. DOPING OF THE SEMICONDUCTOR CAUSES AN UPWARD (N-TYPE) OR A DOWNWARD (P-TYPE) SHIFT OF FERMI LEVEL, WHICH GET CLOSE TO ONE OF THE BAND EDGES.

In a solid, we can consider that instead of having discrete energies as in the case of free atoms, the available energy states form bands[28]. Two bands can be identified: the valence band, made of filled states, and the conduction bands, made of empty states. For conductors like metals, the two bands overlap each other, so that electrons can move across available electronic states. For semiconductors and insulators, instead, the two bands are separated by an energy gap. If the band gap is small enough, thermal energy or other stimuli can promote one electron from valence band to conductivity band, generating two charge carriers (the electron in the conduction band and the hole in the valence band).

The increase of semiconductor conductivity can be obtained by enhancing charge carrier concentration through doping. Doping consists in controlled introduction of impurities to create states within the bandgap, which can accept electrons from valence band (as, for instance, boron states in silicon) or donate electrons to the conduction band (as phosphorus states in silicon). In the first case, an excess of holes will be generated, and the resulting doping is designed as p-type. In the second one, the excess of electrons in conduction band makes the semiconductor n-type doped.

Conductivity in semiconductors is owed to the processes described of promotion of electron to higher energy states, which usually requires thermal energy. In standard conditions, semiconductor conductivity is thermally activated.

At high doping levels, the semiconductor can become degenerate. This means that the density of impurity atoms is so large that localized states in the bandgap form an impurity band. In such a condition, the Fermi level gets close to the conduction band (or valence band) and might even end up inside the band. In this case, electrical conductivity is no longer thermal activated, and becomes more similar to a metallic one.

From the given description, it is possible to understand why such model seems to provide a fair interpretation of ICP electrical behaviour. The concept of p-type doping, together with the thermal activated electrical conductivity which becomes metallic-like at high doping levels are all features that are validated through ICP physical characterization. Nevertheless, the absence

a of a long-range order in most of ICPs studied strongly limits the rigorous application of this model[25].

2.2.2.2 Hopping model

The main implication of disorder in ICPs (both at molecular and at supramolecular levels) is the presence of localized states. These states do not build up bands, but conduction is still possible from one state to the other due to hopping process. Marcus theory[29] can be useful to describe the process, when only two sites are considered.

If we consider two localized states and we assume that one of them is excited because of an excess of charge, the transfer of the charge carrier from one site to the other is ruled by three main parameters:

- The reorganization energy, λ, which is due to structural reorganization coupled the transfer of the charge, together with the polarization of the surrounding medium;
- The electron coupling between the two sites, which accounts for the interaction among the molecular orbitals. It is expressed by the electron coupling matrix $\langle\psi_i|V|\psi_f\rangle$;
- The presence of a driving force, usually an electric field $\vec{\varepsilon}$, that sets also the direction of transfer.

The rate of electron migration from one site to the other can be expressed as:

$$k_{if} = \frac{2\pi}{\hbar}\left|\langle\psi_i|V|\psi_f\rangle\right|^2\left\{\frac{1}{\sqrt{4\pi k_B T}}exp\left[\frac{-(\Delta G° + \lambda)^2}{4k_B\lambda T}\right]\right\} \quad (2.43)$$

where $\langle\psi_i|V|\psi_f\rangle$ is the electronic coupling matrix in which $\Delta G°$ is the Gibbs free energy associated to the transition. If we consider a transition from the generic site i to the generic site j, in the presence of an electric field $\vec{\varepsilon}$, $\Delta G° \equiv \Delta G_{ij}$ becomes:

$$\Delta G_{ij} = E_j - E_i - e(\vec{\varepsilon}\cdot\vec{d}_{\mathrm{ij}}) \quad (2.44)$$

where E_j and E_i are the energies associated with the two sites and $\vec{d}_{\mathrm{ij}}$ is the vector distance among them.

As already said, this description is valid for a single hop between two localized sites, which are poorly electronically coupled.

Hopping is considered as the basic transport mechanism in polymers. We can consider the crystallites as ordered domains with a band-like transport, while amorphous material is made up of localized states in which charge carriers can be trapped and move by hopping (multiple trap-and-release model). Otherwise, we can consider the amorphous material as the dominant part. In this case, charge carrier hopping can be considered the main responsible mechanism for electrical conduction (variable range hopping model.

2.2.2.3 Multiple Trap and Release (MTR) Model

The multiple trap-and-release (MTR) model has been developed by Shur and Hack[30] to describe the mobility in hydrogenated amorphous silicon. Later, Horowitz et al.[31] extended it to organic semiconductors. The model assumes that charge transport occurs in extended band-like states, but that most of the carriers injected in the semiconductor are trapped in states

localized in the band gap. These traps can be deep, if their energy level is near the middle of the band gap, or shallow, if they are located within 2-3 k_BT of the band edge.

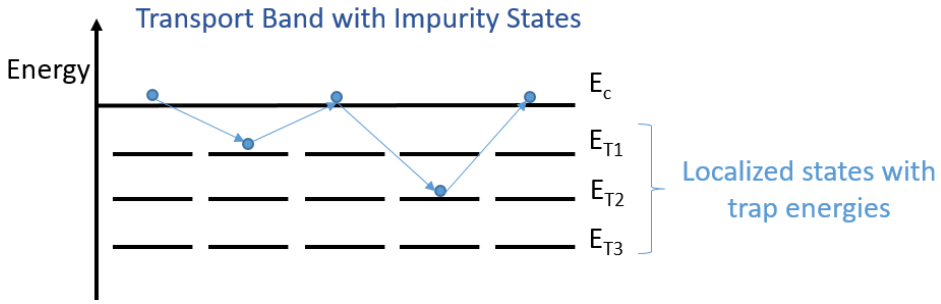

FIGURE 2.12: SKETCH OF MTR BAND STRUCTURE REPRESENTATION. E_C IS THE ENERGY OF THE CONDUCTION BAND, E_{T1}, E_{T2} AND E_{T3} ARE LOCALIZED STATES DUE TO DISORDER. IF A CHARGE CARRIER (LIGHT BLUE DOT) MOVING IN CONDUCTION BAND GETS CLOSE TO A TRAP STATE, IT CAN BE TRAPPED WITH A PROBABILITY CLOSE TO 1. ONCE IT IS TRAP, IT CAN BE RELEASED DUE TO AN EXTERNAL STIMULUS, SUCH AS THERMAL ENERGY OR ELECTRIC FIELD.

The trap states are highly localized, and carriers trapped in these states cannot move easily from these locations in the energy bandgap. The release of the trapped carriers is controlled by a thermally-activated process.

Two key parameters will rule the slowing of the charges as they move through the semiconductor: 1) the energy levels of the traps E_T and 2) the density of traps, expressed by the parameter θ.

For this model, the effective mobility μ_{eff} can be written as:

$$\mu_{eff} = \mu_0 \, \theta \, exp\left[\frac{-(E_C - E_T)}{k_B T}\right] \tag{2.45}$$

where μ_0 is the mobility in the absence of traps. This parameter requires the possibility of defining a band-like transport, and of introducing its modification due to the disorder of the material. This is often not possible for ICPs, so a hopping-based model is usually preferred.

2.2.2.4 Variable Range Hopping (VRH) Model

For ICPs which present a poor degree of crystallinity, the conduction of charges is governed by thermally activated hopping. Variable range hopping (VRH) model was developed by Mott[32] to describe hopping dominated conduction in non-crystalline solids. This is the most effectively used model for ICPs, considering a Gaussian distribution of localized states[26] and has been developed in different boundary conditions[33,34].

If we consider a generic hop from site 1 to site 2, the probability P_{12} for it to happen is considered equal to the probability described for tunneling from site 1 to site 2:

$$P_{12} = P_0 exp\left[\frac{-2R}{R_0}\right] exp\left[\frac{-(E_2 - E_1)}{k_B T}\right] \tag{2.46}$$

where P_0 is a material specific parameter related to phonon frequency, R is the distance between the two sites and R_0 is the delocalization radius of each site. So, the probability of hopping depends both on spatial and energetic terms, and is thermally activated.

It can be shown that in such conditions, electrical conductivity becomes:

$$\sigma = \sigma_0 exp\left[-\left(\frac{T_0}{T}\right)^{1/d}\right] \tag{2.47}$$

with $d = n + 1$, where n is the dimensionality of the system and T_0 is a characteristic temperature given by:

$$T_0 = \frac{128}{9k_B}\frac{\pi a^3}{N_F} \tag{2.48}$$

where a is the size of the localized state (Bohr radius) and N_F is the density of states at the Fermi level. Mott's VHR model can be used also to define Seebeck coefficient, assuming a slowly varying DOS, as[35]:

$$\alpha = \frac{k_B^2 (T_0 T)^{1/2}}{2e}\frac{\partial lnN(E)}{\partial E}\Big|_{E_F} \tag{2.49}$$

where the $T^{1/2}$ -dependence indicates a non-linear decrease of Seebeck coefficient due to the temperature, while the presence of the density of states N(E) sets a dependency of α upon the DOS shape close to the Fermi level.

VRH model is more effective for doped semiconducting polymers where carriers have sufficient energy to jump to a manifold of nearby sites that are also close in energy. It does not describes metallic conduction effectively, which is the domain of Mott mobility edge model already described previously in this section.

2.2.2.5 Novel models

Even though it is possible to use different models to describe different regimes in the same ICP, due to the oxidation level, the lack of a unified model implies the impossibility to obtain an overall comparison. The optimization of ICPs for specific application would benefit from such comparison among different regimes.

Moreover, it must be noticed that none of the presented models accurately represent both the energy and temperature dependence of the carriers, which is a crucial piece of information for optimizing polymers for devices that interconvert gradients of temperature to produce energy.

Therefore, over in the last years[18,19,36] the scientific community has aimed at finding such unified model. In the following section, a novel unifying model[37] presented by Stephen Kang and Jeffrey Snyder in 2016 will be briefly described.

2.2.2.5.1 Kang and Snyder Model

The starting assumption of Kang and Snyder model is that the two quantities usually defined to describe transport properties of the material, charge carrier mobility μ and charge carrier density n are ill-defined in the case of ICPs.

Thus, their model is based on a single microscopic transport function σ_E, which introduces a strong dependence on the carrier energy E within the transport window, defined as the set of energy values above a critical transport edge E_t.

Transport edge is different from previously described mobility edge. Transport edge was introduced in charge transport theory in 1985 by Monroe[38], studying the temperature dependence of detrapping in amorphous semiconductors. There, E_t acts as a threshold separating localized states that contribute to conduction from trap states, the localized states that release carriers at a given temperature.

Thus, energy dependent conductivity is defined as:

$$\sigma_E(E,T) = \begin{cases} \sigma_{E_0}(T) \times \left(\frac{E - E_t}{k_B T}\right)^s & for\ E > E_t \\ 0 & for\ E \leq E_t \end{cases} \tag{2.50}$$

where s is a transport exponent. Electrical conductivity can be obtained as:

$$\sigma(T) = -\int \sigma_E(E,T)\partial_E f(E,T)dE \tag{2.51}$$

(where f(E, T) is the Fermi–Dirac function) while the Seebeck coefficient becomes:

$$\alpha(T) = -\frac{1}{\sigma(T)}\left(\frac{k_B}{e}\right)\int \frac{E - E_F}{k_B T}\sigma_E(E,T)\partial_E f(E,T)dE \tag{2.52}$$

It should be noted that while $\left[{(E - E_t)}/{k_B T}\right]^s$ accounts for the availability of states with energy larger than E_t and contributing to charge transport at any given temperature, $\sigma_{E_0}(T)$ describes the elemental transport event responsible for conduction. Then, in polymers, where states are sensibly assumed to be localized due to the lack of crystalline order, it embeds the physics of the pertinent hopping mechanism. For pseudo-1D hopping it reads[37,39]

$$\sigma_{E_0}(T) = \sigma_{E_0}^{(0)} exp\left[-\left(\frac{W}{k_B T}\right)^{\frac{1}{2}}\right] \tag{2.53}$$

where W is the pseudo-activation energy for non-adiabatic variable-range hopping[39].

Equations (2.51)–(2.52) are simply integrated in two limits. In a degenerate system (where $\eta \equiv \left[{E_f - E_t}/{k_B T}\right]$), setting $E_t = 0$, one obtains that[37]

$$\sigma \sim \sigma_{E_0}\eta^s \tag{2.54}$$

While

$$\alpha \sim \left(\frac{k_B}{e}\right)\frac{\pi^2}{3}s\eta^s \tag{2.55}$$

The transport energy and coefficient correlate σ and α to each other as

$$\alpha = \left(\frac{k_B}{e}\right)\frac{\pi^2}{3}s\left(\frac{\sigma}{\sigma_{E_0}}\right)^{-1/s} \tag{2.56}$$

In the opposite limit, for a lightly doped material ($\eta \ll -1$), Fermi statistics maybe replaced by Boltzmann statistics. Thus, one obtains instead that[37]

$$\sigma \sim \sigma_{E_0} s\Gamma(s)\exp(\eta) \tag{2.57}$$

while

$$\alpha \sim \left(\frac{k_B}{e}\right)(s + 1 + \eta) \tag{2.58}$$

so that

$$\alpha = \left(\frac{k_B}{e}\right)\left(s + 1 - ln\left(\frac{\sigma}{\sigma_{E_0}} s\Gamma(s)\right)\right) \tag{2.59}$$

2.3 References

1 L. Onsager, *Phys. Rev.*, 1931, **37**, 405–426.

2 H. B. G. Casimir, *Rev. Mod. Phys.*, 1945, **17**, 343–350.

3 G. J. Snyder and E. S. Toberer, *Nat. Mater.*, 2008, **7**, 105–114.

4 P. Pichanusakorn and P. Bandaru, *Mater. Sci. Eng. R Reports*, 2010, **67**, 19–63.

5 K. Nielsch, J. Bachmann, J. Kimling and H. Böttner, *Adv. Energy Mater.*, 2011, **1**, 713–731.

6 G. R. Strobl, *Phys. Polym.*, 2007.

7 C. K. Chiang, C. R. Fincher, Y. W. Park, A. J. Heeger, H. Shirakawa, E. J. Louis, S. C. Gau and A. G. MacDiarmid, *Phys. Rev. Lett.*, 1977, **39**, 1098–1101.

8 H. Shirakawa, J. Louis and A. G. Macdiarmid, *J. C. S. Chem. Comm*, 1977, 578–580.

9 A. Ajayaghosh, *Chem. Soc. Rev.*, 2003, **32**, 181–191.

10 W. R. Salaneck and J. L. Brédas, *Synth. Met.*, 1994, 15–22.

11 A. G. MacDiarmid, R. J. Mammone, R. B. Kaner, S. J. Porter, R. Pethig, A. J. Heeger and D. R. Rosseinsky, *Philos. Trans. R. Soc. A Math. Phys. Eng. Sci.*, 1985, **314**, 3–15.

12 W. R. Salaneck, R. H. Friend and J. L. Brédas, *Phys. Rep.*, 1999, **319**, 231–251.

13 J. Bredas and G. Street, *Acc. Chem. Res.*, 1985, **1305**, 309–315.

14 A. Elschner, W. Kirchmeyer, Stephan Lovenich, U. Merker and K. Reuter, *PEDOT: Principles and Applications of an Intrinsically Conductive Polymer*, 2010.

15 O. Bubnova and X. Crispin, *Energy Environ. Sci.*, 2012, **5**, 9345.

16 S. R. Amrutha and M. Jayakannan, *J. Phys. Chem. B*, 2008, **112**, 1119–1129.

17 A. B. Kaiser, *Adv. Mater.*, 2001, **13**, 927–941.

18 R. Noriega, J. Rivnay, K. Vandewal, F. P. V Koch, N. Stingelin, P. Smith, M. F. Toney and A. Salleo, *Nat. Mater.*, 2013, **12**, 1038–44.

19 S. A. Mollinger, B. A. Krajina, R. Noriega, A. Salleo and A. J. Spakowitz, *ACS Macro Lett.*, 2015, **4**, 708–712.

20 O. Bubnova, Z. U. Khan, H. Wang, S. Braun, D. R. Evans, M. Fabretto, P. Hojati-Talemi, D. Dagnelund, J.-B. Arlin, Y. H. Geerts, S. Desbief, D. W. Breiby, J. W. Andreasen, R. Lazzaroni, W. M. Chen, I. Zozoulenko, M. Fahlman, P. J. Murphy, M. Berggren and X. Crispin, *Nat. Mater.*, 2014, **13**, 190–4.

21 A. J. Heeger, *Phys. Scr.*, 2002, **T102**, 30.

22 N. F. Mott, *J. Non. Cryst. Solids*, 1968, **1**, 1–17.

23 B. Kramer and A. MacKinnon, *Rep. Prog. Phys.*, 1993, **56**, 1469–1564.

24 X. Wu, C. O. Yoon, M. Reghu, D. Moses, A. J. Heeger, Y. Cao, T. Chen and R. D. Rieke, 1995, **75**, 229–239.

25 V. I. Arkhipov, I. I. Fishchuk, A. Kadashchuk and H. Bassler, in *Photophysics of Molecular Materials*, ed. G. Lanzani, Wiley, 2006, pp. 262–366.

26 S. D. Baranovskii, *Phys. Status Solidi*, 2014, **251**, 487–525.

27 P. Stallinga, *Adv. Mater.*, 2011, **23**, 3356–3362.

28 P. Y. Yu and M. Cardona, *Fundamentals of Semiconductors*, 1999.

29 R. A. Marcus, *J. Chem. Phys.*, 1956, **24**, 966–978.

30 M. Shur and M. Hack, *J. Appl. Phys.*, 1984, **55**, 3831–3842.

31 G. Horowitz and P. Delannoy, *J. Appl. Phys.*, 1991, **70**, 469–475.

32 N. F. Mott, *Phil. Mag.*, 1969, **19**, 835.

33 A. Miller and E. Abrahams, *Phys. Rev.*, 1960, **120**, 745–755.

34 V. N. Prigodin and K. B. Efetov, *Phys. Rev. Lett.*, 1993, **70**, 2932–2935.

35 I. P. Zvyagin, in *Hopping Transport in Solids*, eds. M. Pollak and B. Shklovskii, Elsevier Science Publishers B. V., Amsterdam, Netherlands, 1991, vol. 28, pp. 145–172.

36 G. Kim and K. P. Pipe, *Phys. Rev. B - Condens. Matter Mater. Phys.*, 2012, **86**, 1–5.

37 S. Dongmin Kang and G. Jeffrey Snyder, *Nat. Mater.*, 2016, **16**, 252–257.

38 D. Monroe, *Phys. Rev. Lett.*, 1985, **54**, 146–149.

39 N. Mott and E. Davis, *Electronic Processes in Non-Crystalline Materials*, Oxford: OUP Oxford, 2012.

Goal of the Thesis

The experimental work described in this thesis was carried out within the research group of professor Dario Narducci, at the Department of Material Science at the University of Milano-Bicocca. The research group has an established experience in the study of thermoelectricity[1,2] and of thin film[3–6] and nanostructured[7–11] silicon as thermoelectric material. The aim of this thesis was to extend investigations to the ICP field, exploring a novel and challenging sets of materials for thermoelectricity. Therefore, the first efforts focused on defining a protocol to prepare ICP thin film, making efficient metallic contacts and characterizing them to obtain information on charge transport behaviour. Then, the work focused on three main areas of investigation.

The first one regarded the influence of parameters involved in polymerization reaction of a specific ICP, poly(3,4-ethylenedioxythiophene) or PEDOT, on its final thermoelectric performances. The use of different polymerization techniques, oxidants and solvents has been studied. This work has been paired with the study of doping (i.e. oxidation) level tuning, carried out on samples of highly performing PEDOT:Tf. The material was obtained through a novel combination of the parameters previously reported by the Laboratory of Organic Electronics at University of Linköping, Sweden. This work is described in Chapter 4.

A second area of investigation considered the possibility of modifying PEDOT properties thanks to molecular modifications. In other words, we studied how the inclusion of different molecular structures into the polymer chains affects charge transport. A study was performed on PEDOT-based copolymers, prepared through synthetic route by research group of professor Luca Beverina, at University of Milano-Bicocca. The work done is reported in Chapter 5.

The third investigated area was nanocomposites. In this case, PEDOT-based nanocomposites were prepared including different metal oxide nanostructures (Mn_3O_4 and CuO). The resulting impact on charge transport was studied for both the nanocomposites with two different tools. In one case, the investigation focused on humidity-dependent changes in electrical conductivity. In the other case, a study on electrochemically modified oxidation level was carried out in collaboration with the research group of professor Riccardo Ruffo at University of Milano-Bicocca. The work on nanocomposites is reported in Chapter 6.

The goal of the thesis was to explore the modification on PEDOT thermoelectric properties at three different level of system perturbation.

First, the modification of "intrinsic" parameters leads to small modifications in material nature (Chapter 4), and can be considered a light perturbation.

On a second level, the modification of the molecular structure through the development of a copolymer (Chapter 5) is a deeper perturbation of the system, at a molecular level.

A third level of perturbation is reached through the inclusion of inorganic material nanostructure (Chapter 6). In this case, the perturbation can be considered supramolecular, since it involves the interaction among the two phases at nanometric level.

The novel insights gained through this work contribute in obtaining a deeper comprehension of PEDOT system, which is the key to open paths to enhancing its thermoelectric performances.

3.1 References

1 D. Narducci, *Appl. Phys. Lett.*, 2011, **99**, 102104.

2 X. Zianni and D. Narducci, *J. Appl. Phys.*, 2015, **117**, 35102.

3 N. Neophytou, X. Zianni, H. Kosina, S. Frabboni, B. Lorenzi and D. Narducci, *J. Electron. Mater.*, 2014, **43**, 1896–1904.

4 D. Narducci, B. Lorenzi, X. Zianni, N. Neophytou, S. Frabboni, G. C. Gazzadi, A. Roncaglia and F. Suriano, *Phys. Status Solidi*, 2014, **1258**, 1255–1258.

5 N. Neophytou, X. Zianni, H. Kosina, S. Frabboni, B. Lorenzi and D. Narducci, *Nanotechnology*, 2013, **24**, 205402.

6 D. Narducci, S. Frabboni and X. Zianni, *J. Mater. Chem. C*, 2015, 3, 12176–12185.

7 D. Narducci, G. Cerofolini, M. Ferri, F. Suriano, F. Mancarella, L. Belsito, S. Solmi and A. Roncaglia, *J. Mater. Sci.*, 2013, **48**, 2779–2784.

8 M. Ferri, F. Suriano, A. Roncaglia, S. Solmi, G. F. Cerofolini, E. Romano and D. Narducci, *Microelectron. Eng.*, 2011, **88**, 877–881.

9 F. Suriano, M. Ferri, F. Moscatelli, F. Mancarella, L. Belsito, S. Solmi, A. Roncaglia, S. Frabboni, G. C. Gazzadi and D. Narducci, *J. Electron. Mater.*, 2015, **44**, 371–376.

10 N. Neophytou, X. Zianni, M. Ferri, A. Roncaglia, G. F. Cerofolini and D. Narducci, *J. Electron. Mater.*, 2013, **42**, 2393–2401.

11 L. Fonseca, J.-D. Santos, A. Roncaglia, D. Narducci, C. Calaza, M. Salleras, I. Donmez, A. Tarancón, A. Morata, G. Gadea, L. Belsito and L. Zulian, *Semicond. Sci. Technol.*, 2016, **31**, 84001.

Poly(3,4-ethylenedioxy)thiophene: Tuneable Intrinsic Parameters

Poly(3,4-ethylenedioxythiophene) or PEDOT is one of the most studied and exploited conjugated polymer in organic electronic applications (Chapter 1). One may quite obviously wonder why it is so, which are the features that make this specific polymer so interesting. The answer to this question can be found in the history of the research efforts that led to PEDOT discovery.

Soon after the discovery of conducting polyacetylene[1], attempts to use these new compounds in technical applications started. Bayer Central Research Department quickly realized that the main issue to be addressed was the instability of polyacetylene, so focused the attention on polyheterocycle development. Even though characterized by a lower electrical conductivity than polyacetylene, polyheterocycles presented a fair environmental stability due to aromatic structures (Figure 4.1).

First, polypyrrole was chosen as object of study, particularly for antistatic layers on thermoplastics. After less than two years, though, drawbacks which were impossible to overcome (such as toxicity) limited further developments of studies on this material. The interest was then moved to poly(3-alkyl-thiophene) class, which was already known at that time, since some studies demonstrated a remarkable conductivity of these polymers in the doped state.

Even if poly(3-alkyl-thiophenes) proved to be a better choice than polypyrrole, still presented the fundamental drawback of instability when they were in highly conductive form.

This phenomenon is easy to explain if one considers that high conductivity is related with a high number of charge carriers. In ICPs, carriers can be chemically interpreted as dications and radical cations, therefore very reactive states of the molecule. The shortcoming is that an increase of the conductivity of the polymer leads also to an increase of its reactivity with the environment and, therefore, of the speed of its degradation due to it.

A way to deal with this issue relies on chemical modification of the monomer molecular structure. In fact, the inclusion of an electron-rich moiety (e.g., oxygen-bearing substituent) can stabilize the charged state by increasing delocalization.

After the development of monoalkoxy- and 3,4-dialkoxysubstitutedthiophenes, the step to obtain a decisive improvement was taken with the extension of thiophene structure to bicyclic

ring systems. Bayer researchers Friedrich Jonas and Gerhard Heywang decided to close the two alkoxy substituents and form dioxolane-, dioxane-, and dioxepane 3,4-anellated thiophenes.

The combination of mesomeric stabilization by two oxygen atoms and the smaller steric hindrance provided by a cyclic structure appeared to be extremely appealing. The resulting scientific breakthrough was 3,4-ethylenedioxythiophene (EDOT) and the resulting polymer, PEDOT, which can be obtain by chemical reaction of the monomer with an oxidizing agent.

After patent publication in 1988[2] an intensive research activity arose on PEDOT and its possible applications. At the end of the same year, a new polymerization route was discovered, the electrochemical polymerization. This second route to obtain PEDOT films proved that different paths can lead to the synthesis of namely the same polymer, but, at the same time, that the chosen path influences material macroscopic features.

Another parameter that was found crucial in PEDOT study was the counterion. Since, once doped, PEDOT can be considered a polycation, several counterions (anions) are required to balance the charges. Such counterions are usually products of oxidation reactions (e.g., using iron (III) chloride as oxidant, resulting complex will be PEDOT:Cl).

A determining step for PEDOT wide diffusion was the use of a particular counterion, due to the collaboration between laboratories at Bayer and Agfa-Gevaert AG[3]. The use of waterborne poly(styrenesulfonic acid) (PSS) and the corresponding polyanion was found to be a convenient choice as the counterion for positively charged doped PEDOT, forming a new PEDOT:PSS complex.

Moreover, the complex was easily dispersible in water and was not detrimentally affected by it, as other polythiophenes were. The discover led to a completely new way to process this ICP, since a solution of the polymerized material could be spread to obtain thin films.

Regarding the thermoelectric application of PEDOT, PEDOT was one of the first to be studied for such a purpose[4,5]. Its good stability appeared promising for an application which required the presence of a temperature gradient. In the last few years a lot of works concerning the use of PEDOT and its composites as thermoelectric material have been publishing, with remarkable increase of performances recorded (especially for electrical conductivity)[6,7].

The achievement of a better PEDOT can be pursued by several different pathways, since both parameters involved in polymerization reaction[8–10] and post polymerization treatment[4,11,12] can dramatically affect material features. In the first part of this chapter, the work done changing three parameters involved in polymerization reaction (polymerization technique, oxidant/counterions and solvent) is reported. In the second part, a study on the modification of the oxidation level on one of the material will be presented.

4.1 Polymerization Techniques, Counterions and Solvents

Three polymerization techniques have been developed for PEDOT: wet chemical polymerization (WCP), electrochemical polymerization and vapor phase polymerization

(VPP). The first one was discovered together with the discovery of ICPs. It consists basically in mixing the monomer in a solution with an oxidative agent, and using the solution itself to coat the substrate. The second one was discovered a few years later, and involves the application of an electrochemical potential to an electrode in a solution of the monomer[13]. The oxidative potential induces the monomer reaction and then the deposition of the ICP on to the electrode surface. The last technique is quite recent[14,15], and consists in the reaction of the monomer in the vapor phase with a layer of oxidant deposited on the substrate.

The first and the third techniques have been used in this thesis work and will be further described later. On the other side, the necessity of a conductive substrate to allow polymer growth with electrochemical technique is a major issue. A conductive substrate is mostly inconvenient for measurements that involve potential and temperature difference, such as thermoelectric measurements. Therefore, this technique is usually avoided.

Several oxidative agents have been proposed to be used in PEDOT polymerization. The choice not only affects the reaction, due to the reactivity of the chosen oxidant, but also the nature of the final material itself, since the oxidant is often also the source of counterions. In the following work two oxidants have been used: iron (III) tosylate and iron (III) triflate (Figure 4.1). The first has been popular to be used to obtain highly performing PEDOT[4,12], while the second one have been only recently exploited in this field, but with excellent results[16].

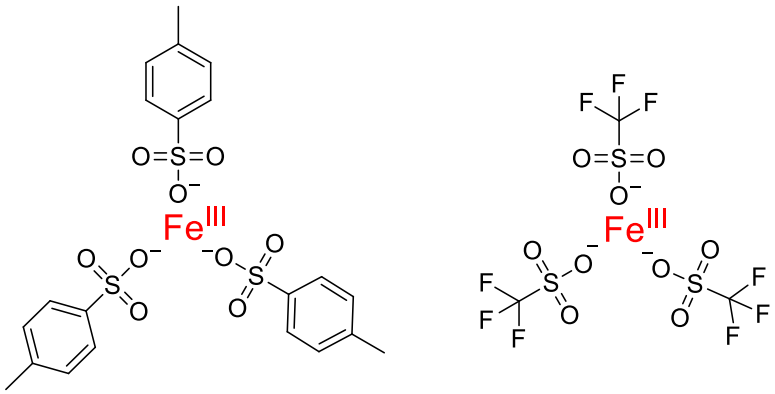

FIGURE 4.1: MOLECULAR STRUCTURE OF THE TWO OXIDANTS USED. THE OXIDATION IS CARRIED OUT BY THE IRON CENTRE, WHILE THE COUNTERIONS ARE RELEASED IN PEDOT TO BALANCE ITS POSITIVE CHARGES.

Moreover, the solvent used affects the reaction due to the speed of evaporation and its interaction with the anionic species[8]. The use of two alcoholic solvents has been investigated in the following, possibly in combinations with the two mentioned techniques and the two oxidants, as reported in Table 4.1.

		OXIDANT			
		$FeTos_3$		$FeTf_3$	
		SOLVENT		SOLVENT	
		Ethanol	Butanol	Ethanol	Butanol
POLYMERIZATION TECHNIQUE	WCP	PEDOT:Tos WCP in EtOH	PEDOT:Tos WCP in BuOH	PEDOT:Tf WCP in EtOH	PEDOT:Tf WCP in BuOH
	VPP	PEDOT:Tos VPP in EtOH	PEDOT:Tos VPP in BuOH	PEDOT:Tf VPP in EtOH	PEDOT:Tf VPP in BuOH

TABLE 4.1: SAMPLES PREPARED TO CHECK THE IMPACT OF DIFFERENT PARAMETERS ON PEDOT FINAL PERFORMANCES.

The work on different polymerization conditions is still in progress to further extent the combination of polymerization techniques, oxidants and solvents. Herein preliminary results are presented.

4.1.1 Polymerization Mechanism

EDOT polymerization mechanism (Figure 4.2) can help understand how different conditions affect the final PEDOT quality and the reasons behind different steps in polymerization procedure.

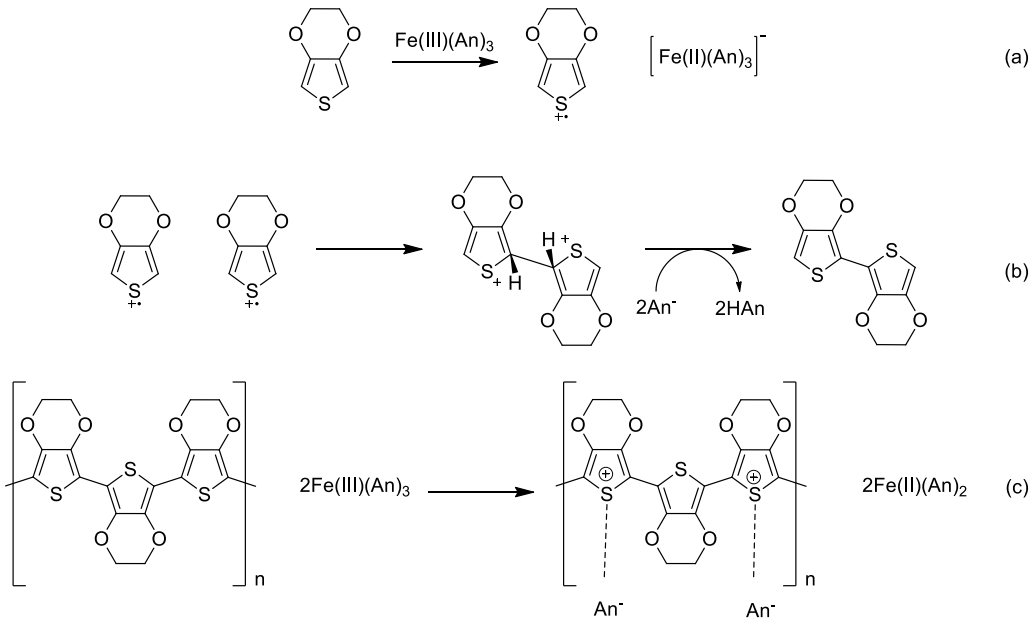

FIGURE 4.2: PROPOSED POLYMERIZATION MECHANISM FOR PEDOT: A) EDOT IS OXIDIZED BY FE(III) TO A CATION RADICAL; B) EDOT CATION RADICALS FORM DIMERS THAT SUBSEQUENTLY GET DEPROTONATED; C) PEDOT POLYMER IS DOPED AND ANIONS RESIDE IN THE FILM TO ACT AS COUNTER IONS.

The mechanism involves as first step (a) EDOT oxidation to radical cation by an oxidative agent, herein an iron(III) salt. The use of different oxidant have been explored[17], such as $Ce(SO_4)_2$, MnO_2 and $CuCl_2$. Iron salts, though, are the most commonly used.

EDOT radical cation is extremely reacting, and quickly forms a bond with another EDOT radical cation (step (b)). The resulting dimer present two positive charges. Its deprotonation restores structure aromaticity. In the reaction mechanism, anion (An^-) produced in oxidation reaction acts as proton scavenger, generating the corresponding acid (HAn). It must be noticed that also water can act as proton scavenger, implying that environmental humidity has an important impact on polymerization reaction[18].

Chain growth progresses with the oxidation of the dimer and its reaction with another EDOT radical cation. The charged trimer loses two protons and originates the neutral specie. The mechanism reiterates on longer chains. The side products of the polymerization are iron(II) salt reduced (step (a)) and the corresponding acid of the third anion (HAn), step (b).

Average chain length is difficult to be estimated since the absorption spectrum of chemically polymerized PEDOT may result from various chemical species present, but it is commonly believed that the main contribution stems from oxidatively charged oligomers consisting of 5 to 15 monomeric units.[17]

Polymerization reaction requires 2 equivalents of iron (III) salt for each EDOT equivalent. A small excess of oxidant is then added to oxidise PEDOT chains (step (c)). Since a positive charge can be stably delocalized over 3-4 monomeric units, 0.25-0.33 equivalents of iron (III) salt are usually added as excess.

Since EDOT oxidation is the rate determining step of polymerization reaction[17], kinetic control over this step is crucial. The inhibition of oxidation reaction is provided by a small amount of weak bases[19] (such as imidazole and pyridine) included in polymerization solution. Decreasing polymerization kinetic is particularly important for film final quality, due to the lessening of conjugation defects. Moreover, a slower reaction allows a better organization of polymer chains, which is crucial to obtain highly conductive crystalline domains.

Bases not only enhance pot-life, but also increase solution pH, which is crucial to avoid detrimental side reactions caused by too acidic environment[15].

Recently, the inclusion of a block copolymer as inhibitor has been proven to be extremely beneficial[20]. The tri-block copolymer is poly(ethylene)-*ran*-poly(propylene)-*ran*-poly(ethylene) or PEPG, sold with the commercial name of Pluronic P-123 (Figure 4.3).

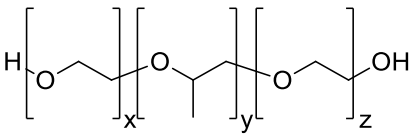

FIGURE 4.3: MOLECULAR STRUCTURE OF THE TRIBLOCK COPOLYMER PEPG

Studies reported this copolymer playing different roles into the polymerization solution. It was originally introduced to suppress iron (III) salt crystallization[10], which was deleterious for PEDOT film quality. Additionally, it was proven that the copolymer has the ability to slow down the polymerization rate of PEDOT by means of reducing the effective reactivity of the oxidant[21]. In this aspect, PEPG has a similar effect to that of pyridine, imidazole or other weak

bases, but achieves through the complexation of the iron centre rather than raising the pH of the solution[22]. However, in both cases, the result is a decrease of Fe(III) salt formal potential.

Moreover, a more recent work showed that PEPG has also the role of water reservoir in vacuum VPP[18]. Water presence is essential when the anion is a bad proton scavenger, such as tosylate and triflate.

In all the recipes used, PEPG has been added as inhibitor.

4.1.2 Experimental Procedures

4.1.2.1 Wet Chemical Polymerization (WCP)

A scheme of EDOT WCP is reported in Figure 4.4. The procedure started with glass substrate preparation. The substrate was immersed in DI water, then in acetone and eventually in isopropanol. For each solvent, the substrate was kept in a sonication bath for 15 minutes. After the washing step, the glass was carefully dried with a nitrogen flux. A shadow mask was then applied on the substrate and golde electrodes were evaporated on it with thermal evaporation (a few nanometer chromium layer was deposited before gold, to enhance metal adhesion). A layer of 100-150 nm of gold was deposited, and then the substrate was washed again following the procedure already described.

An alcoholic solution of an iron (III) salt was prepared (usual concentration of 20%wt for $FeTos_3$ and 3%wt for $FeTf_3$). A copolymer PEG-PPG-PEG, i.e. Pluronic P-123 or PEPG (20% wt) was added and the solution was sonicated until its complete dissolution.

1 equivalent of EDOT was then poured into the solution for each 2.25 equivalents of iron (III) salt. The resulting mixture was stirred at room temperature for 15 minutes, then dropped on the substrate and spin coated. The spin coating program was set to 600 rpm for the first 30 seconds followed by 1200 rpm for 10 seconds.

The resulting layer was annealed for 10 minutes at 80°C and then washed in ethanol to remove unreacted material and side products.

The sample was annealed again after the rinsing step for a few minutes, to evaporate ethanol in excess.

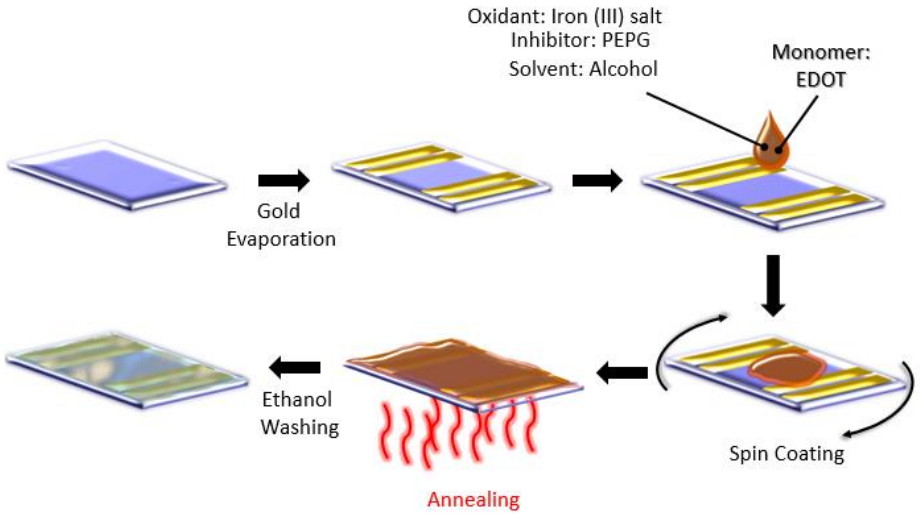

FIGURE 4.4: DESCRIPTION OF WCP PROCESS. GOLD ELECTRODES ARE EVAPORATE ON THE CLEANED GLASS SUBSTRATE (I STEP). THEN THE POLYMERIZATION SOLUTION IS DROPPED (II STEP) AND SPIN COATED (III STEP) ON IT. THE RESULTING LAYER IS ANNEALED (IV STEP) AND EVENTUALLY RINSED IN ETHANOL (V STEP).

4.1.2.2 Vapor Phase Polymerization (VPP)

VPP process is described in Figure 4.5. More exactly, the process used in this thesis work is better described as a low-pressure vapor phase polymerization, since the polymerization takes place in a vacuum chamber. The cleaning of the substrate and gold evaporation on it are the same as described in Section 4.1.2.

An alcoholic solution of iron (III) salt was prepared including Pluronic P-123 or PEPG (20%wt). The solution was stirred until the complete dissolution of the copolymer, and then spin coated on the cleaned substrate.

The sample was then annealed for 2 minutes at 70°C to remove solvent in excess and seated in a vacuum chamber. Few drops of EDOT were placed on the bottom of the vacuum chamber, which was heated up to 60°C to increase EDOT vaporization. The polymerization took 15 minutes. After that time, the samples were removed from the chamber and washed with ethanol.

A final annealing of the sample at 70 °C for 10 mins allowed the removal of residual ethanol.

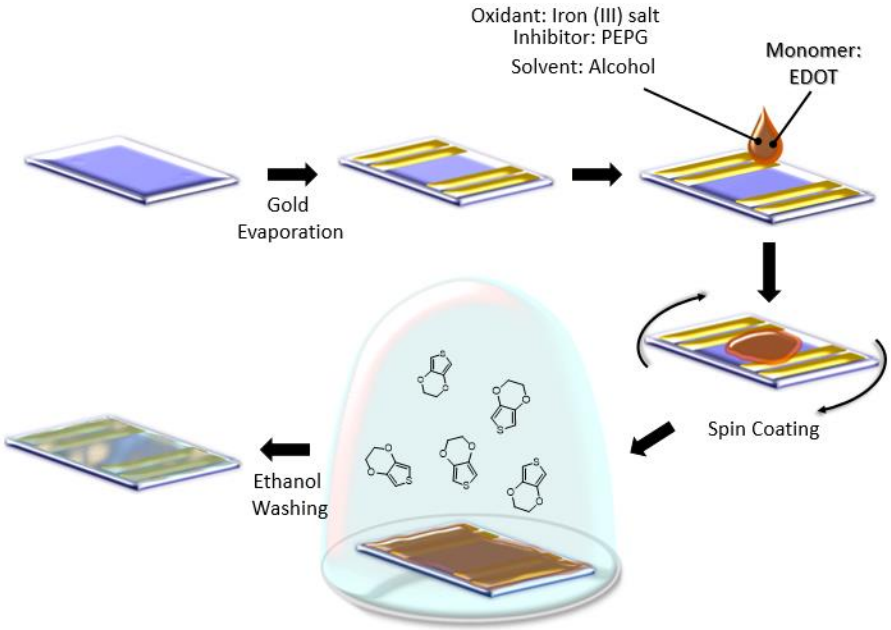

FIGURE 4.5: DESCRIPTION OF VPP PROCESS. GOLD ELECTRODES ARE EVAPORATE ON THE CLEANED GLASS SUBSTRATE (I STEP). THEN THE POLYMERIZATION SOLUTION IS DROPPED (II STEP) AND SPIN COATED (III STEP) ON IT. THE RESULTING LAYER IS EXPOSED TO MONOMER VAPOR (IV STEP) AND EVENTUALLY RINSED IN ETHANOL (V STEP).

4.1.3 Characterization

Optical (UV-vis spectroscopy) and morphological (Atomic Force Microscopy, AFM) characterizations were performed on the samples. This last technique was also used to measure thin film thickness.

Thermoelectric measurements and electric measurement at different temperatures were performed with home-made setups, which will be described in next sections.

4.1.3.1 Electric and Thermoelectrical Characterizations

Room temperature electric and thermoelectric characterizations of the samples were performed using a set up (shown in Figure 4.6) connected with two Keithley 4200 multimeters. Samples must be shaped in a rectangular form (40 mm x 8mm) and two electrodes must be evaporated at the two sides (4mm x 8mm). Sample is placed on two copper blocks, while the central part is suspended, as shown. Two electrical probes are located on the two gold electrodes, and are used for a two-point measurement of resistance (R). To this aim, various voltages (V) values are applied in a user-defined range, and electrical currents (I) are measured with the same probes. The resistance is calculated from Ohm law as:

$$R = \frac{V}{I} \tag{4.1}$$

From resistance, it is possible to calculate the electrical conductivity from the following relation:

$$\sigma = \frac{l}{R \cdot w \cdot t} \tag{4.2}$$

where the geometrical parameters are the length (l), the width (w) and the thickness (t) of the sample.

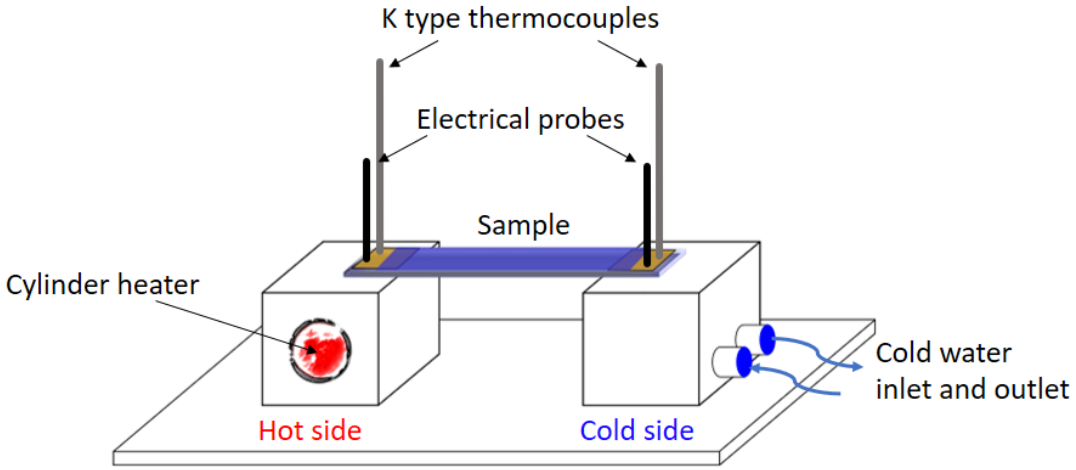

FIGURE 4.6: SCHEME OF HOME-MADE EXPERIMENTAL SETUP FOR RESISTANCE AND ELECTRICAL CONDUCTIVITY MEASUREMENTS.

While resistance measurements were performed under isothermal conditions (25°C), the Seebeck coefficient must be measured in the presence of a thermal gradient. Therefore, in the setup, one of the two edges is cooled down at a fixed temperature (10°C) by a water cooling system, while the other is heated up by an electrical heater at different temperatures. For PEDOT samples, the range for the hot side was set from 30°C to 80°C.

This configuration enables a measurement of the Seebeck coefficient value through the integral method[23]. If the Seebeck voltage increases linearly with temperature difference among the two edges, the slope $\frac{dV}{dT}$ is expected to be constant. Since this was verified for PEDOT samples in the chosen range of temperatures, Seebeck coefficient value could be calculated as a constant value according to the cited method. Temperature difference was checked using two thermocouples seated on the two electrodes.

Data were acquired through a digital voltmeter equipped with a voltage scanning card interfaced with a computer and controlled by a LabView program. For all samples, three or four measurements at different hot-side temperatures were collected and then a linear fit was performed in order to obtain the Seebeck coefficient value.

The setup was placed in a closed dark box, in which the humidity could be controlled by using a flux of dry nitrogen (N_2). Since one of the two blocks is kept at 10°C, water might condense on the cold side of the sample, detrimentally affecting the measurements. The measurements reported are performed at 0% of humidity level, in a flux of nitrogen, unless otherwise stated.

4.1.3.2 Measurements of Resistance vs. Temperature

Measurements of electrical conductivity at different temperatures were performed on square samples (30mm x 30mm) with four gold electrodes evaporated at the four corners. Samples were inserted in a cryostat and the four electrodes were contacted with four electrical probes

connected with a digital voltmeter. The data were collected by a computer interfaced with the instrument through a LabView program.

When the cryostat was pumped down to vacuum, an automated chiller with liquid helium was used to cool down the temperature of the sample. The temperature was then set by heating the sample with an electrical resistor. Sample resistance was measured in the temperature range 170K-320K, with a temperature step of 10K. For each temperature step, resistance was measured three times applying an electric current and measuring the voltage.

4.1.4 Results

Room temperature electrical conductivity data are displayed in Table 4.2, while data obtained from Seebeck coefficient measurement are reported in Table 4.3. For sake of simplicity, in following description the terms 'electrical conductivity' will refer to room temperature electrical conductivity, unless otherwise explicitly stated.

TABLE 4.2: ELECTRICAL CONDUCTIVITY VALUES ($\Omega^{-1}cm^{-1}$) FOR THE PREPARED SET OF SAMPLES.

		OXIDANT			
		$FeTos_3$		$FeTf_3$	
		SOLVENT		SOLVENT	
		Ethanol	Butanol	Ethanol	Butanol
POL. TECH.	WCP	657±22	503±72	1515±83	177±25
	VPP	171±17	154±12	804±94	174±21

TABLE 4.3: SEEBECK COEFFICIENT VALUES (μVK^{-1}) FOR THE PREPARED SET OF SAMPLES.

		Oxidant			
		$FeTos_3$		$FeTf_3$	
		SOLVENT		SOLVENT	
		Ethanol	Butanol	Ethanol	Butanol
POL. TECH.	WCP	11.5±2.1	19.2±1.1	21.5±1.4	23.3±1.7
	VPP	17.9±2.6	21.2±2.3	18.9±2.4	33.4±5.1

Table 4.4 shows the resulting power factor values, calculated according to equation 1.2.

TABLE 4.4: SEEBECK COEFFICIENT VALUES (μVK^{-1}) FOR THE PREPARED SET OF SAMPLES.

		OXIDANT			
		$FeTos_3$		$FeTf_3$	
		SOLVENT		SOLVENT	
		Ethanol	Butanol	Ethanol	Butanol
POL. TECH.	WCP	8.7±3.5	18.5±4.7	70.0±12.9	9.6±2.8
	VPP	5.5±2.1	6.9±2.0	28.7±10.6	19.4±8.3

As a general consideration, it must be noticed that sample electrical conductivity is higher for samples obtained with WCP technique, rather than VPP technique, especially when iron (III) tosylate is used as oxidant. Moreover, a decrease in conductivity was observed when butanol was used as solvent instead of ethanol.

Seebeck coefficient showed an opposite behaviour. It reached higher value (with only one exception) when VPP is used. Moreover, it can be noticed that higher Seebeck values result from using butanol as solvent.

As for the power factor values, it is interesting to notice the highest value of PEDOT:Tf made through WCP technique in ethanol. Such a result leads to the consideration that the peculiar combination of the parameters makes this material particularly performing and different from all the others.

A deeper understanding of the differences among the materials can be achieved through UV-vis absorption spectra (Figure 4.7)

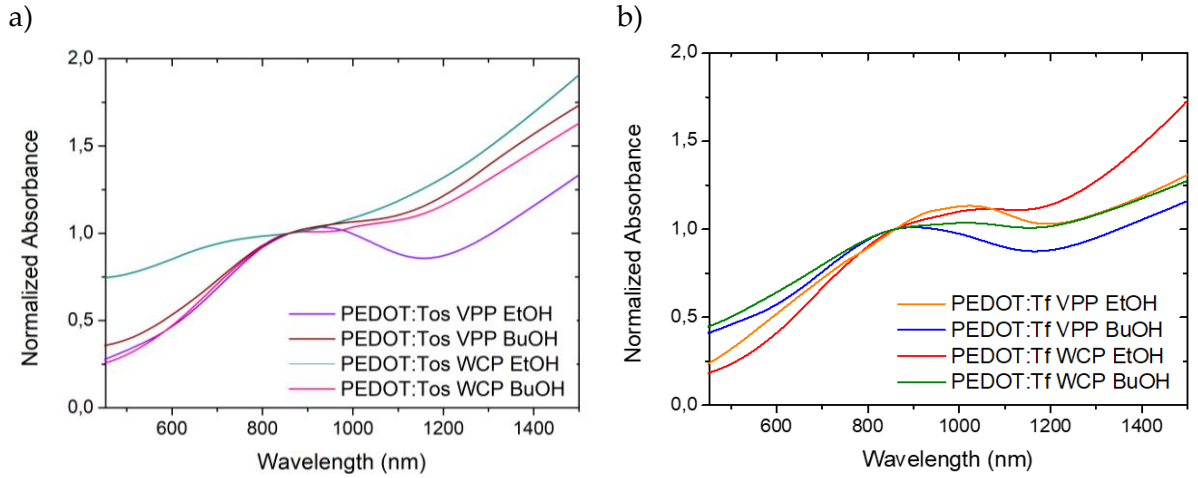

FIGURE 4.7: UV-VIS SPECTRA OF PEDOT SAMPLES OBTAINED WITH IRON (III) TOSYLATE (A) AND OBTAINED WITH IRON (III) TRIFLATE (B).

The absorption spectra were collected right after the polymer preparation and normalized at 860 nm. Among the samples prepared with iron (III) tosylate, it can be noticed that PEDOT:Tos prepared with WCP in ethanol (dark cyan line) presents higher absorption above 1400 nm. It can be stipulated that this material is characterized by a higher oxidation level, which is consistent with the low Seebeck coefficient recorded, and with the high electrical conductivity measured. The use of VPP in the same conditions leads otherwise to a decrease of the oxidation level (purple line), consistent with the recorded electric and thermoelectric data.

PEDOT:Tos samples prepared in butanol present very similar absorption profile, independently of the technique used, which is consistent with the similar Seebeck coefficient recorded, although in contrast with conductivity data.

For samples prepared with iron (III) triflate (Figure 4.7b), it can be noticed that PEDOT:Tf obtained from WCP in ethanol presented higher absorption above 1400 nm, and it is therefore characterized by a higher oxidation level, which is consistent with higher electrical conductivity.

On the other side, the lowest oxidation level can be attributed to PEDOT:Tf polymerized in butanol through VPP, consistent with the Seebeck value and the electric conductivity recorded.

As a general trend, it can be observed that PEDOT prepared in butanol is characterized by lower oxidation levels than the one prepared in ethanol, with the only exception of PEDOT:Tos prepared with VPP, which presents a trend inversion.

Further information about charge transport in the material can be obtained through electrical conductivity measurements at different temperatures (Figure 4.8).

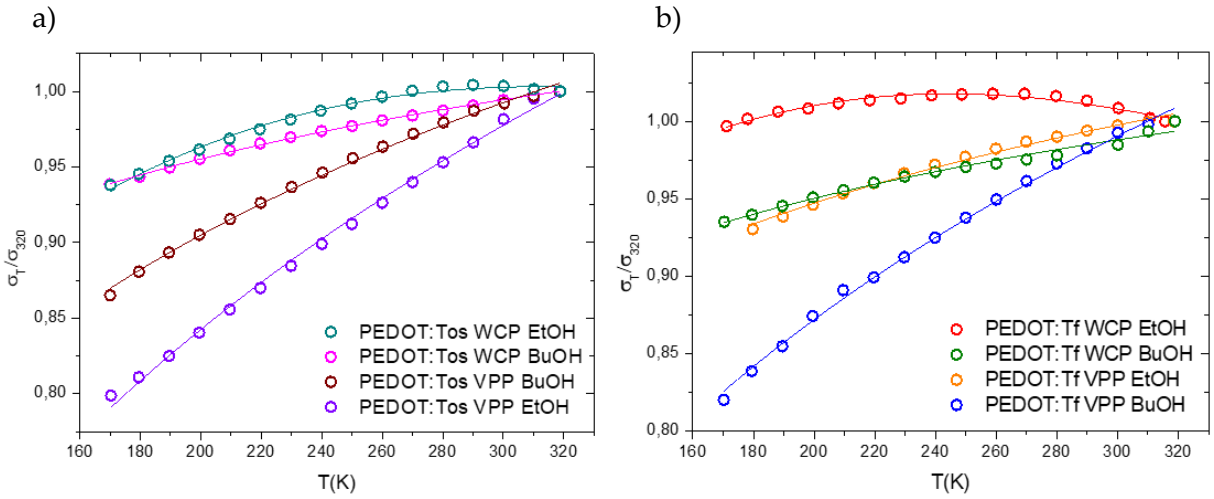

FIGURE 4.8: NORMALIZED ELECTRICAL CONDUCTIVITY *VERSUS* TEMPERATURE MEASURED FOR SAMPLES PREPARED WITH IRON (III) TOSYLATE (A) AND PREPARED WITH IRON (III) TRIFLATE (B) IN DIFFERENT CONDITIONS.

The trend of electrical conductivity at different temperatures can be usually ascribed to thermally activated hopping of charge carriers, which can be fitted with the VHR model, as reported in equation 2.48 (Section 2.2.2.4). It can be rewritten as:

$$\sigma = \sigma_0 exp\left[-\left(\frac{T_0}{T}\right)^{1/4}\right] \tag{4.3}$$

considering the dimensionality parameter γ equal to ¼ for a 3D system[24]. This fitting is satisfactory for most of the samples, with the two exceptions of WCP samples in ethanol (dark cyan dots in Figure 4.8a and red dots in Figure 4.8b). In this case, it is possible to notice a maximum in the trend followed by conductivity decrease at higher temperatures, especially for PEDOT:Tf. These two curves are poorly fitted by VHR model, which is therefore insufficient for explain this behaviour.

This different trend in conductivity temperature dependence was already observed in highly conducting polymers and explained with an heterogeneous model by Kaiser[25]. He suggested that the intrinsic heterogeneous disorder in ICPs is the key to understand this behaviour. In ICP crystalline domains, charge transport can assume the character of quasi-one dimensional metal[26]. If the ICP presents a good amount of crystalline portions, the resulting electrical conductivity is made up of two contributions: metallic behaviour (first term) and hopping in

amorphous portions among crystallites (second term). In heterogeneous model, this is expressed as a series resistance, namely:

$$\sigma^{-1} = f_c \rho_m exp\left(-\frac{T_m}{T}\right) + f_n \rho_0 exp\left[\left(\frac{T_0}{T}\right)^{1/4}\right] \quad (4.4)$$

where f_c and f_n are geometric factors describing the relative extension of respectively, crystalline and not crystalline domains. ρ_m is the intrinsic resistivity in crystalline portions, while T_m gives the energy of phonons that can backscatter carriers, usually taken equal to 1000K for ICPs[25].

Using this equation for PEDOT:Tos WCP in ethanol and PEDOT:Tf WCP in ethanol provided more satisfying fittings. The weight of metallic contribution in these two samples proves a larger extension of crystalline domains, than in other samples. The preparation route is fundamental to tune morphological features of the polymer.

4.1.5 Counterion and Solvent Effect

The data collected on the prepared set of samples suggest that several effects are involved in the polymerization reaction that deeply affect polymer final features. Even though more work is needed to give a full account of these effects, it is possible to advance some interesting observations by the work done till now.

First, the general higher conductivity values of WCP samples might be owed to slower reactions. While VPP chamber is saturated with monomer vapor, in WCP samples the reaction occurs in a liquid environment, in which a smaller EDOT amount is involved in the reaction. A slower reaction allows a better organization of polymer chains and, therefore, an increase in PEDOT crystallinity, as proved by electrical conductivity measurements *versus* temperature.

The effect of the solvent can be explained in relation with its interaction with the counterion[8]. Alcoholic solvents lead to hydrogen bonds with the negative charge of the counterion. In this interaction (Figure 4.9) solvent molecules can interpose among chains, worsening chain packing. This is consistent with the worse conductivity results obtained for materials prepared with butanol, a larger molecule than ethanol.

The effect is stronger when smaller counterions are used, since a larger counterion, such as tosylate, already displaces chains. This is confirmed by the more dramatic decrease in electrical conductivity recorded for samples prepared with iron (III) triflate.

In principle, hydrogen bonds could be formed also between the hydrogen in ethanol molecule and the fluorine atom in triflate counterion, leading to a more effective solvatation of the anion. Even though this theory sounds interesting and could furtherly motivate triflate better performances, intermolecular bonds among hydrogen and covalently bond fluorine are reported to be weak and less likely to be formed[27]. Therefore, a more specific study should address the validation of this specific hypothesis.

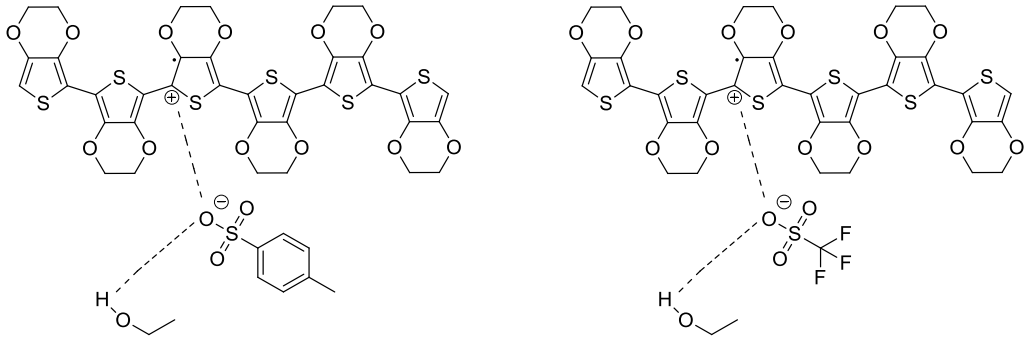

FIGURE 4.9: MOLECULAR STRUCTURES OF PEDOT HEXAMER INTERACTING WITH THE COUNTERION (TOSYLATE, ON THE LEFT, AND TRIFLATE, ON THE RIGHT) IN PRESENCE OF SOLVENT MOLECULE (ETHANOL) WHICH IS SUPPOSED TO DEVELOP HYDROGEN BOND WITH NEGATIVE CHARGED SULFONATE GROUP OF THE COUNTERION.

From the data collected, the use iron (III) triflate in ethanol, along with WCP, appears to be the best strategy to obtain highly performing PEDOT, as proved by the thermoelectric power factor achieved of 70 $\mu WK^{-2}m^{-1}$. The combination of a small counterion, together with small solvent molecules, helped obtain also a good degree of crystallinity, which is responsible for the high electrical conductivity measured.

4.2 Oxidation Level

As already stated, the oxidation level of an ICP strongly impacts on its electrical conductivity. For PEDOT:Tos the impact of the oxidation level on the thermoelectric performance has been already studied[4].

Interestingly, Bubnova et al.[4] reported that a slight reduction of PEDOT allows to reach the maximum of thermoelectric power factor[4]. In order to verify if the observed trend for PEDOT:Tos was reproducible in PEDOT:Tf, a similar study was carried on PEDOT:Tf samples.

4.2.1 Study on Oxidation Level on VPP PEDOT:Tf

PEDOT:Tf samples were prepared according to the procedure reported in Sect. 4.1.1.2, using iron (III) triflate as oxidant and ethanol as solvent. Moreover, samples were immersed in diluted sulfuric acid (1M) for 30 minutes to obtain an increase in oxidation level and a partial counterion exchange, which has been proved to be beneficial for thermoelectric properties[11,16]. Since the work done was performed at Laboratory of Organic Electronics (LOE) at Linköping University (Sweden), the characterization apparatus used for measuring Seebeck coefficient was different from that previously described.

Progressive modification of PEDOT oxidation level can be achieved exposing the film to oxidizing or reducing vapor. In the first case, iodine (I_2) at room temperature was used. In the case of reduction, vapors of diethylentriamine (DETA) (Figure 4.10) at 60°C were used to treat the sample.

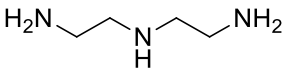

FIGURE 4.10: MOLECULAR STRUCTURE OF DIETHYLENTRIAMINE (DETA), USED AS REDUCING AGENT.

The first part of the study focused on the stability in air of the sample at different oxidation level, while the second part concerned a study using three parameters (electrical conductivity, Seebeck coefficient and UV-vis spectrometry) to follow the effect of a progressive reduction on PEDOT:Tf features.

4.2.2 Characterization

The optical (UV-vis) characterization was performed with a PerkinElmer Lamba 900 spectrofotometer, while morphological characterization (AFM) was performed in tapping mode with Veeco Dimension 3100. Electrical resistance was measured with 4-point method, using four rectangular gold electrodes (as depicted in Figure 4.11). The data were collected with a Keithley 4200 digital voltmeter. The same sample was used for electric and thermoelectric measurements.

4.2.2.1 Thermoelectric Characterization

Seebeck coefficient measurements were performed using a LabVIEW controlled setup where the sample was placed between two Peltier elements with adjustable separation, as shown in Figure 4.11. One of the Peltier elements was heated, while the other one was kept at room temperature.

Glass substrates with golden electrodes like the ones used for resistance measurements were used.

Thermovoltage was measured with nanovoltmeter Keithley 2182, sitting one probe on each electrode on the cold and on the hot side of the sample, while thermocouples were used to measure the temperature at the two sides of the sample. The resulting Seebeck coefficient was calculated with integral method[23] for temperature differences between the two sides of the sample in the range 1-8 K.

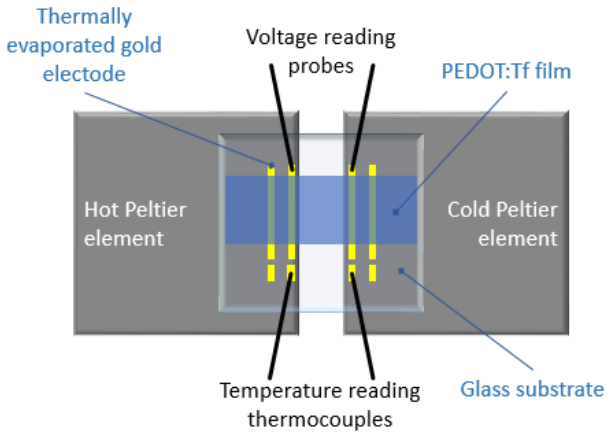

FIGURE 4.11: EXPERIMENTAL SETUP USED FOR SEEBECK COEFFICIENT MEASURAMENTS

4.2.3 Results

4.2.3.1 Investigation on Doped and Dedoped State Stability

Resistance was measured at different time after exposure of the sample to I_2 and DETA.

In case of iodine exposure, only a small decrease of resistance was recorded after a few second exposure, as reported in the graph (resistance *versus* time delay) in Figure 4.12. Moreover, the more oxidised level reached by the polymer appeared to be unstable, since a progressive increase of resistance in time after the exposure was recorded.

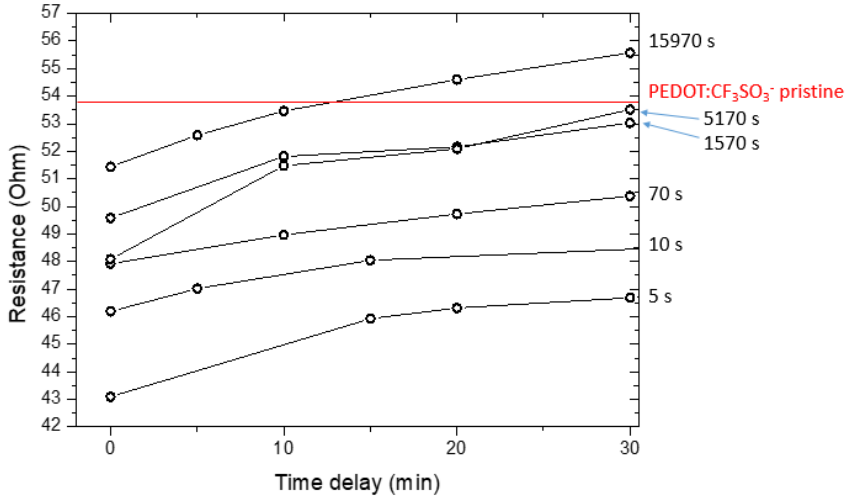

FIGURE 4.12: STABILITY INVESTIGATION ON I_2 EXPOSED SAMPLES. THE RESISTANCE IS PLOTTED AGAINST DELAY TIME AFTER THE EXPOSURE OF THE SAMPLE FOR DIFFERENT TIME OF EXPOSURE (REPORTED IN SECONDS ON THE GRAPH RIGHT SIDE). PRISTINE PEDOT:TF VALUE IS MARKED IN RED.

Following treatments for longer times resulted in lower resistances than pristine one. Interestingly, though, resistances increased with the exposure time. This might be related with the instability of the polymer in such highly doped states. A strong increase in the reactivity of the material due to the doping can lead to degradation reactions[28].This can also explain why the sample treated for the longest time (more than 4 hours) showed a higher resistance than pristine PEDOT:Tf, 20 minutes after the exposure.

Due to the instability of the polymer in such a condition, progressive doping was not considered for further studies.

In the case of DETA exposure (dedoping) samples showed a better stability was shown by the samples. Figure 4.13 shows resistance variation in time after DETA treatment for different exposure times.

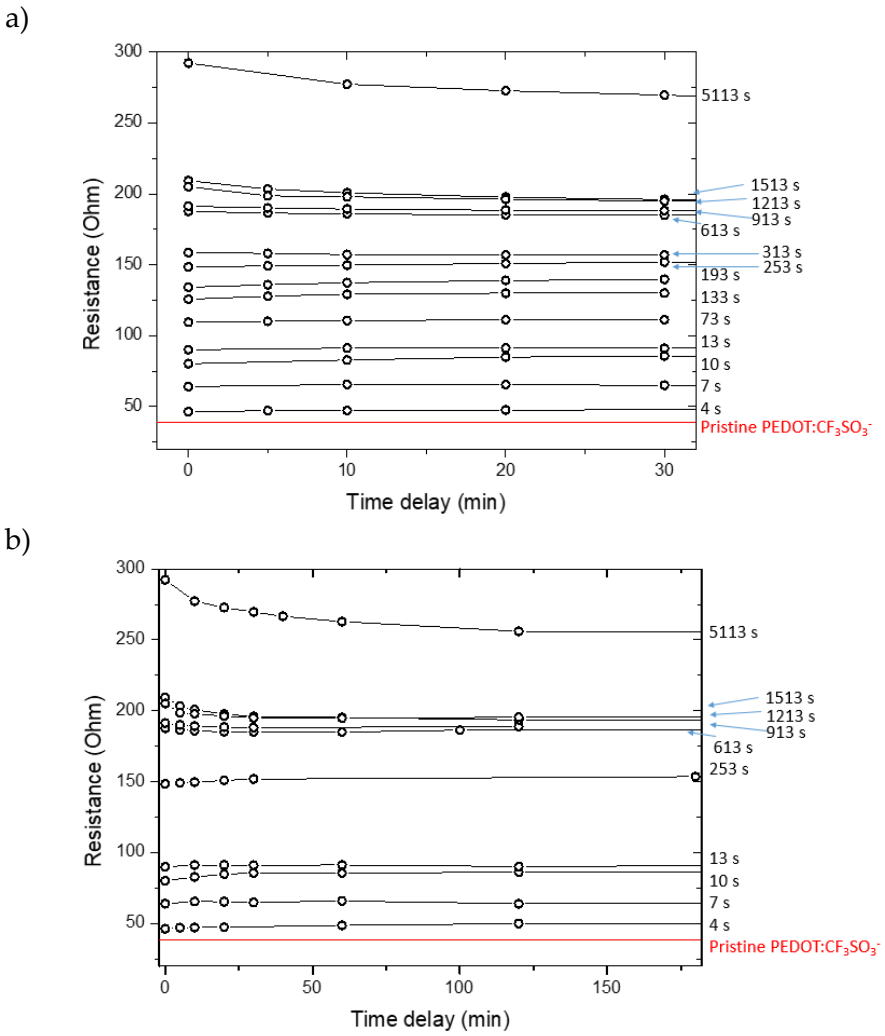

FIGURE 4.13: A) RESISTANCE OF PEDOT:TF SAMPLES FOR THE FIRST 30 MINUTES AFTER EXPOSURE TO DETA. B) RESISTANCE OF PEDOT:TF SAMPLES FOR 180 MINUTES AFTER EXPOSURE TO DETA.

It can be observed that DETA exposure has a more dramatic effect on PEDOT:Tf resistance than on PEDOT:I_2, for shorter treatment times. Moreover, decrease of resistance due to ICP oxidation by air is found to be negligible for treatment times lower than 600 seconds. Therefore, the study on feature modification was focused on reduction effect on PEDOT:Tf.

The rate of PEDOT:Tf reduction is not linear with exposure time, as reported in Figure 4.11. After a sharp increase of resistance over the first seconds of exposure, the curve becomes flatter. Eventually, it reaches a plateau (Figure 4.14c).

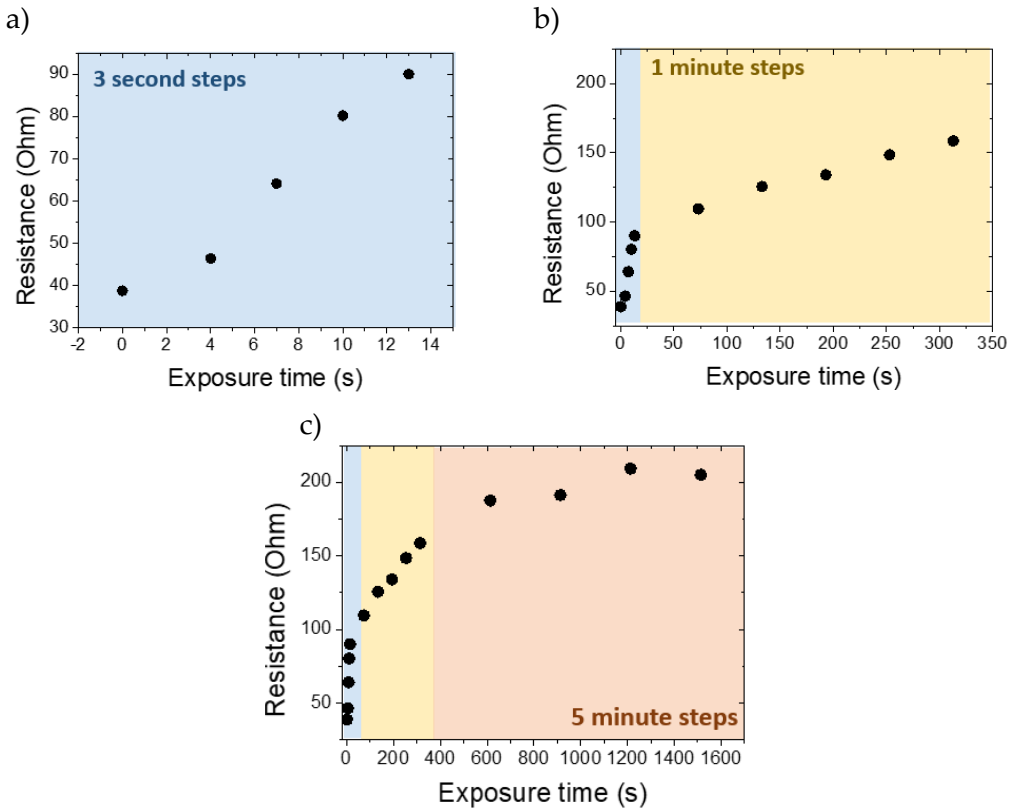

FIGURE 4.14: A) RESISTANCE MEASURED FOR CONSECUTIVE TREATMENTS WITH DETA, EACH ONE LASTING 5 SECONDS, B) RESISTANCE MEASURED FOR CONSECUTIVE TREATMENTS WITH DETA, EACH ONE LASTING 1 MINUTE, C) RESISTANCE MEASURED FOR CONSECUTIVE TREATMENTS WITH DETA, EACH ONE LASTING 5 MINUTES.

Such a trend is consistent with resistance decrease of highly dedoped PEDOT in time. It has been previously observed both chemically and electrochemically dedoped PEDOT gets redoped under ambient conditions by air oxygen, as traced by a sharp increase of conductivity[29]. This phenomenon is related to the good stability of cationic moieties in PEDOT, which does not allow a complete reduction. Another driving force is the high tendency of less stable radical-cationic PEDOT (polaron) to rapidly oxidize to dicationic (bipolaronic) PEDOT form.

4.2.3.2 Investigation on Progressive Reduction

Thermopower, electrical conductivity and UV-vis absorption spectra were measured at different oxidation levels, by means of reduction with DETA vapor.

Figure 4.15a and 4.15b show the dedoping effect on electrical conductivity and Seebeck coefficient, and the resulting thermoelectric PF for each oxidation level reached. It is interesting to notice that, as for PEDOT:Tos[4], a remarkable increase in thermoelectric power factor is recorded after a few second of exposure. In PEDOT:Tf case, the dedoping process led to a PF maximum of 69 $\mu W/K^2m$ after 5 second exposure treatment.

It should be notice that the recorded data for the untreated material (t=0 seconds) are sensibly different from the ones shown in Sect. 4.1.4 for PEDOT:Tf prepared through VPP in ethanol. This might be linked to two main factors: the first one is the sulfuric acid treatment performed on these samples, which was not performed on samples in previous sections. The oxidation

caused by sulfuric acid leads to an increase of electrical conductivity together with a decrease of Seebeck coefficient, as reported for t=0 seconds in Figure 4.15. The second factor is linked with the reactor used for VPP procedure. Since this second set of samples was prepared in University of Linköping, the reactor was different from the one used in University of Milano-Bicocca, an aspect that likely led to a difference in final material.

Then, the progressive decrease of electrical conductivity is no more compensated by the increase of Seebeck coefficient, so a worsened power factor is recorded for lower oxidation levels.

The variation in the oxidation level was monitored through the acquisition of UV-vis spectra (Figure 4.15c). As the oxidation level decreases, it is possible to see a decrease in the absorption peak above 1400 nm, owed to bipolaron presence, and an increase of the absorption peak at 900 nm, conventionally assigned to polarons[30]. For the last spectrum, it is possible to identify a small satellite peak at 600 nm, usually attributed to the presence of neutral portions in polymer chains.

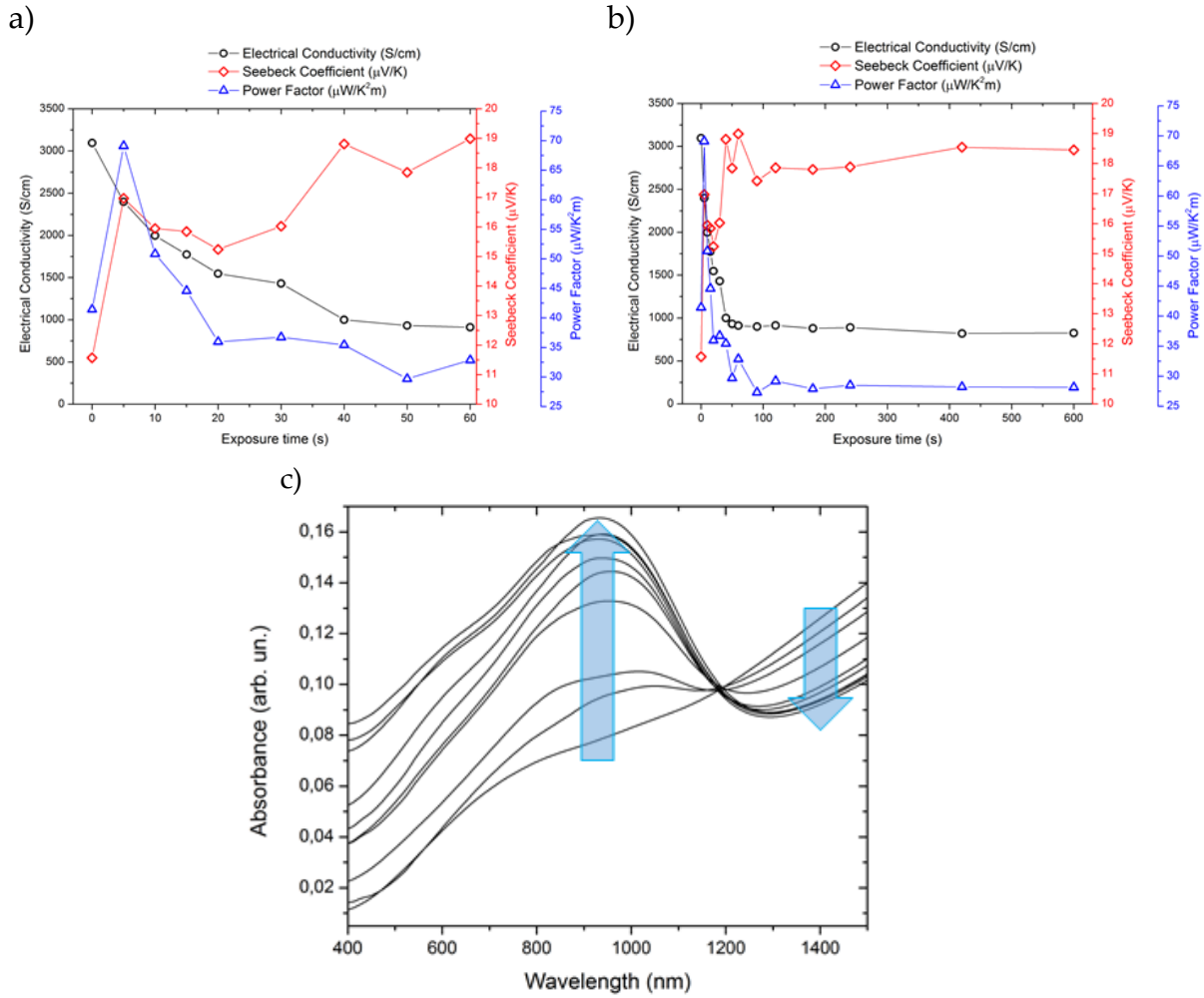

FIGURE 4.15: CHARACTERIZATIONS PERFORMED DURING DEDOPING TREATMENTS ON PEDOT:TF. A) ELECTRICAL CONDUCTIVITY, SEEBECK COEFFICIENT AND THE RESULTING POWER FACTOR ARE REPORTED FOR THE FIRST 60 SECONDS OF EXPOSURE TO THE AMINE AND B) UNTIL 600 SECONDS OF EXPOSURE. C) FOR EACH DOPING LEVEL STUDIED, AN UV-VIS SPECTRUM WAS COLLECTED. LIGHT BLUE ARROWS INDICATE THE INCREASE OF POLARONIC BAND AT 900 NM AND THE DECREASE OF THE BIPOLARONIC BAND ABOVE 1400 NM, AS THE DEDOPING PROCESS TAKES PLACE.

For longer exposure times (Figure 4.15b) all three reported quantities reached a plateau, as expected for treatments in air.

This is further proved by treatments in N_2 inert atmosphere (Figure 4.16a). In this case, remarkably lower electrical conductivity together with remarkably higher Seebeck coefficient values are measured for longer exposure times. UV-vis spectra show also an intense peak at 600 nm (Figure 4.16c), which means that the polymer has been reduced further beyond the reachable state in air, allowing the presence of a good amount of neutral portions.

a)

b)

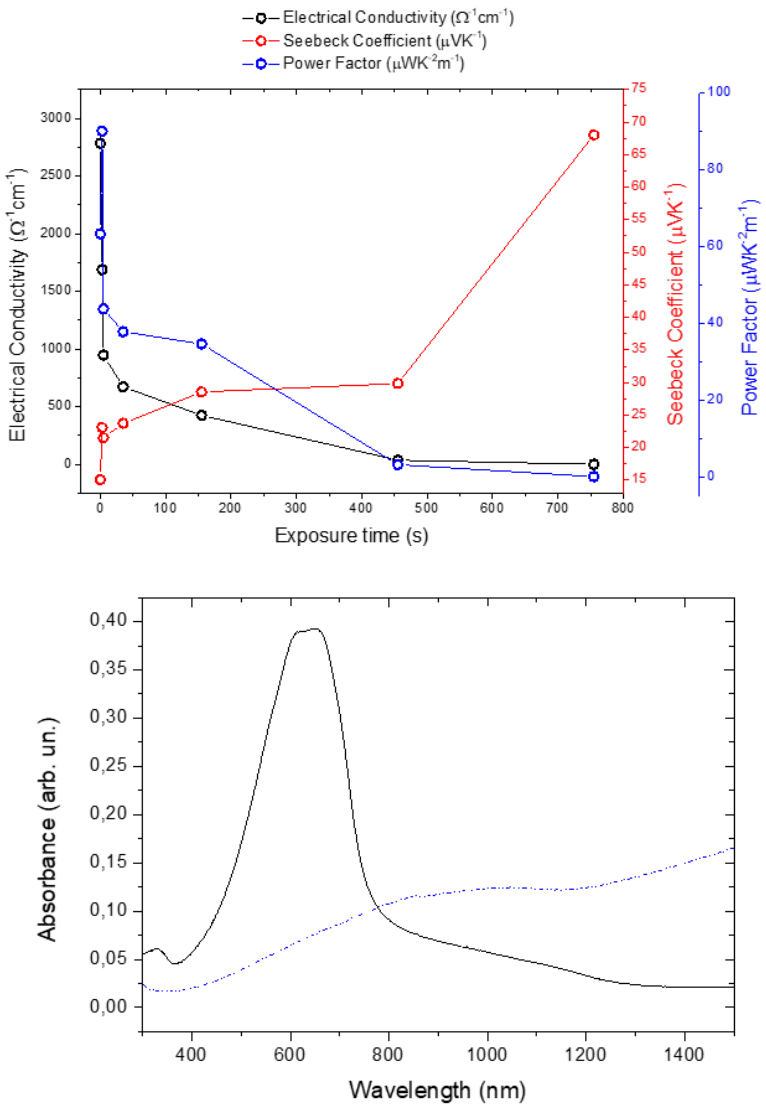

FIGURE 4.16: A) ELECTRICAL CONDUCTIVITY, SEEBECK COEFFICIENT AND THE RESULTING POWER FACTOR ARE REPORTED FOR DIFFERENT STEPS OF EXPOSURE TO DETA. B) THE UV-VIS SPECTRUM OF THE PRISTINE PEDOT:TF (BLUE DASHED LINE) IS COMPARED WITH THE ONE OF THE MATERIAL REDUCED IN INERT ATMOSPHERE, AFTER 750 SECONDS OF DETA EXPOSURE.

4.3 Conclusions

The study on parameters allowed to underline the deep influence that PEDOT intrinsic features have on final thermoelectric performance. The choice of polymerization technique,

oxidants and solvents dramatically affect both oxidation level and crystallinity of the polymer, leading to materials with completely different performances. A further investigation on the different combinations of parameters might be crucial to obtain even better PEDOT performances, based on a deeper understanding of the roles of each parameter and of their mutual interaction.

Dedoping treatment allows an enhancement of PEDOT performances due to the fine tuning of the oxidation level. Reduced PEDOT has been proven to be stable in air for a few hours, which allowed to perform time-consuming characterizations. A power factor increase was recorded after a few second exposure to DETA, almost doubling the pristine value. Such an increase is not comparable with the one observed for PEDOT:Tos[4], but validate the effectiveness of this strategy to reach better performances.

The work described in this chapter allowed to highlight the merits of PEDOT, as the possibility to easily tune its features through chemical aspects, the easiness of preparation routes and reduction treatments, and the possibility to get insights in their microstructural properties through standard techniques.

4.4 References

1 C. K. Chiang, C. R. Fincher, Y. W. Park, A. J. Heeger, H. Shirakawa, E. J. Louis, S. C. Gau and A. G. MacDiarmid, *Phys. Rev. Lett.*, 1977, **39**, 1098–1101.

2 F. Jonas, G. Heywang and W. Schmidtberg, *Ger. Offen.*, 1988, **DE 3814730**, 6.

3 F. Jonas and W. Krafft, *Eur. Pat. Appl.*, 1991, **EP0440957**.

4 O. Bubnova, Z. U. Khan, A. Malti, S. Braun, M. Fahlman, M. Berggren and X. Crispin, *Nat. Mater.*, 2011, **10**, 429–33.

5 Q. Wei, M. Mukaida, K. Kirihara, Y. Naitoh and T. Ishida, *Materials (Basel).*, 2015, **8**, 732–750.

6 O. Bubnova, Z. U. Khan, H. Wang, S. Braun, D. R. Evans, M. Fabretto, P. Hojati-Talemi, D. Dagnelund, J.-B. Arlin, Y. H. Geerts, S. Desbief, D. W. Breiby, J. W. Andreasen, R. Lazzaroni, W. M. Chen, I. Zozoulenko, M. Fahlman, P. J. Murphy, M. Berggren and X. Crispin, *Nat. Mater.*, 2014, **13**, 190–4.

7 B. Russ, A. Glaudell, J. J. Urban, M. L. Chabinyc and R. A. Segalman, *Nat. Rev. Mater.*, 2016, **1**, 16050.

8 M. Yamashita, C. Otani, M. Shimizu and H. Okuzaki, *Appl. Phys. Lett.*, 2011, **99**, 143307.

9 M. Culebras, C. M. Gómez and A. Cantarero, *J. Mater. Chem. A*, 2014, **2**, 10109.

10 K. Zuber, M. Fabretto, C. Hall and P. Murphy, *Macromol. Rapid Commun.*, 2008, **29**, 1503–1508.

11 N. Massonnet, A. Carella, A. de Geyer, J. Faure-Vincent and J.-P. Simonato, *Chem. Sci.*, 2015, **6**, 412–417.

12 Z. U. Khan, O. Bubnova, M. J. Jafari, R. Brooke, X. Liu, R. Gabrielsson, T. Ederth, D. R.

Evans, J. W. Andreasen, M. Fahlman and X. Crispin, *J. Mater. Chem. C*, 2015, **3**, 10616–10623.

13 J. Heinze, B. A. Frontana-uribe and S. Ludwigs, *Chem. Rev.*, 2010, **110**, 4724–4771.

14 A. Mohammadi, M. A. Hasan, B. Liedberg, I. Lundstroem and W. R. Salaneck, *Synth. Met.*, 1986, **14**, 189–197.

15 B. Winther-Jensen and K. West, *Macromolecules*, 2004, **37**, 4538–4543.

16 M. N. Gueye, A. Carella, N. Massonnet, E. Yvenou, S. Brenet, J. Faure-Vincent, S. Pouget, F. Rieutord, H. Okuno, A. Benayad, R. Demadrille and J. P. Simonato, *Chem. Mater.*, 2016, **28**, 3462–3468.

17 A. Elschner, W. Kirchmeyer, Stephan Lovenich, U. Merker and K. Reuter, *PEDOT: Principles and Applications of an Intrinsically Conductive Polymer*, 2010.

18 M. Mueller, M. Fabretto, D. Evans, P. Hojati-Talemi, C. Gruber and P. Murphy, *Polymer (Guildf).*, 2012, **53**, 2146–2151.

19 B. Winther-Jensen, D. W. Breiby and K. West, *Synth. Met.*, 2005, **152**, 1–4.

20 M. Fabretto, C. Jariego-Moncunill, J. P. Autere, A. Michelmore, R. D. Short and P. Murphy, *Polymer (Guildf).*, 2011, **52**, 1725–1730.

21 S. A. Mollinger, B. A. Krajina, R. Noriega, A. Salleo and A. J. Spakowitz, *ACS Macro Lett.*, 2015, **4**, 708–712.

22 Y. H. Ha, N. Nikolov, S. K. Pollack, J. Mastrangelo, B. D. Martin and R. Shashidhar, *Adv. Funct. Mater.*, 2004, **14**, 615–622.

23 C. Wood, A. Chmielewski and D. Zoltan, *Rev. Sci. Instrum.*, 1988, **59**, 951–954.

24 N. F. Mott, *Phil. Mag.*, 1969, **19**, 835.

25 A. B. Kaiser, *Adv. Mater.*, 2001, **13**, 927–941.

26 S. Kivelson and A. J. Heeger, *Synth. Met.*, 1988, **22**, 371–384.

27 J. D. Dunitz and R. Taylor, *Chem. - A Eur. J.*, 1997, **3**, 89–98.

28 A. Zykwinska, W. Domagala, B. Pilawa and M. Lapkowski, *Electrochim. Acta*, 2005, **50**, 1625–1633.

29 T. Johansson, L. A. A. Pettersson and O. Ingana, 2002, **129**, 269–274.

30 O. Bubnova and X. Crispin, *Energy Environ. Sci.*, 2012, **5**, 9345.

System Perturbation at Molecular Level: Conjugated Copolymers

5.1 Copolymers for thermoelectric application

Copolymer (CP) development appears a quite interesting and still barely explored strategy. A CP is defined as a polymer derived from more than one species of monomers[1], so that it is possible to introduce structural modifications to the polymeric chain. This strategy allows to finely tune the electronic properties of the material in order to optimize thermoelectric performances[2–4]. Nevertheless, the difficulty to control copolymer final structure is a main challenge that must be faced to practically achieve this result.

The strategy is incredibly versatile due to all the possible combinations of comonomers and their sequence inside the chain. Even though the use of copolymers in this field is still barely explored, the potentially infinite possibility of choice has led to a widespread variability of materials developed – and of results on this topic as well.

In the fifth part of this thesis, a brief organized oversight of the pioneering works on conjugated copolymers for thermoelectric application will be given to introduce and substantiate the experimental work done on partially conjugated copolymer, a PEDOT derivative and its blends with pristine PEDOT.

Table 5.1 summarizes fundamental features of the copolymers studied in literature for this application, divided in three main categories. These three categories can be thought as increasing levels of difference between the two comonomers.

The first degree of diversity is represented by copolymers made of pristine and structurally modified (P-SM) comonomers, which share a common backbone and differ only for a moiety or a heteroatom. A diversity step further, there are copolymers based on donor and acceptor (D-A) comonomers. In this case the backbone is different, but both units are aromatic, even though characterized by opposite electronic features. Finally, copolymers of conjugated and not conjugated (C-NC) comonomers can be set at the highest level of diversity, since the two units belong to different organic classes, i.e. aromatic and aliphatic.

Comonomer Nature	CP Features		Ref.
Pristine-Structurally modified (P-SM)	Random	Linear	[5,3,6,7,8]
Donor-Acceptor (D-A)	Alternating	Linear	[9,10,11,12,13,14]
	Random	Crosslinked	[15,16]
Conjugated-Not Conjugated (C-NC)	Alternating	Linear	[17]

TABLE 5.1: CLASSIFICATION OF CONJUGATED COPOLYMERS STUDIED FOR THERMOELECTRIC APPLICATION.

The copolymers differ also for the sequence of the comonomers in the chains. For linear copolymer, three sequences: random, if the two comonomers are inserted into the chain without any scheme, alternated, if the two comonomers alternate within the chain and block, if two or three portions can be identified within the chain, each one constituted by the replication of the same comonomer. In case one of the comonomers can react more than twice, the resulting copolymer is not linear anymore, but can be defined as a cross-linked copolymer. The sketch in Figure 5.1 depicts the different copolymers listed above for generic comonomers A and B.

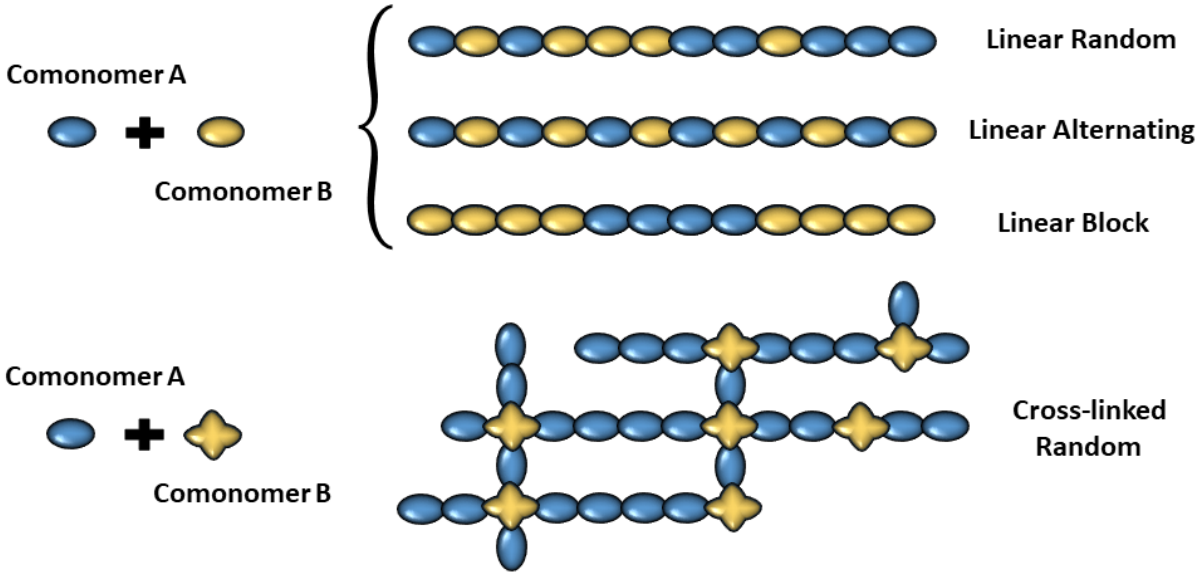

FIGURE 5.1: TWO GENERIC MONOMERS A AND B, WHICH CAN REACT TWO TIMES, ARE CONSIDERED IN THE TOP. THE POSSIBLE RESULTING SEQUENCES IN A COPOLYMERIC LINEAR CHAIN ARE RANDOM, ALTERNATING AND BLOCK. OTHERWISE, IF A COMONOMER (FOR INSTANCE, B) CAN REACT THREE OR MORE TIMES, THE LINEARITY OF CHAINS IS LOST, AND THE RESULTING COPOLYMER WILL BE CROSS-LINKED.

5.1.1 Pristine-Structurally Modified Comonomers

The use of two comonomers which are very similar is usually a strategy pursued to average the final properties observed in the two homopolimers obtained for each comonomers. The introduction of a small modification in the monomer structure can lead to deep variations in the polymer features, particularly from an intermolecular point of view. Since the relative amounts of the two comonomers can be controlled, the resulting averaging of features can be tuned with the feed ratio. Two main strategies relying on this path are worth to be mentioned: the inclusion of side moieties containing hydroxyl groups, which allows the development of hydrogen bonds that modify the interactions among chains; and the substitution of heteroatoms with smaller ones.

Through the first strategy Hiroshige et al.[3] recorded an almost four-time increase of electrical conductivity for the copolymer developed. The introduction of hydroxyl groups, in fact, increased the elasticity of the final material which could undergo to a stretching treatment. This treatment can align polymer chains and, therefore, increase electrical conductivity. It could not be performed on the too fragile homopolymer, so the macroscopic change due to the molecular modifications enabled a performance increase due to the treatment.

Introducing smaller heteroatoms (such as oxygen instead of sulphur) allowed for a better chain-chain stacking in the work of Lu et al.[7], leading to an increase in electrical conductivity. This strategy also let control the quantity of selenium introduced into a PEDOT derivative as a heteroatom alternative to sulphur, in order to see if the supposed appealing features prospected can be achieved[5].

Since the pristine-structurally modified comonomers are electronically similar, i.e. they present similar energy values of HOMO and LUMO, it is usually possible to copolymerize them with the same oxidant agent (chemical path) or at the same oxidative potential (electrochemical path). The advantage to obtain the copolymer through such easy routes is balanced by the lack of any control on the final chain sequence, which therefore will be random.

5.1.2 Donor-Acceptor Comonomers

Donor-acceptor (D-A) CPs are already well known for photovoltaic applications[18]. On a molecular level, the combination of donor and acceptor units into the same polymer leads to the possibility of tuning the band gap, to suite it to light harvesting necessities. At a supramolecular level, such combination allows for stronger intermolecular interactions, providing a better chain packing. Since the charge carrier mobility is strongly affected by the quality of chain π-π stacking, it is sensibly improved by the presence of supporting intermolecular interactions.

For TE applications, the second aspect is particularly interesting. An improvement in charge carrier mobility has a beneficial impact on electrical conductivity, but should not affect, at least not in a major way, Seebeck coefficient. The expected TE PF enhancement motivates the interest in such a strategy.

In order to obtain the features described above, donor and acceptor units should be strictly alternating into the macromolecule[18]. The control of copolymer stereochemistry requires a synthetic path of multiple coupling reaction among precursors of the two comonomers. This requirement is not only costly, but usually means also that the two reference homopolimers may not be available to evaluate the efficacy of the strategy through performance comparison.

5.1.3 Conjugated-Not Conjugated Comonomers

Studies on thermoelectric properties of CPs have shown that decreasing chain oxidation level involves a decrease of electrical conductivity, while enhancing the Seebeck coefficient value. Such procedure has been used to find the best trade-off value of the two quantities to obtain

the highest PF, usually found in slightly reduced polymers[19]. The stability of the CP in this condition depends on the tendency of the material itself to oxidise again, usually through interactions with the environment.

It is possible to mimic the reduction of the CP, obtaining a permanent decrease of charge carriers, including insulating portions into the chains. Such structural modification leads to C-NC CP development.

It should be noticed that this strategy is the least studied among the ones listed. Since performance increasing usually happen through electrical conductivity enhancement, including non-conductive units into the chain appears counterproductive under this point of view. For the pristine copolymer, in fact, the presence of insulating portions causes an extremely high Seebeck coefficient combined with low electrical conductivity, which may lead to poor PF values. Nevertheless, C-NC polymers give the unravelled possibility to tune electrical features of the material by blending the copolymer with fully conjugated homopolymer, as it has been done by Taylor et al.[17].

Unexpectedly, the authors found out that the measured features of the blends are not the simple averaging of the two component properties. A general decrease of electrical conductivity was observed for C-NC CP rich blends, even lower than C-NC CP value itself, and a remarkable increase of the Seebeck coefficient only in one case.

Authors hypothesized that in such conditions of mixing, a phase segregation between the two components is most likely to happen, leading to the unexpected behaviour of the blends.

On the contrary, blends rich in fully conjugated homopolymer showed a higher electrical conductivity than the pristine MEH-PPV, and a Seebeck coefficient value only slightly different. In this case, the explanation proposed focused on the effect of not conjugated chains on the morphology of the final material. In fact, it has already been proven that a small amount of aliphatic glycolic copolymer improves the final CP film quality, leading to a better electrical conductivity[20,21].

Blend development leads to a dramatic increase of system complexity, since not only must the single component features be taken in account in such final mixture, but one should also account for the interaction among the two components and their morphological effect on the final material. Future studies on this kind of materials should address a deep insight in this matter, to provide a complete explanation on the unexpected behaviour of the blend. Nonetheless, such interesting behaviour may be a novel key to reach a further comprehension of CP based material physical-chemical characteristics.

5.2 Development of EDOT based C-NC Copolymer

Inspired by the work of Taylor et al.[17], a C-NC CP has been developed using, as conjugated portions, PEDOT oligomer. The central one is a PEDOT-C6 oligomer, while two lateral aliphatic chains are non-conjugated units.

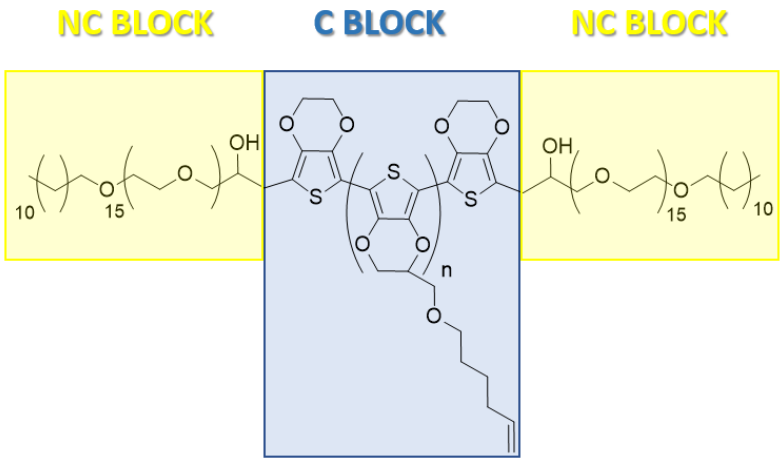

FIGURE 5.2: MOLECULAR STRUCTURE OF C-NC EDOT BASED COPOLYMER. CENTRAL CONJUGATED (C) PORTION IS HIGHLIGHTED IN BLUE, WHILE THE TWO LATERAL NOT CONJUGATED (NC) ONES ARE YELLOW HIGHLIGHTED.

PEDOT, as largely reported in previous chapters, is one of the most studied conjugated polymers for this application and displays various advantages in thermoelectric application. Therefore, it is a convenient choice for the conjugated building block.

The copolymer was synthetized by the Organic Synthesis Laboratory of Prof. Luca Beverina (Department of Material Science at University of Milano-Bicocca), in a nitromethane suspension. Electrical properties of copolymer films were measured and compared with pristine homopolymer (PEDOT) ones. Then, films made of blends of CP and PEDOT were prepared, tuning the concentration of the two components, and characterized in the same way.

5.2.1 Experimental Procedure

5.2.1.1 C-NC Copolymer

The copolymer was obtained through in situ polymerization of EDOT and a functionalized EDOT which acted as terminator[22]. The functionalized EDOT (Structure A) was obtained by the reaction:

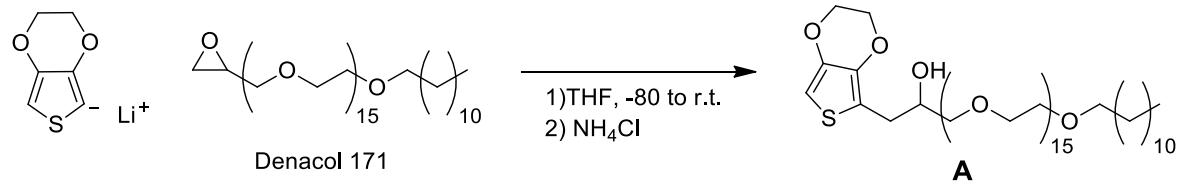

Structure A and EDOT-C6 were then added to an oxidative solution of $FeTos_3$ (0.15M in CH_3CN). Two different feed ratios EDOT-C6:A, 20:1 and 30:1, were used. The oxidative solution containing the two monomers was stirred for 48 hours, and then cyclomixed at 3500 rpm for 20 minutes. The solid was washed several times with ethanol and then dispersed in CH_3NO_2 at 1% wt.

The two different feed ratios led to copolymer CP1 (20:1) and copolymer CP2 (30:1).

5.2.1.2 Film preparation

Film samples of C-NC copolymer itself were prepared simply by filming with blade coating (Doctor Blade, wet thickness 254 μm) the suspension in nitromethane on cleaned Kapton substrates, and then by annealing the film in air at 70°C for 2 hours. The blade coating technique (Figure 5.3) is quite popular to prepare thin films starting from a solution. The solution is spread onto the substrate through an automated blade. The fixed distance between the blade edge and the substrate and the speed of the blade are the two parameters that can been tuned to modify the film thickness.

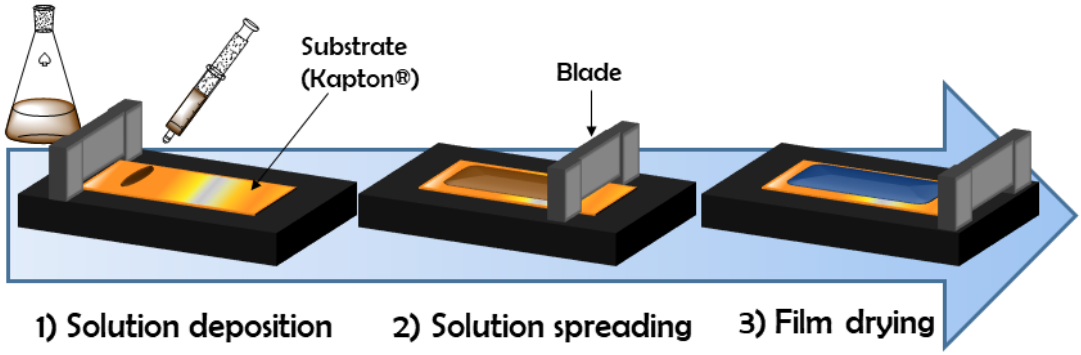

FIGURE 5.3: SKETCH OF FILM MAKING THROUGH BLADE COATING. 1) THE POLYMERIZATION SOLUTION IS DROPPED ON THE SUBSTRATE, 2) THE BLADE RUNS OVER THE SUBSTRATE, HOMOGENOUSLY SPREADING THE SOLUTION ON IT, 3) THE WET FILM IS ANNEALED TO EVAPORATE THE SOLVENT AND PROMOTE THE POLYMERIZATION REACTION IN IT.

Blend film samples have been prepared adding C-NC copolymer suspension to the solution used for *in situ* polymerization[23]. Polymerization solutions were a mixture of Clevios™ CB 40 V2 (1000 mg) and Pluronic® P-123 (200 mg), which were stirred for 8 hours and then immersed in an ultrasound bath for 30 minutes until homogeneous. C-NC copolymer was then added in different concentrations for different samples. The resulting mixture was stirred and then put in an ultrasound bath for several minutes, until homogeneous. EDOT (28 μL) was poured into the cooled down mixture (−20 °C), and everything was stirred for 15 minutes. The final ratio EDOT:$Fe(Tos)_3$:pyridine was 1:2.55:1.1.

Afterwards, the mixture was filmed through blade coating technique (using Doctor Blade, wet thickness 254 μm) on cleaned Kapton® substrates. Films were annealed in air at 70°C for 2 hours, then, after cooling down at room temperature, rinsed in ethanol to wash the residual $Fe(Tos)_3$ and $Fe(Tos)_2$. A final annealing was performed at 70°C for 30 minutes.

PEDOT:Tos films were obtained through the same technique but without including the C-NC adding step.

For electrical measurements, rectangular samples (0.4-0.5x3.0-3.5 cm^2) and square samples (2.5x2.5 cm^2) were cut from the obtained films. On the formers, two gold electrodes (100-150 nm of thickness) were evaporated at the two sides of the sample, while on the latters four gold electrodes were evaporated at the four corners. After electric and thermoelectric characterization, the samples were used for morphological characterization (SEM and AFM).

UV-vis spectra were recorded with a JASCO V-570 using sample prepared on glass substrates.

5.2.1.3 Characterization

Four blends were prepared and characterized, and their properties were compared with the ones recorded for the pristine PEDOT:Tos and copolymer blends. Electrical conductivity and Seebeck coefficient were measured using the set up described in Sect. 4.1.3.1.

Table 5.2 shows the results obtained for the copolymers.

Samples	A:EDOT Feed Ratio %	Electrical Conductivity ($\Omega^{-1}cm^{-1}$)	Seebeck Coefficient (μVK^{-1})	Power Factor ($\mu WK^{-1}m^{-2}$)
CP1 dispersion	5	0.051±0.007	57.7±1.1	0.021±0.003
CP2 dispersion	3.3	0.064±0.009	27.2±0.2	0.005±0.001

TABLE 5.2: ELECTRICAL AND THERMOELECTRICAL CHARACTERIZATION OF COPOLYMER FILMS.

Electrical conductivity is 4 order of magnitude lower than the one recorded for pristine PEDOT:Tos, while the Seebeck coefficient values are remarkably higher. Therefore, as expected the presence of NC portions into the chains impacts both charge carrier density and mobility. Table 5.3 shows the results obtained for blends of copolymers and PEDOT:Tos.

Samples	CP concentration (% wt)	Electrical Conductivity ($\Omega^{-1}cm^{-1}$)	Seebeck Coefficient (μVK^{-1})	Power Factor ($\mu WK^{-1}m^{-2}$)
Blend CP1 A	0.01	510±74	18.3±0.5	17.2±0.6
Blend CP1 B	0.1	320±14	16.4±0.2	8.6±0.2
Blend CP1 C	1	149±26	18.4±0.3	5.0±0.5
Blend CP2 A	0.01	495±25	17.6±0.4	15.4±0.3
Blend CP2 B	0.1	368±41	16.7±0.2	10.3±0.3
Blend CP2 C	1	253±24	19.2±0.4	9.3±0.4
PEDOT:Tos	0	393±22	18.5±0.6	13.5±0.2

TABLE 5.3: ELECTRICAL AND THERMOELECTRICAL CHARACTERIZATION OF COPOLYMER BLENDS.

Electrical conductivity is found to decrease for copolymer-rich samples, while Seebeck coefficient does not display a correspondent increase, leading to the conclusion that copolymer presence mainly affects polymer morphology in blends.

Thus, UV-vis adsorption was analysed for all samples to check if electrical performances were related to the oxidation degree (Figure 5.4).

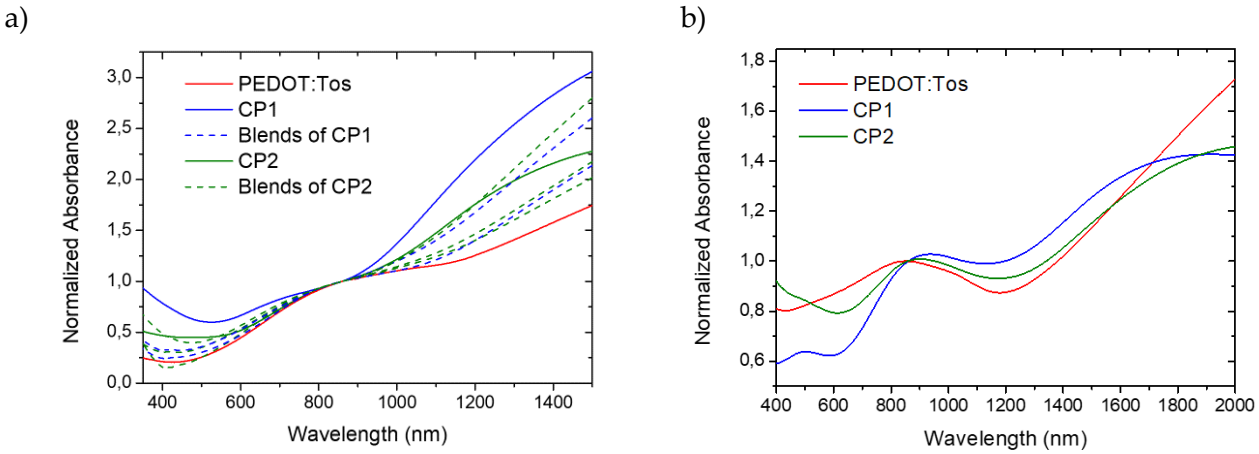

FIGURE 5.4: UV-VIS SPECTRA OF COPOLYMER, BLEND AND PEDOT:TOS FILMS COLLECTED IN THE RANGE 350 NM-1500 NM (A) AND IN THE RANGE (400 NM-2000 NM).

Interestingly, bipolaronic band shows a blue shift with respect to pristine PEDOT:Tos for both copolymer absorption spectra (Figure 5.5b). This might be imputed to shorter conjugation length (larger HOMO-LUMO gaps) in copolymer macromolecules. In other words, copolymer chains are expected to be shorter than PEDOT:Tos ones. This is consistent with the polymerization mechanism involving the presence of a terminator. In fact, copolymers prepared with a larger amount of terminator (CP1) present a bigger blue shift. Unfortunately, the blue shift of the two copolymer spectra makes the evaluation of sample oxidation state not possible. The shift, in fact, forbids the comparison of absorbance at the same wavelength.

A further analysis of the samples was carried out with electrical conductivity measurements at different temperature, obtained with the experimental setup described in Sect. 4.1.3.2.

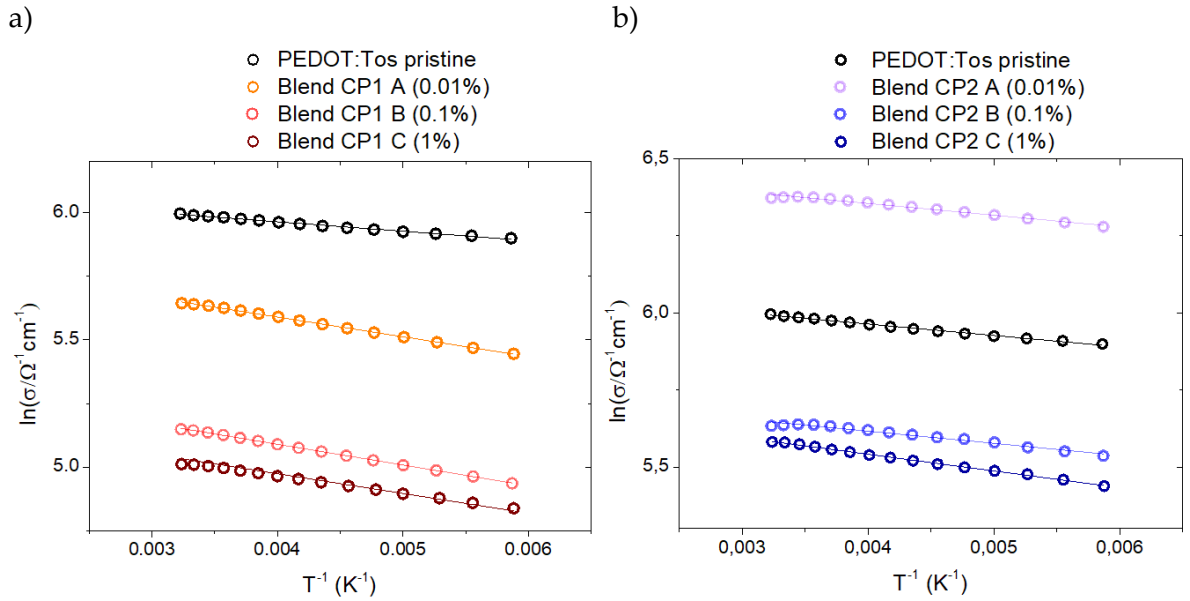

FIGURE 5.5: NATURAL LOGARITHM OF ELECTRICAL CONDUCTIVITY PLOTTED *VERSUS* TEMPERATURE INVERSE FOR CP1 BLENDS (A) AND CP2 BLENDS (B). IN BOTH GRAPHS, PRISTINE PEDOT:TOS IS REPORTED AS BLACK DOTS.

Figure 5.5 shows electrical conductivity values at different temperatures for both the sets of data. Within the assumption charge transport dominated by fixed-range hopping, it is possible to write the following relation[24] for the electrical conductivity (σ):

$$\ln(\sigma) = \ln(\sigma_0) - \frac{E_a}{k_B T} \tag{5.1}$$

For sake of simplicity, fixed-range hopping was used instead variable range hopping (VRH). The use of this model allowed to obtain activation energy (E_a) value, which can be used as a tool to easily compare hopping mechanism in each sample.

The data collected in Figure 5.5 were found in good agreement with equation 5.1. Activation energy (E_a) values can be calculated from curve fitting. This value can be interpreted as the energy that charge carrier needs to hop from one site to another. It is therefore mainly related to the composition and the morphology, i.e. crystallinity, of the polymer. The values are reported in Table 5.4.

Samples	CP concentration (% wt)	Activation Energy Ea (meV)
PEDOT:Tos	-	3.20±0.06
Blend CP2 A	0.01	3.27±0.12
Blend CP2 B	0.1	4.40±0.15
Blend CP2 C	1	4.67±0.05
Blend CP1 A	0.01	3.68±0.05
Blend CP1 B	0.1	7.02±0.03
Blend CP1 C	1	6.7±0.6
CP2	-	46.6±1.6

TABLE 5.4: ACTIVATION ENERGY VALUES FOR THE SAMPLES OF THE SET.

Unfortunately, CP1 presented a resistance too high (> 1 GΩ) to be measured in the setup. For the values calculated for the rest of the sample set, a general increase of activation energy was found in PEDOT blends with CP, with slightly higher values for CP1 blends over CP2 blends. The value calculated for CP2 film is one order of magnitude higher than the ones recorded for pristine PEDOT:Tos. This result validated the idea of a strong morphological impact of the copolymer on the PEDOT:Tos.

A deeper comprehension on material morphology was eventually obtained through the analysis of images acquired with scanning electron microscope (SEM) (Figure 5.6).

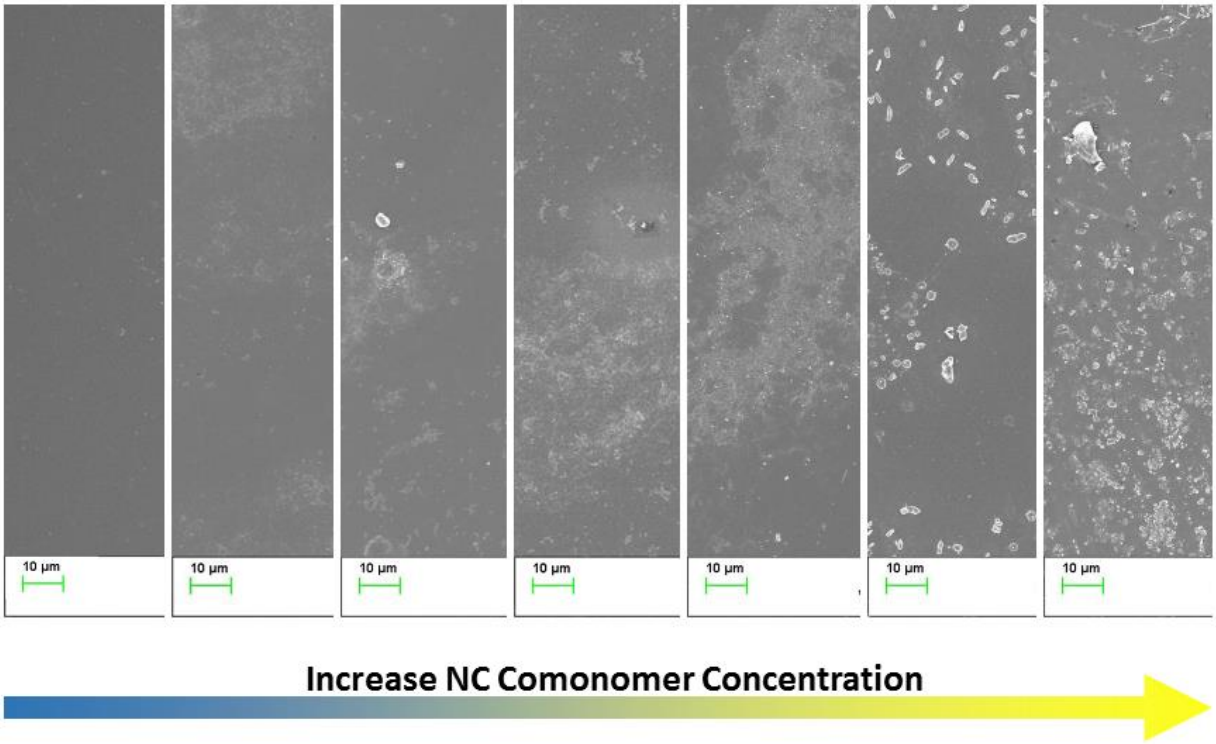

FIGURE 5.6: SEM IMAGES OF PEDOT:TOS, COPOLYMER BLEND AND PRISTINE COPOLYMER FILMS.

Figure 5.6 shows the effect of increasing CP concentration into the film. The first image was taken from a PEDOT:Tos pristine film. It shows a homogeneous dark grey layer. With the increase of the copolymer presence, white spots start to appear and become bigger and denser with the increase of NC comonomer presence.

Such behaviour suggests that long side glycolic chains of the copolymer agglomerate, generating insulating domains within the polymer film.

5.2.2 Charge Transport Percolative Behaviour

The dramatic effect of insulating chains on polymer morphology led to consider the presence of a certain amount of NC comonomer as the determining factor on transport properties of the final material. Therefore, we considered that the feed ratio A:EDOT, used during the preparation of the CP, is preserved in final CP. This is a quite rough estimation, since we consider that reagents completely turn into products, which is not usually the case. However, within this assumption, we could estimate the ratio among the terminator A and the overall EDOT and EDOT-C6 monomers in PEDOT and CP blends, without taking into account the difference among CP1 and CP2.

This information is useful to plot electrical conductivity of different materials *versus* the A:EDOT ratio. Figure 5.7 shows the resulting trend.

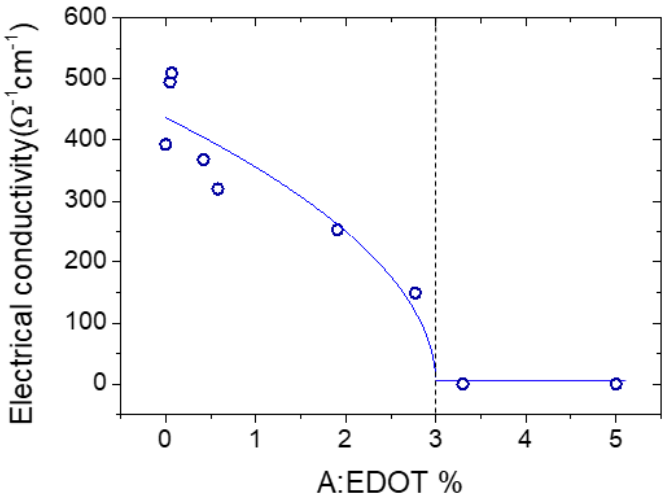

FIGURE 5.7: ELECTRICAL CONDUCTIVITIES PLOTTED VERSUS TERMINATOR (A)/EDOT RATIO. PERCOLATION THRESHOLD VALUE IS MARKED BY THE DASHED LINE.

The data collected seem to follow a percolation regime, with a percolation threshold x_c=3 %. The trend can be fitted by the following[25]:

$$\begin{aligned} \sigma(x) &\propto (x_c - x)^s \qquad if\ x \leq x_c \\ \sigma(x) &= 0 \qquad\qquad\quad if\ x > x_c \end{aligned} \tag{5.2}$$

where s is a constant. A similar behaviour, even though less marked, can be supposed for Seebeck coefficient, as shown in Figure 5.8.

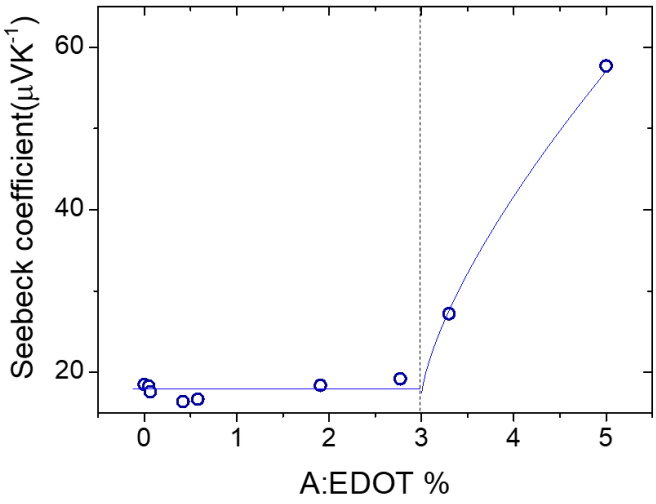

FIGURE 5.8: SEEBECK COEFFICIENT PLOTTED VERSUS TERMINATOR (A)/EDOT RATIO. PERCOLATION THRESHOLD VALUE IS MARKED BY THE DASHED LINE.

In this case the trend has been fitted according to the following:

$$\begin{aligned} \alpha(x) &\propto 18.5 + (x - x_c)^s \qquad if\ x \geq x_c \\ \alpha(x) &= 18.5 \qquad\qquad\qquad\quad if\ x < x_c \end{aligned} \tag{5.3}$$

where the Seebeck coefficient assumes the value recorded for PEDOT:Tos for x values lower than x_c.

As already stated in Chapter 2, percolation concept has been already used in description of charge transport in conjugated polymers[26–28]. Percolation paths are supposed to connect crystallites through the so-called "tie-chains", which cross the less conductive amorphous domains. Such a behaviour is considered responsible for high conductivities in low-crystallinity samples[29]. Figure 5.9a sketches this situation. In this case percolation path can be found connecting different crystallites.

If we think to add to such a system a small amount of copolymer CP1 or CP2, we can obtain the situation in Figure 5.9b. NC portions of the chain are expected to segregate, but for small amounts of CPs the percolation paths are not disrupted and the charge transport behaviour is reasonably the same. Increasing the amount of CP, we should keep in mind two facts. CP side chains are bulky and would most likely make more difficult for the central PEDOT portion to pack with other chains. A second aspect we must deal with is the presence of a third kind of domains, other than crystalline and amorphous, the completely insulating ones (yellow).

This means that, as we increase the concentration of CP, we likely obtain a more amorphous material, in which insulating domains worsen the connection among the different crystallites (Figure 5.9c).

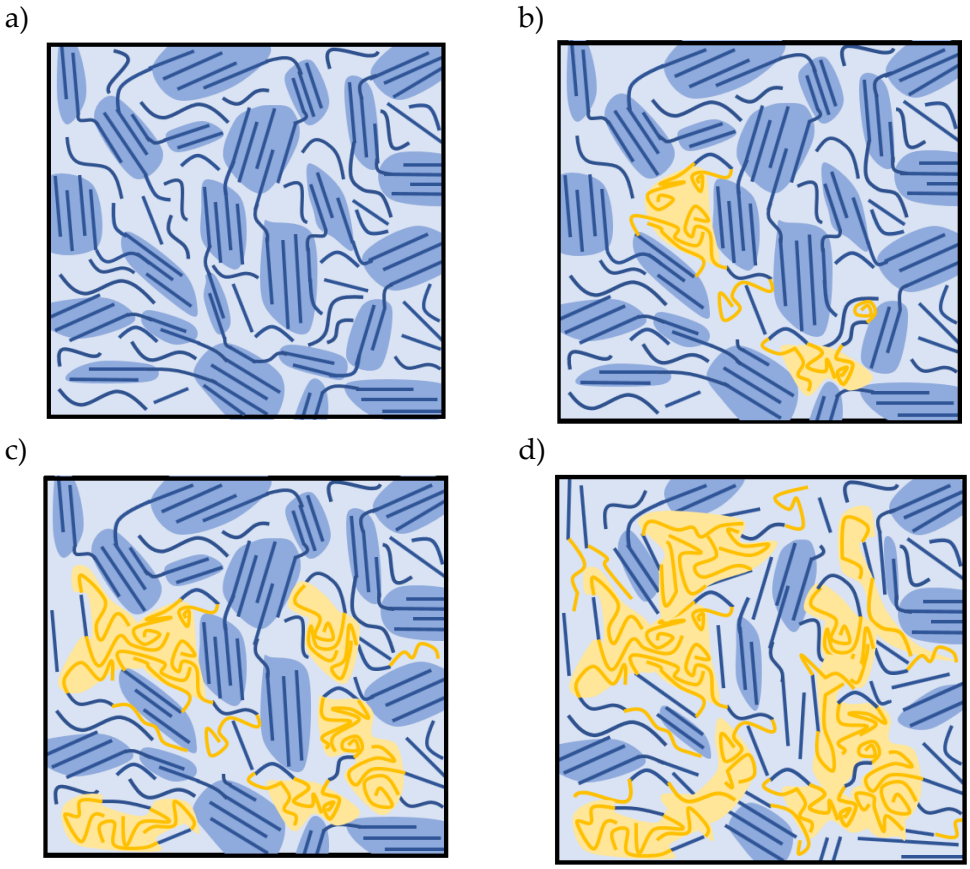

FIGURE 5.9: SKETCH OF MATERIAL SUPPOSED MORPHOLOGY AS CP CONCENTRATION INCREASE. A) PRISTINE PEDOT:TOS REPRESENTATION, WHERE SMALL CRYSTALLITES (DARKER BLUE DOMAINS) ARE CONNECTED AMONG EACH OTHER, SURROUNDED BY AMORPHOUS MATERIAL (LIGHT BLUE). THE ADDITION OF CP CONTAINING INSULATING CHAIN PORTIONS (YELLOW LINES) WILL GENERATE INSULATING DOMAINS INSIDE THE MATERIAL. A SMALL AMOUNT (B) IS NOT DRAMATICALLY AFFECTING THE STRUCTURE. AN INCREASE OF CP (C) CONCENTRATION WILL START TO BE DISRUPTING, BUT STILL WILL NOT PREVENT MOST OF THE PERCOLATION PATHS. FOR A CERTAIN THRESHOLD CONCENTRATION VALUE (D), THE PERCOLATION PATHS ARE DISRUPTED, PREVENTING MOTION OF CHARGE CARRIERS.

Eventually, for a certain threshold value of CP concentration, the percolation paths are disrupted, the material is mainly amorphous and starts to behave as an insulator (Figure 5.9d).

For A:EDOT ratio lower than threshold value, conductivity is affected by the morphology-disrupting effect and the decrease of percolation path density, while Seebeck coefficient is substantially unaltered. Above the percolation threshold, we can suppose that no more percolative paths allow for conduction, leading to electrical conductivity values close to zero. The insulating behaviour is beneficial for Seebeck coefficient, which increases after the threshold.

5.3 Conclusions

The use of copolymers for thermoelectric application opens a great opportunity to obtain specific features through molecular structure tuning. It represents also a challenge, since copolymers imply an increase in structural complexity. Our study aimed to obtain a trade-off between two features, namely exploiting the simultaneous increase of Seebeck coefficient and the decrease of electrical conductivity due to the introduction of insulating portions into the material. We found the presence of a percolative behaviour in the novel material, which is dependent upon the concentration of insulating chain portions, but independent of the length of CP conjugated portion length. This provided insights in the charge transport behaviour of CP and its blends, which can be exploited for further studies on copolymer for thermoelectric application.

It should be also noticed that for small concentration of CPs (A:EDOT=0.04-0.06) a small increase in conductivity was found. Even though further studies are needed to get a precise comprehension of the phenomenon, a possible reason behind this increase might be found in beneficial effects of small amounts of glycolic chains. In previous studies[20,30], an increase in conductivity was found adding small amounts of polyglycols to PEDOT:Tos, followed by a decrease for higher concentrations. The explanation dealt with the screening effect acted by polyglycol chains for counterion charge and improved order of PEDOT chains, similar to the effect attributed to ethylene glycol[31,32].

Therefore, the effect of polyglycolic side chains might be more complex than the one supposed in the discussion presented and further studies will address this topic.

5.4 References

1 A. D. Jenkins, P. Kratochvíl, R. F. T. Stepto and U. W. Suter, *Pure Appl. Chem.*, 1996, **68**, 2287–2311.

2 R. Yue, S. Chen, C. Liu, B. Lu, J. Xu, J. Wang and G. Liu, *J. Solid State Electrochem.*, 2011, **16**, 117–126.

3 Y. Hiroshige, M. Ookawa and N. Toshima, *Synth. Met.*, 2006, **156**, 1341–1347.

4 S. Chen, B. Lu, J. Xu, L. Qin, Z. Wang and X. Duan, *J. Appl. Polym. Sci.*, 2013, **129**, 1717–1725.

5 S. Chen, B. Y. Lu, J. K. Xu, L. Q. Qin, Z. P. Wang and X. M. Duan, *J. Appl. Polym. Sci.*, 2013, **129**, 1717–1725.

6 H. Gu, S. Ming, K. Lin, H. Liu, S. Chen, B. Lu and J. Xu, *J. Electron. Mater.*, 2017, **46**, 3124–3130.

7 B. Lu, S. Chen, J. Xu and G. Zhao, *Synth. Met.*, 2013, **183**, 8–15.

8 Q. Wei, Y. Sugihara, T. Tanabe, M. Mukaida, K. Kirihara, Y. Naitoh and T. Ishida, *Polym. (United Kingdom)*, 2015, **66**, 38–42.

9 R. B. Aïch, N. Blouin, A. Bouchard and M. Leclerc, *Chem. Mater.*, 2009, **21**, 751–757.

10 S. Ming, S. Zhen, K. Lin, L. Zhao, J. Xu, B. Lu, L. Wang, J. Xiong and Z. Zhu, *J. Electron. Mater.*, 2015, **44**, 1606–1613.

11 Q. Zhang, Y. Sun, W. Xu and D. Zhu, *Macromolecules*, 2014, **47**, 609–615.

12 I. Lévesque, P.-O. Bertrand, N. Blouin, M. Leclerc, S. Zecchin, G. Zotti, C. I. Ratcliffe, D. D. Klug, X. Gao, F. Gao and J. S. Tse, *Chem. Mater.*, 2007, **19**, 2128–2138.

13 C. Mai, R. A. Schlitz, G. M. Su, D. Spitzer, X. Wang, S. L. Fronk, D. G. Cahill, M. L. Chabinyc and G. C. Bazan, 2014, 2–5.

14 A. Liang, X. Zhou, W. Zhou, T. Wan, L. Wang, C. Pan and L. Wang, *Macromol. Rapid Commun.*, 2017, **201600817**, 1600817.

15 R. Yue, S. Chen, C. Liu, B. Lu, J. Xu, J. Wang and G. Liu, *J. Solid State Electrochem.*, 2012, **16**, 117–126.

16 R. Yue, B. Lu, J. Xu, S. Chen and C. Liu, *Polym. J.*, 2011, **43**, 531–539.

17 P. S. Taylor, L. Korugic-Karasz, E. Wilusz, P. M. Lahti and F. E. Karasz, *Synth. Met.*, 2013, **185–186**, 109–114.

18 K. Müllen and W. Pisula, *J. Am. Chem. Soc.*, 2015, **137**, 9503–9505.

19 O. Bubnova, Z. U. Khan, A. Malti, S. Braun, M. Fahlman, M. Berggren and X. Crispin, *Nat. Mater.*, 2011, **10**, 429–33.

20 M. Fabretto, C. Jariego-Moncunill, J. P. Autere, A. Michelmore, R. D. Short and P. Murphy, *Polymer (Guildf).*, 2011, **52**, 1725–1730.

21 K. Zuber, M. Fabretto, C. Hall and P. Murphy, *Macromol. Rapid Commun.*, 2008, **29**, 1503–1508.

22 C08F 126/06, 26/06, 234/04, 2003.

23 T. Park, C. Park, B. Kim, H. Shin and E. Kim, *Energy Environ. Sci.*, 2013, **6**, 788.

24 N. F. Mott, *J. Non. Cryst. Solids*, 1972, **8–10**, 1–18.

25 S. Kirkpatrick, *Rev. Mod. Phys.*, 1973, **45**, 574–588.

26 S. A. Mollinger, B. A. Krajina, R. Noriega, A. Salleo and A. J. Spakowitz, *ACS Macro Lett.*, 2015, **4**, 708–712.

27 P. Stallinga, *Adv. Mater.*, 2011, **23**, 3356–3362.

28 S. Dongmin Kang and G. Jeffrey Snyder, *Nat. Mater.*, 2016, **16**, 252–257.

29 R. Noriega, J. Rivnay, K. Vandewal, F. P. V Koch, N. Stingelin, P. Smith, M. F. Toney and A. Salleo, *Nat. Mater.*, 2013, **12**, 1038–44.

30 T. Wang, Y. Qi, J. Xu, X. Hu and P. Chen, *Chinese Sci. Bull.*, 2003, **48**, 2444.

31 A. Dkhissi, D. Beljonne and R. Lazzaroni, *Synth. Met.*, 2009, **159**, 546–549.

32 A. Dkhissi, D. Beljonne, R. Lazzaroni, F. Louwet and B. Groenendaal, *Theor. Chem. Acc.*, 2008, **119**, 305–312.

System Perturbation at Supramolecular Level:
Inorganic Nanostructure Inclusion

6.1 ICP Based Nanocomposites

In the third part of the thesis, the influence of the presence of inorganic nanostructures on PEDOT thermoelectric properties has been studied. Inclusion of inorganic nanostructures in ICPs has already been explored as possible path to obtain TE performance implementation.

Such an assumption is based on Hicks and Dresselhaus seminal papers, published in early 1990s, which postulated that control over material dimensionality could be the key to obtain extremely high TE performances[1]. This hypothesis led to the development of a large variety of complex thermoelectric materials[2] over the last three decades, made of mixture of phases, patterned superlattices, embedded structures and composite materials. ICP based nanocomposites represent the newest offspring of this area.

These nanocomposites are usually made of two separate phases, one of which is an ICP, while the other is an inorganic (metallic or semiconductor) nanomaterial or a carbon-based one (graphene or carbon nanotubes CNTs). The enhancement of TE performance in these materials is owed to a change in charge transport properties thanks to polymer/nanostructure interaction.

Charge transport properties of a composite are, quite obviously, affected by the component ones. Particularly, for thermoelectric properties, Bergman and Levy demonstrated that composite ZT can never exceed each component ones[3]. Nevertheless, in ICP nanocomposites, the nanoscale interaction can lead to novel effects that allow to overcome such limit and to achieve higher performances than those of each components.

Different effects have been hypothesized for such increase[4]: energy filtering, heterojunction charge transfer, thermal conductivity reduction and polymer structural change at polymer/nanostructure interface. They are schematically depicted in Figure 6.1.

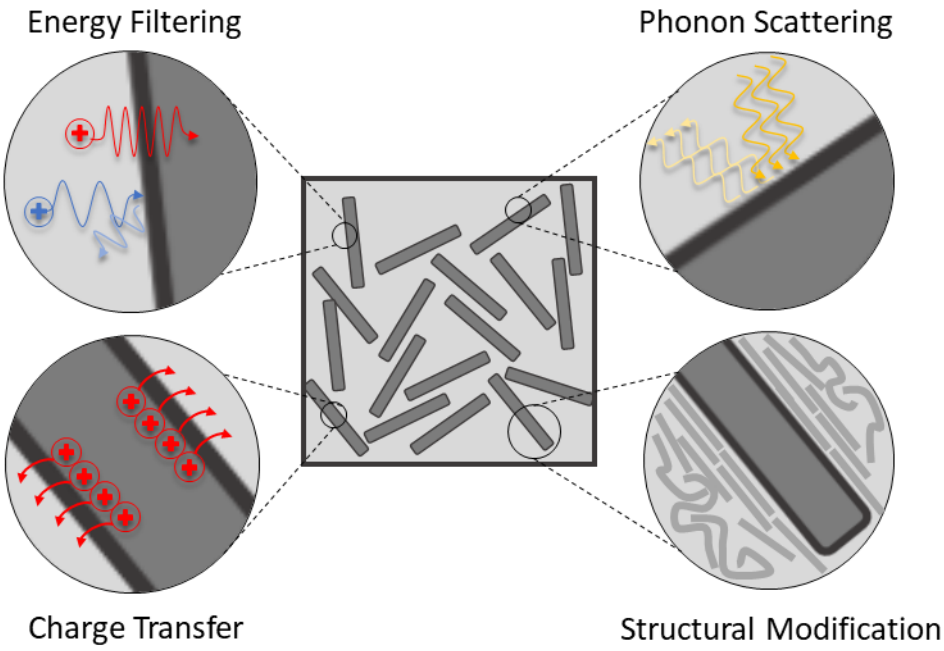

FIGURE 6.1: IN THE CENTRAL SQUARE IS REPORTED A SKETCH OF A GENERIC POLYMER (LIGHT GREY)/NANOSTRUCTURE (DARK GREY RODS) BLEND. THE FOUR ZOOMS SCHEMATICALLY DEPICT THE FOUR EFFECTS SUPPOSED TO HAPPEN AT THE INTERFACE BETWEEN THE TWO PHASES AND THAT WILL BE BRIEFLY DESCRIBED IN THE NEXT PARAGRAPHS.

All the effects hypothesized to motivate nanocomposite peculiar behaviour are yet to be fully experimentally proven, mainly because it is quite difficult to obtain direct evidences of nanostructure/ICP interactions.

The experimental work described in Sect. 6.2 focused on the attempt to analyse such ICP nanostructure interaction. PEDOT based nanocomposites were obtained embedding two nanostructured metal oxides, manganese (II,III) oxide (Mn_3O_4) and copper (II) oxide (CuO) in *in situ* polymerized films. The choice of these metal oxides was guided by different requirements. First, a p-type semiconducting material was needed, to avoid the generation of a p-n junction within the composite. The second parameter was a work function close to PEDOT one, to avoid the development of large potential barriers, which would have localized most of the carriers at interfaces. In third place, metal oxides nanostructures were easily made through wet chemical process and easily dispersible in alcoholic polymerization solution. We decide not to use high performing TE material as nanostructured fillers for two main reasons: on one side, since organic TE has been developed to replace toxic and expensive TE material, i.e. Bi_2Te_3, using it as a filler would be in contrast with this aim. On the second hand, we wanted to base the choice of the material on the parameters that influence its interaction with the ICP, rather than just using the ICP as a conductive matrix in which dispersing highly performing nanostructures.

Set of the two nanocomposite materials were made with different concentrations of nanostructured oxides and their properties were studied in comparison with PEDOT itself, to understand changes owed to nanostructure presence.

Before getting to the description of experimental work on this topic, a brief explanation on each of the four effects hypothesized to happen due ICP/nanostructure interaction will be given. Since the subject is still under investigation, a more detailed explanation of the expected phenomena can give a better idea on such materials behaviours.

6.1.1 Energy Filtering of Charge Carriers

The possibility to filter charge carriers at polymer/nanostructure interface relies on the generation of potential barriers due to an energetical mismatching between the two phases. "Cold" charge carriers, i.e. the less energetic ones, can be localized by the potential barrier, while the hot ones have enough energy to overcome it and keep on migrating in the material.

Such effect, usually called "energy filtering", has been proven to be beneficial for the thermoelectric properties of materials in inorganic samples[5]. In fact, localization of part of charge carriers leads to a Seebeck coefficient increase, while, on the other side, the selection of fastest carriers provides an enhancement of charge carrier average mobility $\mu(E)$. Thus, the detrimental effect of charge carrier decrease on electrical conductivity σ is partially compensate by mobility increase. The overall effect is a TE PF enhancement.

This effect was first demonstrated in inorganic systems[6], and only subsequently it was also observed for organic/inorganic nanocomposites in single-molecule junctions[7,8].

Even though this phenomenon has been observed more than once in single-molecule junctions, its presence in polymer/inorganic nanocomposite is still scarcely reported[9] and discussed by the scientific community.

6.1.2 Heterojunction Charge Transfer

Differences in energy, carrier density and energy levels among organic and inorganic material cause a charge carrier migration through the junction between the two materials. This is owed to the necessity to reach a new equilibrium in the composite.

Such charge transfer may be engineered to obtain a modulation of charge carrier densities or to fill trap sites, leading to an improvement of material performance.

For ICPs, thermoelectric performance can be enhanced with this effect for different reasons. For instance, in CNT based nancomposites, charge transfers from the polymer to the nanostructure are considered favourable due to either the high-mobility carrier transport along the axis of the nanotube or the doping of the conjugated polymer[10]. Similar phenomena are used to explain the high TE performance recorded in PEDOT:PSS/Te nanowires composite[11].

The decrease of ICP charge carrier concentration due to the transfer has also been supposed as performance implementing reason, since such decrease is beneficial for the Seebeck coefficient, as already discussed in Sect. 2.1.2.4. This mechanism was proposed as an explanation for Seebeck coefficient increase in PEDOT:PSS/gold nanoparticles nanocomposite.

Heterojunction charge transfer is challenging to be exploited in this application, since it requires a fine tuning to lead to the desired effect. In a complex system as an inorganic/organic nanocomposite, charge transfer depends on specific electronic and structural features of the two components and on their interaction, which means that several parameters must be finely controlled to succeed and this is the reason why this strategy is so challenging.

6.1.3 Thermal Conductivity Tuning

As already reported in Sect. 2.1.2.4, a decrease in thermal conductivity is favourable for thermoelectric performance, as can be easily understood by zT dependence k. It has also been observed that thermal conductivity is composed of two contributes, an electronic one k_e, which is owed to the thermal energy transported by charge carriers, and a lattice one k_l, which is generated by the vibrations of the lattice.

The first term, k_e, is directly related to the electrical conductivity of the material by Wiedemann-Franz law:

$$k_e = \sigma L T \tag{6.1}$$

where L is the Lorenz constant. Equation 6.1 states that it is not possible to decrease k_e term without detrimentally affecting electrical conductivity, which represent a limit to thermoelectric performance enhancing.

It has been demonstrated[12], though, that in 1D systems σ and k_e can be entirely decoupled. It can be shown that for this kind of single channel transport k_e becomes zero:

$$k_e = k_0 - S^2 \sigma_0 T = 0 \tag{6.2}$$

where k_0 is the electronic heat conduction for a zero-potential gradient, S is the Seebeck coefficient, σ_0 is the reduced conductivity for a monodimensional system and T is the temperature.

Therefore:

$$\frac{k_e}{\sigma} = 0 \tag{6.3}$$

Such fruitful decoupling of the two quantities is related with 1D conduction, which is compatible both with long crystalline domains in conjugated polymers and with 1D nanostructures, such as nanowires. Even though such performance implementing strategy has not be proven yet in ICP based nanocomposite, it appears extremely interesting.

On the other side, the lattice contribution to the thermal energy, k_l, can also be reduced thanks to material engineering. Since phonons are responsible of thermal conductance of the lattice, their scattering can be a strategy to decrease k_l. Nanocomposites are characterized by an elevated number of boundaries and surfaces among the two phases which can effectively scatter phonons, leading to the desired effect.

It must be noticed that current studies on ICP based nanocomposites are focused on power factor enhancement, rather than thermal conductivity decrease, since thermal conductivity in ICPs is already expected to be low[13].

6.1.4 Structural Changes at Organic-Inorganic Interface

A final phenomenon that was hypothesized in ICP based nanocomposites is the change in ICP morphology due to the presence of inorganic nanostructures. In a study on PEDOT:PSS/Te nanowires[11], a local increase of polymer crystallinity was supposed to happen in regions close to the nanowire surfaces.

Such local crystallinity causes an enhancement of carrier mobility, which increases σ along with the volume fraction of the (3D) interfacial region. As discussed for energy filtering effect, an increase of mobility only marginally affects Seebeck coefficient value, leading to an overall increase of TE PF.

In the cited work, an empirical model has been proposed, based on in-series connection of the two different phases through such high mobility interfacial regions. Even though the model is quite successful in explaining composite behaviour, it is still difficult to experimentally prove the occurrence of such structural changes in small regions of the polymeric material.

6.2 Manganese (II,III) Oxide Nanoparticle Inclusion

The first nanocomposite material developed in the experimental work done for this thesis was based on PEDOT:Tos including Mn_3O_4 nanoparticles (NPs). To ensure the interaction among the two phases, a procedure of NP functionalization was developed before mixing them into the polymerization solution. NPs used were decorated with an organic moiety, terminating with monomer structure (as showed in Figure 6.3). This structure reacts as a monomer in the polymerization solution, allowing the chain to grow directly on the surface of the NP. The chemical interaction among NP and polymer chain would support the development of a good interface among the two phases.

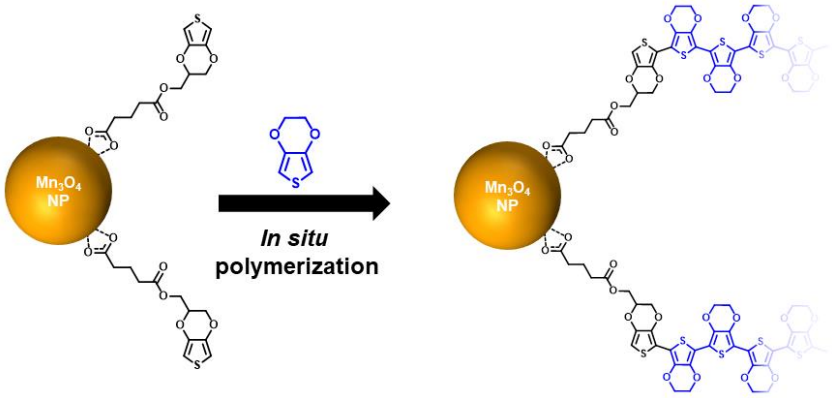

FIGURE 6.2: FUNCTIONALIZED NP (*LEFT*) CAN BE DISPERSED INTO THE OXIDANT SOLUTION, TOGETHER WITH THE MONOMER. IN SITU POLYMERIZATION OCCURS IN THE FILM, LEADING TO THE DEVELOPMENTS OF PEDOT CHAINS STARTING ALSO FROM THE NP ITSELF (*RIGHT*).

A set of samples with different NP concentrations were prepared. The study allowed to correlate electrical conductivity and Seebeck coefficient with the rateo among the two phases. Moreover, electrical conductivity was studied at different humidity levels, to understand morphology related aspects of charge transport properties in the composite material.

6.2.1 Experimental Procedure

6.2.1.1 Manganese Oxide NP synthesis

Mn_3O_4 was synthetized according to a known procedure reported by Lei et al. [14], which started with the dissolution of $MnCl_2{\cdot}4H_2O$ in ethanolamine (20 g/l). The resulting mixture was put into an ordinary ultrasonic bath for some minutes. Afterwards, distilled water was poured into the solution, and the mixture was stirred at room temperature for 5 h. The resulting dark brown suspension was centrifuged at 4500 rpm for 5 min. The black precipitate obtained was then dispersed in ethanol. After centrifugation at 4500 rpm for 40 minutes, a dark brown powder was isolated, which was characterized by FTIR to prove its composition.

6.2.1.2 Manganese Oxide NP functionalization

The NP functionalization was carried out following the procedure reported by Giri et al. [15] for α-hydroxyl carboxylate ligands. Modified EDOT monomer was used as ligand, the 4-((2,3-dihydrothieno[3,4-b][1,4]dioxin-2-yl)methoxy)-4-oxopentanoic acid (4-EDOT-MeO-4-oxopentanoic acid), obtained according to the procedure reported by Sassi[16]. An esterification between EDOT-methanol and glutarric anhydride was performed, to obtain a monomer decorated with a glutaryl moiety. For NP functionalization, 5 mL of a solution 0.5 M of glutaryl-EDOT in ethanol was added to approximately 100 mg powder Mn_3O_4 NPs and the resulting suspension was centrifuged for 12 hours at 4500 rpm.

6.2.1.3 Nanocomposite Sample Preparation

Nanocomposite material was prepared by in situ polymerization, according to Park et al.[17] modified procedure. Polymerization solutions were obtained starting from a mixture of CleviosTM CB 40 V2 (1000 mg) and Pluronic® P-123 (200 mg), which was stirred for 8 hours and then immersed in an ultrasound bath for 30 minutes. Functionalised nanoparticles have has been added to the mixture, in different concentration for different samples. The resulting suspension has been stirred and then put in an ultrasound bath for several minutes. Pyridine (23 µl) was poured into the final mixture. Afterwards, the mixture was cooled down to −20 °C and then EDOT (28 µl) was added. The final ratio EDOT:$Fe(Tos)_3$:pyridine was 1:2.55:1.1.

The resulting mixture was stirred for 15 minutes and it was filmed by blade coating technique (using Doctor Blade, wet thickness 254 µm). Films were annealed in air at 70°C for 2 hours, rinsed in ethanol to wash the residual $Fe(Tos)_3$ and $Fe(Tos)_2$ once cooled down at room temperature, and then annealed again at 70°C for 30 minutes.

The same receipt was followed for the PEDOT:Tos sample, without including Mn_3O_4 NP adding step.

6.2.1.4 Characterizations

Five samples of NC with different concentration of Mn_3O_4 NPs were prepared according to the procedure described in Sect. 6.2.1.3. Table 6.1 reports their Seebeck coefficient and their electrical conductivity, which were measured with the set up described in Sect. 4.1.3.1.

	NP concentration (cm^{-3})	Electrical conductivity ($\Omega^{-1}cm^{-1}$)	Seebeck coefficient (μVK^{-1})	Power factor ($\mu WK^{-1}m^{-1}$)
PEDOT:Tos	0	242±9	15.8±0.9	6.0±0.8
Mn_3O_4 NC1	$1.5 \cdot 10^{14}$	240±9	14.8±0.5	5.5±0.7
Mn_3O_4 NC2	$3.0 \cdot 10^{14}$	147±6	15.5±0.7	3.8±0.5
Mn_3O_4 NC3	$2.2 \cdot 10^{15}$	98±4	15.0±0.2	2.2±0.6
Mn_3O_4 NC4	$3.0 \cdot 10^{15}$	89±3	15.5±0.8	2.0±0.3

TABLE 6.1: ELECTRICAL CONDUCTIVITY AND SEEBECK COEFFICIENT DATA MEASURED FOR PEDOT:TOS AND FOUR NANOCOMPOSITES. THE CALCULATED TE POWER FACTOR IS ALSO REPORTED.

The FTIR characterization of the NPs proved their composition (observed IR peaks: 407 cm^{-1} Mn^{3+}-O vibrational modes in octahedral sites, 517 cm^{-1} Mn-O stretching modes in octahedral sites, 630 cm^{-1} Mn-O stretching modes in tetrahedral sites[18]), while SEM analysis provided the average diameter of 25±6 nm (Figure 6.3).

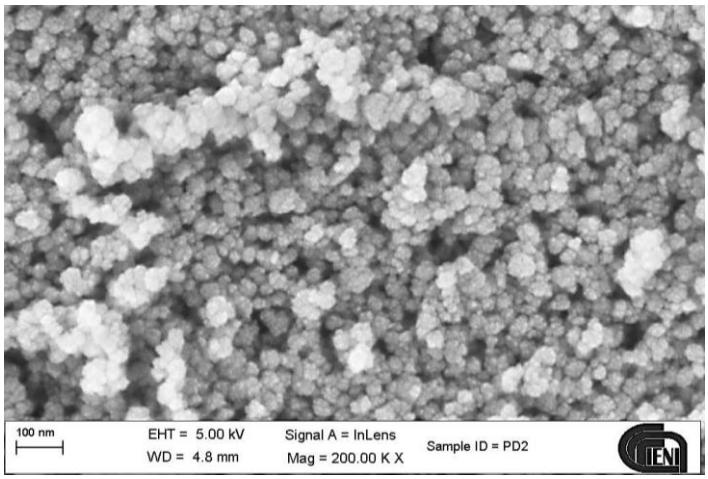

FIGURE 6.3: SEM IMAGE OF Mn_3O_4 NPS

The UV-vis spectrum of functionalized NPs dispersed in ethanol shows a ligand-metal charge transfer (LMCT) band at 292 nm that can be interpreted as caused by the functionalization of the NP surface[15].

Functionalized NP concentrations per unit volume of polymerization solution were estimated using the weight of the NPs inserted into the polymerization solution and the average NP size obtained through SEM analysis.

Electrical conductivity σ was found to decrease upon increasing NP concentration, while the Seebeck coefficient is found to be only slightly lower than in PEDOT:Tos, remaining otherwise constant when increasing the NP density. A comparison between AFM analyses for

PEDOT:Tos film and the hybrid material with the highest NP concentration ($3.0 \cdot 10^{15}$ cm^{-3}) is shown in Figure 6.4.

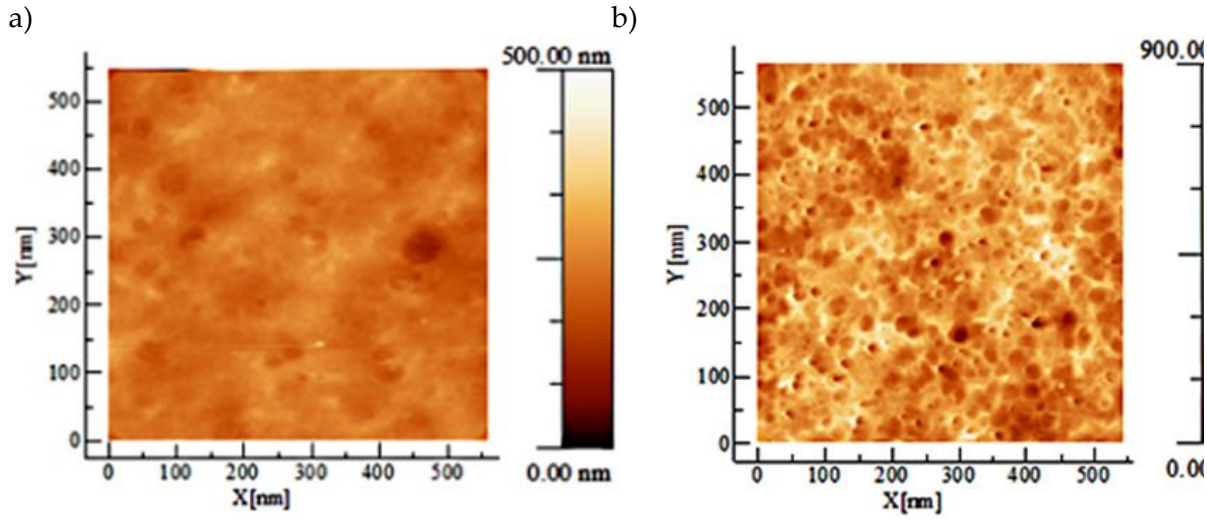

FIGURE 6.4: (A) TAPPING MODE AFM IMAGE OF PEDOT:TOS FILM SAMPLE, (B) TAPPING MODE AFM IMAGE OF SAMPLE Mn_3O_4 NC4, NP CONCENTRATION OF $3.0 \cdot 10^{15}$ CM^{-3}.

6.2.2 Humidity effect as a tool to study microscopical disorder

The electrical conductivity is found to depend on both humidity level and NP concentration. Figure 6.5 displays the conductivity of films measured in dry air as a function of the NP concentration. An exponential decay for increasing NP content is observed.

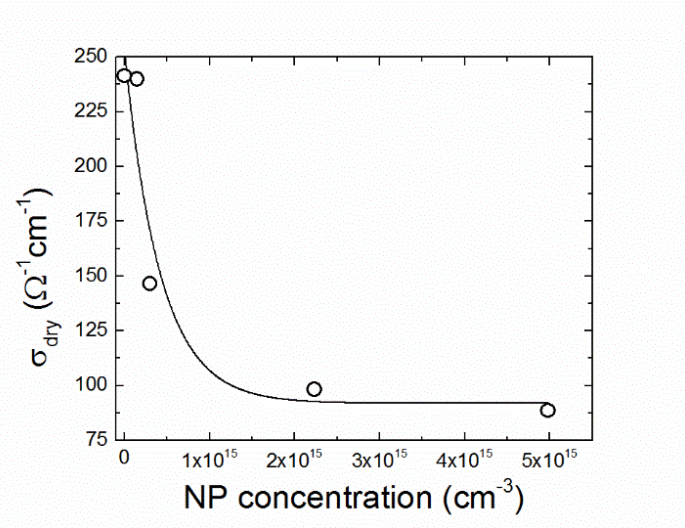

FIGURE 6.5: DEPENDENCY OF THE ELECTRICAL CONDUCTIVITY IN DRY AIR ON THE NANOPARTICLE CONCENTRATION.

The dependence of the electrical conductivity on the humidity was also measured for each film. Ionic transport is known to be negligible in PEDOT:Tos[19]. Consistently, no evidence of polarization upon application of d.c. bias was observed in our samples. Electrical conductivity was instead found to change with the humidity level. No dependence of the Seebeck coefficient upon the humidity level was observed, instead.

In a study on ionic contribution in conjugated polymer Seebeck effect[19], Wang et al. actually hypothesized that water dissolved into PEDOT may act on σ in two ways (Figure 6.6). It may interpose across the polymer, thereby lessening the chain stack so that the conductivity decreases. However, water is also supposed to solvate the PEDOT counterion (p-toluenesulfonate), thereby trapping holes. Thus, it may increase the electrical conductivity by counterion solvation in the polymer.

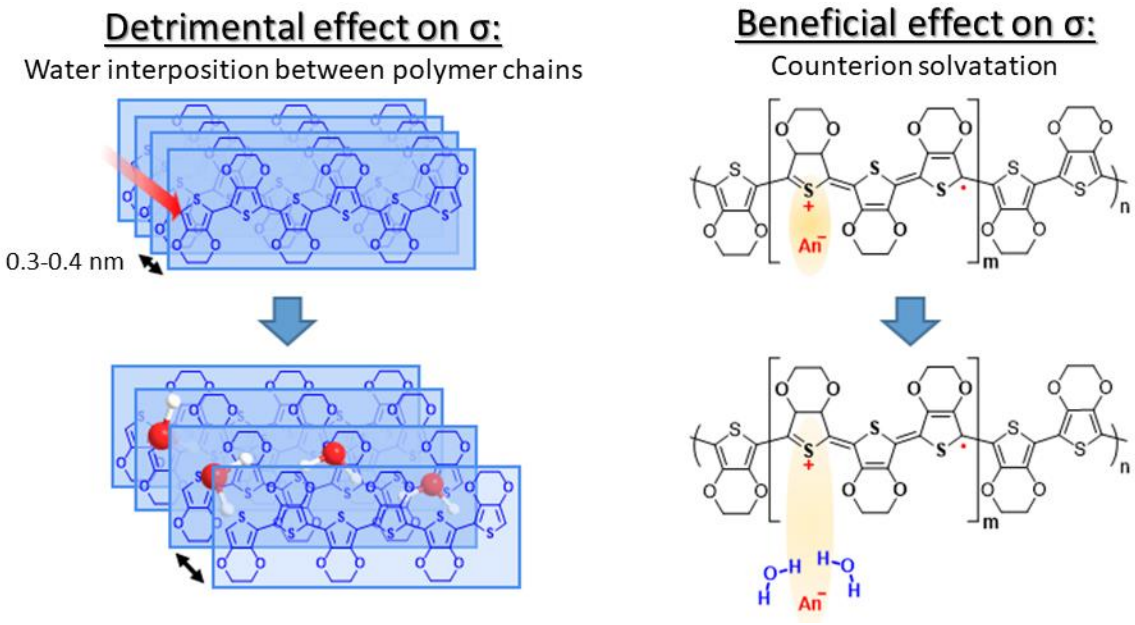

FIGURE 6.6: SKETCH OF WATER EFFECT ON PEDOT IN PRESENCE OF A MOLECULAR COUNTERION. ON ONE SIDE THERE IS A DETRIMENTAL EFFECT (*LEFT*) DUE TO THE INTERPOSITION OF WATER MOLECULES WITHIN POLYMER CHAINS, WHICH LEAD TO A WORSE Π-Π STACKING. ON THE OTHER HAND, THE SOLVATION OF COUNTERIONS (*RIGHT*) IS EXPECTED TO LESSEN THE ELECTROSTATIC TRAP THAT IT CREATES INTERACTING WITH HOLES.

In the NC system the first mechanism is sensibly negligible, as NPs are clearly more effective than water to spoil chain stacking (Figure 6.7). Thus, water may only operate by increasing the conductivity through counterion solvation.

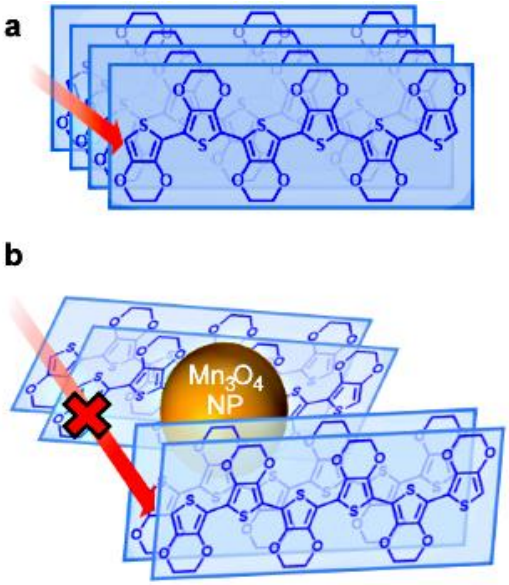

FIGURE 6.7: SUPPOSED EFFECT OF SPHERICAL NPS ON CHAIN PACKING. (A) CHAIN PACKING ALLOWS CARRIERS HOPPING FROM ON CHAIN TO ANOTHER THANKS TO Π-Π INTERACTIONS (RED ARROW). (B) WHEN AN EXTERNAL AGENT, AS A NP, DISRUPTS SUCH ORDER, INTERCHAIN HOPPING IS SEVERELY COMPROMISED.

A simple model may be then advanced, where the mobility is assumed to depend on the NP concentration only. It was already noted that in dry air the conductivity exponentially decreases with the NP concentration [NP]. Then

$$\sigma = ep(x_w, [NP])\mu_0 + \mu_1 e^{-[NP]/N_0} \tag{6.4}$$

where $-e$ is the electron charge, x_w is the molar fraction of water dissolved into the polymer, and μ_0, μ_1 and N_0 are constants. About $p(x_w, [NP])$, the charge carrier density as dependent upon the humidity level and the nanoparticle concentration, no obvious model for such dependency may be put forward, we can use the ansatz

$$p(x_w, [NP]) = p(0, [NP]) + \left(\frac{\partial p}{\partial x_w}\right)_{x_w=0} x_w \equiv p_0(1 + \beta([NP])x_w) \tag{6.5}$$

(where β is a dimensionless function, $\beta > 0$) is advanced. Thus Eq. (6.4) may be rewritten as

$$\sigma - \sigma_{dry} = \beta([NP])x_w(\sigma_0 + \sigma_1 e^{-[NP]/N_0}) \tag{6.6}$$

where σ_{dry} is the conductivity in dry air.

The water molar fraction is simply correlated to the water vapor pressure through the vapor-liquid equilibrium condition for non-ideal solutions, namely:

$$\frac{P_w^{(0)}}{P^0} = \frac{P_w/P^0}{a_w(x_w)} \tag{6.7}$$

where $P_w^{(0)}$ is the equilibrium water vapor pressure, $P^0 = 1$ bar, and a_w is the water activity. We take a standard sigmoidal $a_w(x_w)$ [20]:

$$a_w(x_w) = csch\left(\frac{1}{2\delta_x}\right) sinh\left(\frac{x_w}{2\delta_x}\right) cosh\left(\frac{x_0 - 1}{2\delta_x}\right) sech\left(\frac{x_w - x_0}{2\delta_x}\right) \tag{6.8}$$

Inverting the function and in view of Eq. (6.7) one gets with a little of algebra that

$$x_w = 2\delta_x coth^{-1}\left(\frac{(RH-1)tanh\left(\frac{x_w}{2\delta_x}\right)+coth\left(\frac{1}{2\delta_x}\right)}{RH}\right) \equiv \xi(RH;\delta_x,x_0) \qquad (6.9)$$

(with $0 \leq RH \leq 1$) so that finally

$$\sigma - \sigma_{dry} = \beta\xi(RH;\delta_x,x_0)(\sigma_0 + \sigma_1 e^{-[NP]/N_0}) \qquad (6.10)$$

The three unknowns in Eq. (6.6) may be computed (*not* fitted) for each set of σ(RH) data (Figure 6.8a). The overall agreement confirms the physical picture the model relies upon.

More specifically, Figure 6.8b shows the dependency of β upon the NP density and that of the water molar fraction x_w upon the relative humidity. The β term displays an exponential decay with [NP].

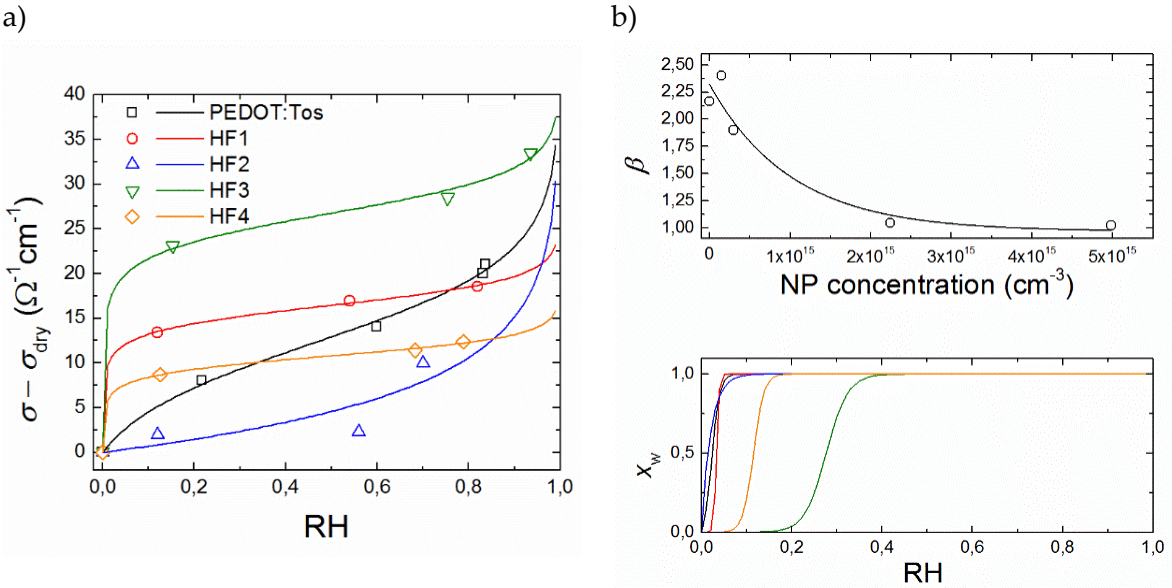

FIGURE 6.8: A) CHANGE OF THE ELECTRICAL CONDUCTIVITY DUE TO HUMIDITY FOR ALL SAMPLES CONSIDERED IN THIS WORK; B) (*TOP*) DEPENDENCE OF THE *B* PARAMETER UPON THE NP CONCENTRATION; (*BOTTOM*) MOLAR WATER FRACTION IN THE POLYMER VS. RELATIVE HUMIDITY FOR ALL SAMPLES CONSIDERED IN THIS WORK.

A decrease of the counterion solvation efficiency of water with increasing NP density suggests that NPs also adsorb water, making it less available to solvate tosylate molecules. Activity also depends on NP. This is not surprising as the water solubility in PEDOT reasonably depends on the NP concentration. Steeper x_w(RH) are found at low NP densities, with a major broadening for the two samples displaying larger NP contents. NP apparently helps solubilize water, a piece of evidence consistent with the decrease of counterion solvation efficiency if one assumes that NPs also sequestrate water by adsorbing it on their surface. It is worth noting that while carrier density is controlled by RH, its reduction never exceeds 30%. This quite explains the marginal dependency of the Seebeck coefficient on the humidity level. Since the Seebeck coefficient logarithmically depends upon the carrier density, counterion solvation slightly affects α, so that no major beneficial effect on the thermopower is observed.

6.3 Copper oxide nanolamellae inclusion

The second nanocomposite material was developed starting from the observations made on Mn_3O_4 nanocomposite material. In fact, since morphology of nanostructures plays a crucial role in final nanocomposite material performances, 2D nanostructured material was chosen as nanofiller. CuO NL were synthetized and mixed into the polymerization solution without any functionalization step. The NL quite homogeneously suspend in the polymerization solution. As it has been done for the Mn_3O_4 nanocomposite, a set of samples with increasing NL concentration was prepared, to evaluate the effect of PEDOT charge transport properties.

In this case, a deeper analysis on nanocomposites was performed by modifying their oxidation level through electrochemical procedure and characterizing electrical conductivity at different temperatures.

6.3.1 Experimental Procedure

6.3.1.1 CuO NL Synthesis

CuO NL were synthetized accordingly to Li et al.[21]. 200 mg of $Cu(NO_3)_2{\cdot}3H_2O$ were dissolved in 50 ml deionized water. 1.7 mL of PEG200 were poured into the resulting solution. The mixture was stirred for 2 hours, to obtain a homogeneous dispersion, then 300 mg of NaOH pellets were added. The solution turned from light blue to blue almost immediately and was stirred at room temperature for 20 hours. The resulting black suspension was filtered and then washed with water to purify the product. During the purification, ethanol was used several times to dissolve any unreacted PEG200. A dark grey solid was isolated and characterized.

6.3.1.2 CuO NL Characterization

SEM images of CuO NL provided information about their size and shape (Figure 6.9). The choice of a 2D nanosized material is usually driven by the necessity to lessen the detrimental effect on polymer morphology [22,23], considering that their shape is more compatible with PEDOT chain packing[24].

The graphical size evaluation of NL gives to an approximate diameter value of 470±80 nm and a thickness value around 30±4 nm.

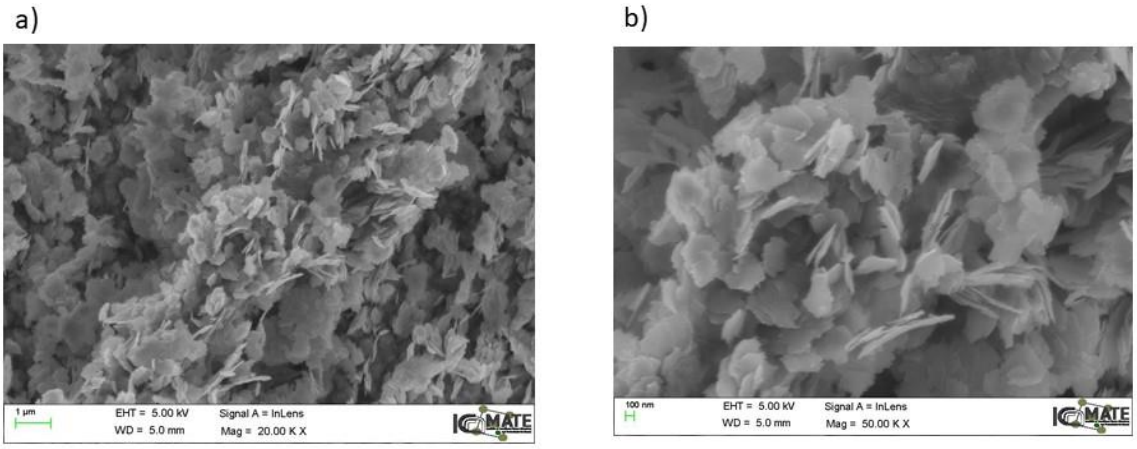

FIGURE 6.9: SEM IMAGES OF CUO NL

6.3.1.3 Nanocomposite Sample Preparation

The polymerization solution was prepared according to the route in Sect. 6.1.2.3, including a CuO NL adding step instead of functionalized Mn_3O_4. An increase in PEDOT:Tos film quality was obtained through a more careful rinsing in ethanol as final step of sample preparation.

The main change in the procedure was imposed by the choice of the substrate. Here, a mostly conductive substrate is required to properly apply the electric potential during the electrochemical processing. Nonetheless, a completely conductive substrate would have led to problems, e.g. short-circuits, during electrical conductivity and Seebeck coefficient measurement. The strategy pursued to avoid this problem is schematized in Figure 6.7. A gold pattern was thermally evaporated on a cleaned Kapton® foil, obtaining a partially conductive substrate (Step 3), on which PEDOT can be filmed through the procedure described above (Step 4-5). Such sample was used as the working electrode in a three-electrode cell, to modify its oxidation level and, therefore, its charge carrier density.

The resulting sample was prepared for electrical conductivity and Seebeck coefficient measurements by cutting its lateral edges (Step 7) to avoid electrical contacts between the top and the bottom of the sample through the gold film (Step 9). Top and bottom parts of the sample act as the hot and the cold sides during the Seebeck coefficient measurement.

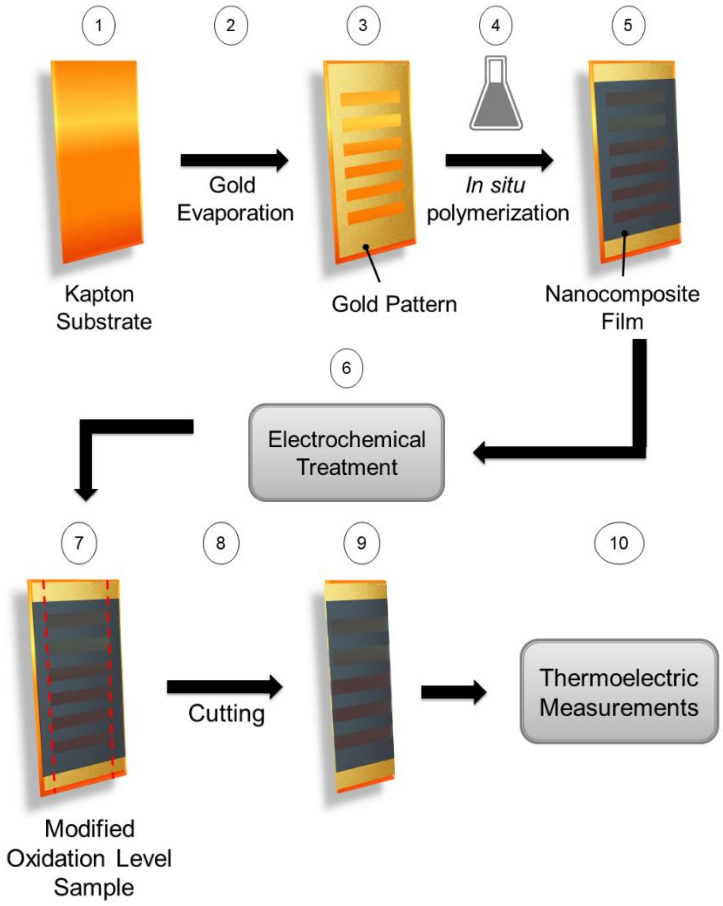

FIGURE 6.10: SKETCH OF THE SAMPLE PREPARATION PROCEDURE. (1) THE CLEANED KAPTON FOIL UNDERGOES TO A THERMAL GOLD EVAPORATION (2) TO OBTAIN A GOLDEN PATTERN ON IT (3). ON SUCH SUBSTRATE IN SITU POLYMERIZATION IS PERFORMED (4), ACHIEVING A NANOCOMPOSITE THICK LAYER (5). ELECTROCHEMICAL TREATMENT (6) OF THE SAMPLE LEADS TO A MODIFIED OXIDATION LEVEL FILM (7). THE SAMPLE IS THEN CUT (8) ALONG THE RED DASHED LINES, IN ORDER TO OBTAIN (9), ON WHICH THERMOELECTRIC MEASUREMENT (10) (SEEBECK COEFFICIENT AND ELECTRICAL CONDUCTIVITY) CAN BE PERFORMED.

6.3.1.4 Electrochemical Treatment

A single compartment three electrode cell was used for the electrochemical oxidation level modification of the sample prepared as described in Sect. 6.3.1.3, used as working electrode, in N_2 filled glove box (residual O_2 < 0.1 ppm; residual H_2O < 0.1 ppm). An electrolyte solution of tetrabutylammonium perchlorate ($TBAClO_4$) in acetonitrile (0.1 M) was employed. A Pt net counter electrode and an Ag/AgCl pseudo-reference electrode were used. The latter was calibrated before each measurement using 1 mM ferrocene solution in the supporting electrolyte. All potentials are reported vs. Fc^+/Fc^0couple[25].

The treatment consisted in three to five cycles of cyclic voltammetry on each sample at 3 mV/s, followed by a slow potential linear scan (1 mV/s) to the desired potential. After the oxidation/reduction, the sample was let equilibrate until voltage reached its electromotive force (emf) value (Figure 6.13).

6.3.2 Electrical and Thermoelectrical Characterization

First, the investigation focused on the effect of the NL presence on PEDOT:Tos electrical and thermoelectrical properties. Therefore, six nanocomposites with different NL concentration

were prepared following the procedure already described (Sect. 6.1.3.1) and PEDOT:Tos reference sample. The data obtained from their characterization are reported in Table 6.2.

	CuO NL conc. (g/L)	Electrical Conductivity ($\Omega^{-1}cm^{-1}$)	Seebeck Coefficient (μVK^{-1})	Power Factor (μVK^{-1})
PEDOT:Tos	0	393±12	18.0±0.8	12.7±0.1
NC CuO 1	0.58	155±15	15.5±1.0	2.8±0.5
NC CuO 2	0.88	223±20	20.3±1.2	9.2±0.3
NC CuO 3	1.18	163±16	14.4±1.3	3.4±0.8
NC CuO 4	1.76	164±16	19.2±0.9	6.0±0.2
NC CuO 5	2.33	152±20	15.9±1.1	3.8±0.6
NC CuO 6	2.94	90±22	16.5±0.9	2.4±0.7

TABLE 6.2: ELECTRICAL CONDUCTIVITY AND SEEBECK COEFFICIENT DATA MEASURED FOR PEDOT:TOS AND SIX NANOCOMPOSITES. THE CALCULATED TE POWER FACTOR IS ALSO REPORTED.

As already pointed out for Mn_3O_4 based nanocomposites, electrical conductivity shows a decrease as the nanostructure concentration increase, while no major change of the Seebeck coefficient was observed. All the values measured are in typical PEDOT:Tos range (15-20 μVK^{-1}). From the graph displayed in Figure 6.13, it is possible to see that the electrical conductivity present an exponential decrease when the NL concentration is increased.

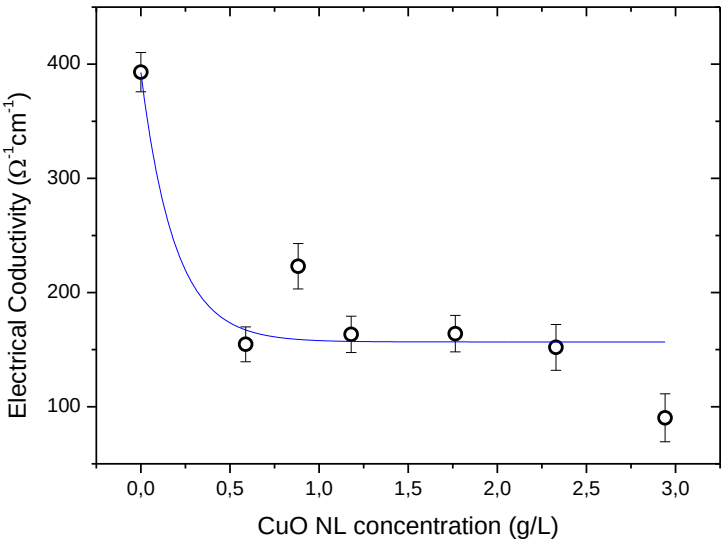

FIGURE 6.11: ELECTRICAL CONDUCTIVITY OF SAMPLES VERSUS CUO NL CONCENTRATION.

It is possible to hypothesise the same exponential decrease of mobility that was supposed for Mn_3O_4 based nanocomposite (Sect.6.2.2). According to this interpretation, even with a 2D shape, the presence of nanostructure still detrimentally affects the morphology of the material. A study on the modification of charge carrier concentration was performed in order to achieve a deeper comprehension of nanocomposite charge transport behaviour.

6.3.3 Oxidation Level Tuning

Among the prepared samples, samples 1, 3 and 6 were selected for further investigations. The samples were prepared according to procedure reported in Sect. 6.3.1.3 and characterized at different oxidation level achieved by the electrochemical treatments.

UV-vis spectra were performed to obtain a qualitative information about the oxidation level of the samples right after the polymerization route (i.e., without any modification of the oxidation state). The comparison is shown in Figure 6.12.

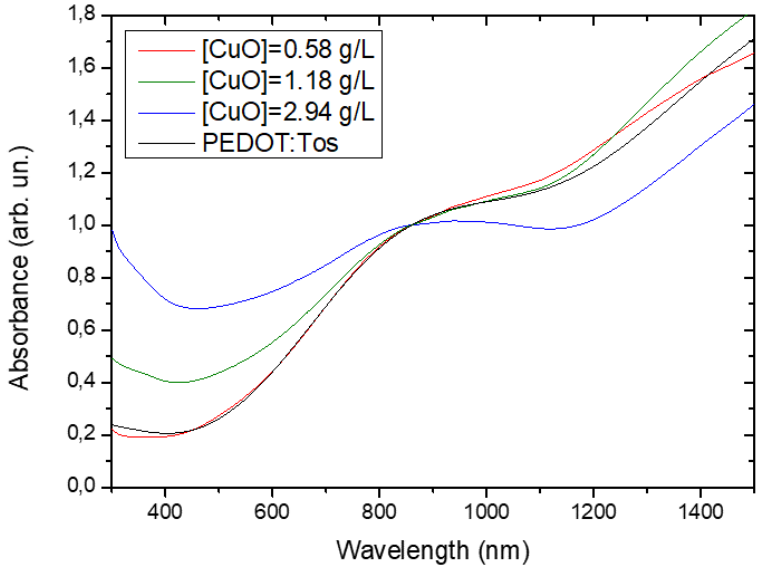

FIGURE 6.12: UV-VIS SPECTRA OF CUO NL BASED NCS AND PEDOT:TOS IN PRISTINE OXIDATION STATE. THE SPECTRA ARE NORMALIZED ON 860 NM ABSORBANCE VALUE TO MAKE A COMPARISON AMONG EACH OTHER.

All spectra present quite the same shape, with two polaronic bands (at 900 nm and above 1400 nm) which indicates a rather high oxidation level. This is a typical condition for in situ polymerized films, due to the use of an oxidative agent as reactant. The spectra differ for a peak below 300 nm, which is originated by the CuO NL presence. Since before any treatment samples were at the same oxidation level, it can be state that CuO NL do not interfere with oxidation reaction during polymerization.

Further information on nanocomposite behaviour can be obtained from the electrochemical treatment itself. The cyclic voltammetries (Figure 6.13) acquired during sample processing showed the characteristic anodic and cathodic peak values of PEDOT:Tos for all the samples (cathodic peak range:-950/-900mV vs $Fc^{+/0}$, anodic peak: -500/-450 mV vs $Fc^{+/0}$), meaning that the polymer only incurs in oxidation/reduction reaction, and that NLs are not involved.

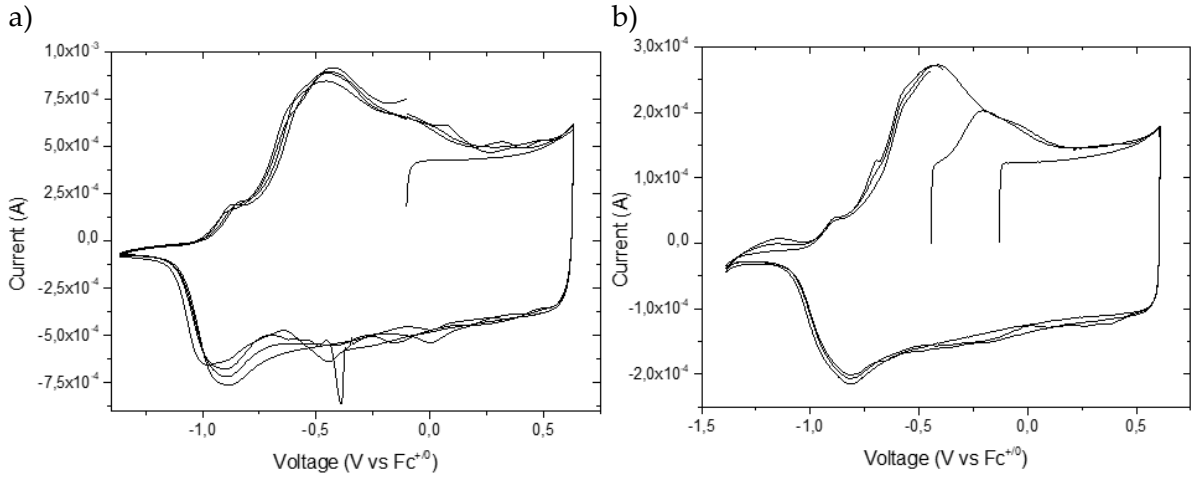

FIGURE 6.13: COMPARISON AMONG CYCLIC VOLTAMMETRIES OF A) PEDOT:TOS AND B) PEDOT:TOS NANOCOMPOSITE WITH HIGHEST CUO NL CONCENTRATION (2.94 G/L).

Electrical conductivity and Seebeck coefficient were measured for samples at three or four different oxidation levels, reached through electrochemical treatments. Results are summarized in two graphs in Figure 6.14, in which electrical conductivity and Seebeck coefficient are reported *versus* electromotive force (EMF).

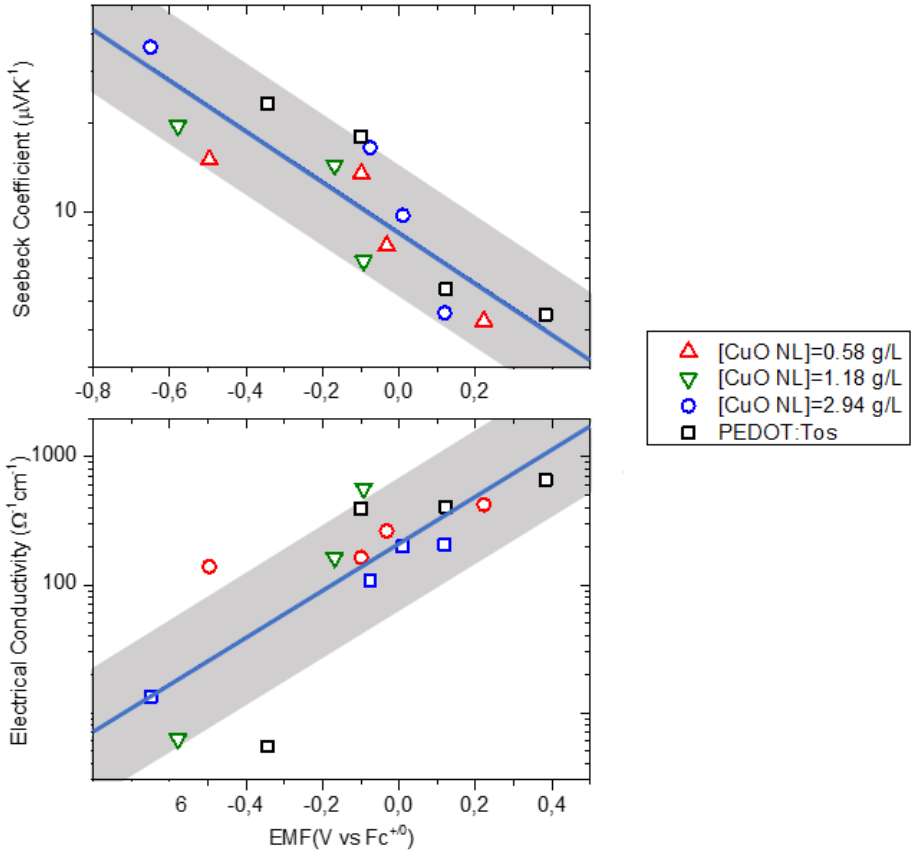

FIGURE 6.14: SEEBECK COEFFICIENT (TOP) AND ELECTRICAL CONDUCTIVITY (BOTTOM) OF NANOCOMPOSITE SAMPLES AT DIFFERENT OXIDATION LEVELS (REPORTED AS ELECTROMOTIVE FORCE, EMF).

All data follow the expected general trend (blue line). Such results agree with the hypothesis of a merely morphological effect of the NL on PEDOT.

Recalling the description given at the beginning of this chapter, two effects related to charge carrier density were supposed to happen in nanocomposite: energy filtering effect and heterojunction charge transfer. Considering a charge carrier density modification in the polymeric phase, as it happens thanks to electrochemical treatments, a deviation from the trend would be expected in presence of the two effects. Oxidising/reducing PEDOT impacts also on electronic structure of the material, leading to a new mismatching among the energetic levels of the two phases. In case of energy filtering, this would mean an increase or a decrease of the potential barrier, while in case of heterojunction charge transfer, the result would be an enhanced or a decreased driving force for the transfer. Both phenomena would severely impact Seebeck coefficient and electrical conductivity values.

A charge transport model is needed to confirm this hypothesis of PEDOT transport behaviour retention in its nanocomposites. As already reported in Chapter 2, identification of the optimal model might not be an easy task, since several interpretations of charge transport phenomena have been proposed.

In this case, we decided to exploit Kang and Snyder model, since it aimed to be as inclusive as possible (Sect. 2.2.2.5.1).

Although Eqs. (2.51)–(2.52) may not be analytically integrated in finite terms for arbitrary s values, a general expression for the conductivity and the Seebeck coefficient is computable for s = 1. This is a fortunate circumstance since, differently from all other polymers, PEDOT and its related composites are believed to be better described by taking the transport exponent equal to 1[26]. One may easily verify that

$$\sigma(T) = \sigma_{E_0}(T)\ln(1 + e^{\eta}) \tag{6.11}$$

where $\eta \equiv \left[{E_f - E_t}/{k_B T}\right]$

while

$$\alpha(T) = -\left(\frac{k_B}{e}\right)\frac{\pi^3 - 3\eta\ln(1 + e^{-\eta}) + 6Li_2(-e^{-\eta})}{3\ln(1 + e^{\eta})} \tag{6.12}$$

where $Li_n(z)$ is the polylogarithm function:

$$Li_n(z) \equiv \frac{1}{\Gamma(n)}\int_0^{+\infty}\frac{t^{n-1}}{1 + e^t/z}\,dt \tag{6.13}$$

Note that α depends upon η only.

It is immediate to verify that Eq. (6.11) reduces to $\sigma_{E_0}(T)e^{\eta}$ for $\eta \ll -1$ ($e^{\eta} \ll 1$) and to $\sigma_{E_0}(T)\eta$ for $\eta \gg 1$ ($e^{-\eta} \ll 1$). Instead, Eq. (6.12) simplifies to $(k_B/e)(2 - \eta)$ and to $\left(k_B\,{\pi^2}/{3e}\right)\eta^{-1}$ in the same two limits.

In view of Eq. (6.12), Seebeck coefficients may be used to immediately obtain η. As mentioned, we expect that $E_f - E_t$ depends on the oxidation level, that sets both energies, while it should

not be affected by the presence and the density of NL. Figure 6.15 displays η vs. EMF. It confirms how in all specimens, independently of the eventual NL density, $E_f - E_t$ increases with the PEDOT oxidation level. Stated differently, modulating the ionization degree of the polymer chain also consistently modulates the difference between Fermi and transport energies. It should be remarked that in all samples $\eta \gg 1$. Samples are then strongly degenerate. Manifestly enough, this does not imply the samples to be metallic, with a negative resistance temperature coefficient, since electronic states in the polymer are anyway localised, and conductions occur by hopping among non-extended states.

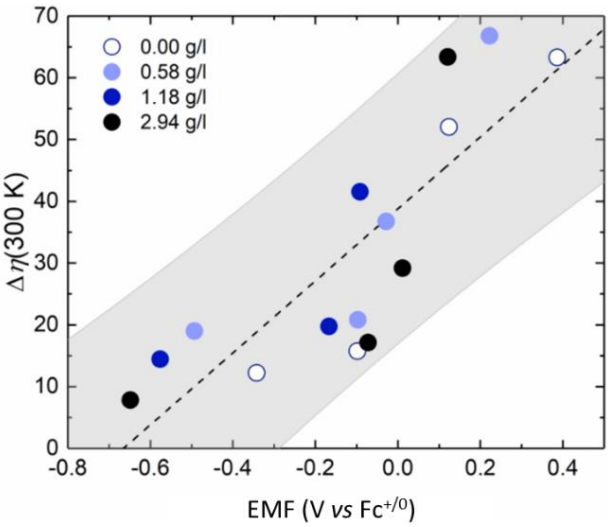

FIGURE 6.15: INCREASE OF η WITH THE EMF. NOTE THAT NP DENSITY (REPORTED AS THE CUO NP CONCENTRATION IN THE POLYMERIZATION SOLUTION) DOES NOT IMPACT η. DATA REFER TO 300K

6.3.4 Conductivity Temperature Dependence

The hypothesis on charge transport behaviour is confirmed by the analysis of the temperature dependence of σ in pristine samples.

Using η values computed once again out of α through Eq. (6.21), hopping energies W and pre-exponential factors $\sigma_{E_0}^{(0)}$ [Eq. (6.11)] are obtained (Fig. 6.16). Hopping energies were found to range between 100 and 115 meV, a value remarkably smaller than those observed in polyacetylene[26].

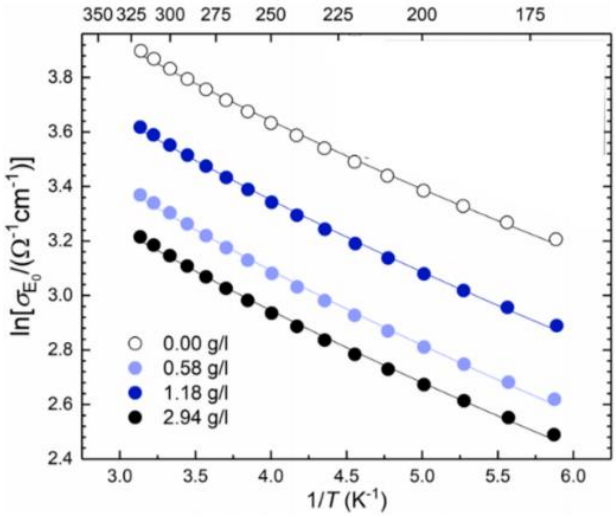

FIGURE6.16: ELECTRICAL CONDUCTIVITY NORMALIZED ON THE VALUE MEASURED AT 170 K REPORTED VERSUS TEMPERATURE FOR THE SET OF SAMPLES PREPARED.

Interestingly, the larger hopping energy is found for the sample with the lowest concentration of NL. This may be rationalized considering that a higher density of NL increases the probability of their aggregation. Aggregates can still perturb polymer morphology, but the portion perturbed is smaller than the one of well dispersed nanostructures.

Such hypothesis is supported by SEM images of nanocomposite sample external surfaces (Figure 6.17). In nanocomposites with highest concentration, Figure 6.17 b, SEM analysis shows the generation of some nanostructure aggregates, while such phenomenon is not observed in the most diluted nanocomposites (Figure 6.17a).

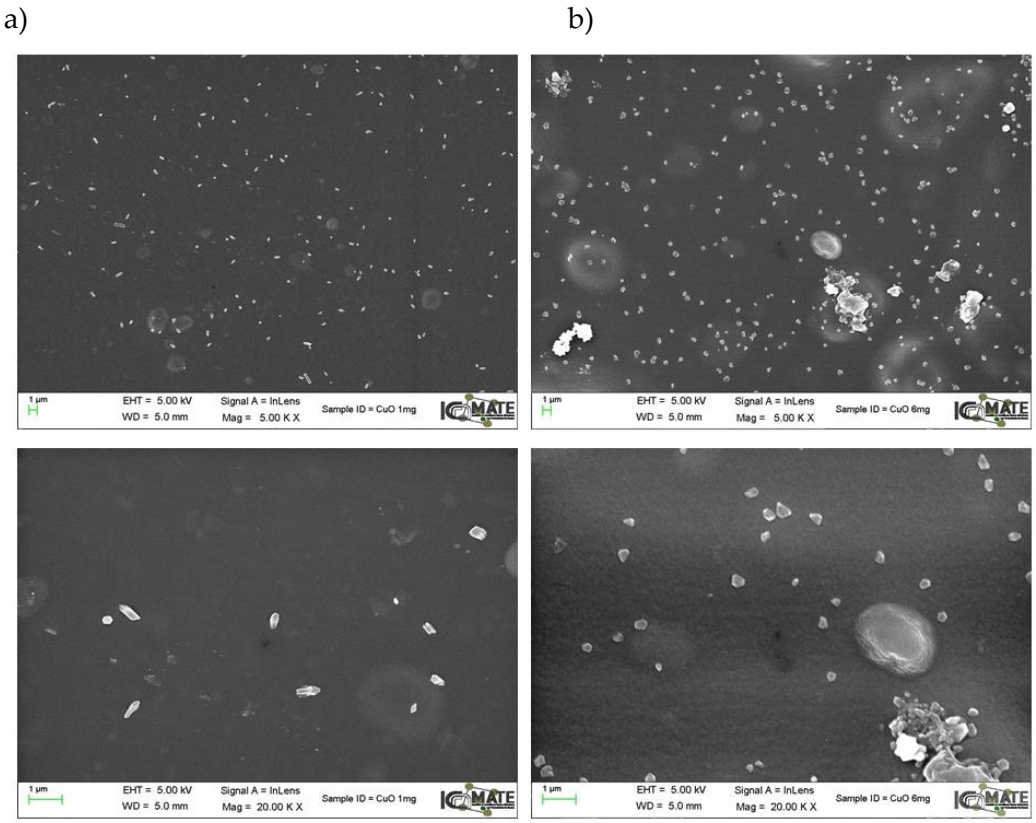

FIGURE 6.17: SEM IMAGES OF CUO BASED NANOCOMPOSITES. THE DARK GREY BACKGROUND IS THE POLYMER, WHILE THE WHITE SPOTS ARE THE NL. A) SAMPLE NC CUO 1 (NL CONCENTRATION OF 0.58 G/L), MAGNIFICATION 5.00K X (*TOP*) AND MAGNIFICATION 20.00K X *(BOTTOM)*; B) SAMPLE NC CUO 6 (NL CONCENTRATION OF 1.94 G/L), MAGNIFICATION 5.00K X (*TOP*) AND MAGNIFICATION 20.00K X *(BOTTOM)*.

6.4 Conclusions

Control the final quality of ICP film is not a trivial task, as it has been described in previous chapters. The inclusion of nanostructured materials in such systems leads to further increase of their complexity and, thereof, a lower degree of control on it. Even with the proper comprehension of the thermoelectric behaviour of both ICP and nanostructures, effects rising from their interaction are still difficult to understand and properly prove. With the work described in this chapter, we aimed to make a little step further in this difficult task, exploring different experimental paths to study on ICP/nanostructure interactions to analyse the behaviour of novel nanocomposites.

Two inorganic nanomaterials were used to probe the behaviour of PEDOT nanocomposite. First, Mn_3O_4 spherical nanoparticles were embedded in the polymeric matrix, after being functionalized with an organic moiety. The electrical measurements at different humidity conditions led to the conclusion that nanoparticles have a detrimental impact on polymer morphology, which lead to a substantial decrease of charge carrier mobility in nanocomposite. Second, CuO nanolamellae have been used, without any surface functionalization. In this case, developed nanocomposite were studied in different oxidation states to obtain information about their behaviour in presence of higher and lower charge carrier densities. Even in this

second set of samples, the effect of NL has been proven to be only morphological, thanks to the study of material at different oxidation levels and electrical conductivity measurements performed at different temperatures.

Application of the Kang–Snyder model to PEDOT-Tos and related CuO nanocomposites is found to successfully construe the whole set of experimental data. PEDOT is confirmed to set apart from all other conductive polymers considered up to now as candidates for thermoelectric applications. Specifically, a transport exponent s of 1 (instead of 3, as in almost all other conductive polymers) is confirmed to appropriately fit the temperature dependence of the electrical conductivity and the effect of the polymer oxidation level on both the electrical conductivity and the Seebeck coefficient.

The material (both in the presence and in the absence of CuO NL) is found to be degenerate, with the Fermi level sitting within electronic states contributing to charge transport. This is consistent with the high values of electrical conductivity observed in our samples and in all PEDOT:Tos samples[27].

Of the two terms ruling the electrical conductivity, we confirmed our starting hypothesis that η is controlled by the oxidation level, being instead irresponsive to the NL density. The adverse effect of NL on the polymer stacking is witnessed instead by the $\sigma_{E_0}(T)$ term, which reports about the elemental hopping event. An increase of the NP density, while not fully destroying local stacking of the aromatic rings as observed with spherical nanoparticles[22], decreases the interchain hopping rate, leading to a decrease of the average hopping rate.

Although it would be inappropriate to link η to the carrier density and $\sigma_{E_0}(T)$ to the carrier mobility, it is apparently confirmed that also in disordered material the two quantities are functionally reminiscent of the above parameters, with η being controlled by processing aimed at modulating the PEDOT ionization and $\sigma_{E_0}(T)$ being instead sensitive to modifications of the material micromorphology.

6.5 References

1 L. D. Hicks and M. S. Dresselhaus, *Phys. Rev. B*, 1993, **47**, 727–731.

2 G. J. Snyder and E. S. Toberer, *Nat. Mater.*, 2008, **7**, 105–114.

3 D. J. Bergman and O. Levy, *J. Appl. Phys.*, 1991, **70**, 6821–6833.

4 H. E. Katz and T. O. Poehler, *Innovative Thermoelectric Materials*, Imperial College Press, London, 2016.

5 N. Neophytou, X. Zianni, H. Kosina, S. Frabboni, B. Lorenzi and D. Narducci, *Nanotechnology*, 2013, **24**, 205402.

6 N. Neophytou, X. Zianni, H. Kosina, S. Frabboni, B. Lorenzi and D. Narducci, *Nanotechnology*, 2013, **24**, 205402.

7 M. Paulsson and S. Datta, *Phys. Rev. B*, 2003, **67**, 241403.

8 P. Reddy, S.-Y. Jang, R. A. Segalman and A. Majumdar, *Science (80-.).*, 2007, **315**, 1568–

1571.

9 B. Poudel, Q. Hao, Y. Ma, Y. Lan, A. Minnich, B. Yu, X. Yan, D. Wang, A. Muto, D. Vashaee, X. Chen, J. Liu, M. S. Dresselhaus, G. Chen and Z. Ren, *Science*, 2008, **320**, 634–8.

10 F. S. Liu, J. X. Zheng, M. J. Huang, L. P. He, W. Q. Ao, F. Pan and J. Q. Li, 2014, **4**, 1–7.

11 S. K. Yee, N. E. Coates, A. Majumdar, J. J. Urban and R. A. Segalman, *Phys. Chem. Chem. Phys.*, 2013, **15**, 4024.

12 A. Casian, *Phys. Rev. B - Condens. Matter Mater. Phys.*, 2010, **81**, 1–5.

13 Q. Wei, M. Mukaida, K. Kirihara, Y. Naitoh and T. Ishida, *Materials (Basel).*, 2015, **8**, 732–750.

14 S. Lei, K. Tang, Z. Fang and H. Zheng, *Cryst. Growth Des.*, 2006, **6**, 1757–1760.

15 A. Giri, N. Goswami, M. Pal, M. T. Zar Myint, S. Al-Harthi, A. Singha, B. Ghosh, J. Dutta and S. K. Pal, *J. Mater. Chem. C*, 2013, **1**, 1885.

16 M. Sassi, 2010.

17 T. Park, C. Park, B. Kim, H. Shin and E. Kim, *Energy Environ. Sci.*, 2013, **6**, 788.

18 F. Buciuman, F. Patcas, R. Craciun and D. R. T. Zahn, *Phys. Chem. Chem. Phys.*, 1999, **1**, 185–190.

19 H. Wang, U. Ail, R. Gabrielsson, M. Berggren and X. Crispin, *Adv. Energy Mater.*, 2015, **5**, 1–6.

20 T. a. Zawodzinski, *J. Electrochem. Soc.*, 1993, **140**, 1041.

21 Y. Li, X. Yang, J. Rooke, G. Van Tendeloo and B. Su, *J. Colloid Interface Sci.*, 2010, **348**, 303–312.

22 D. Galliani, S. Battiston and D. Narducci, *J. Nanosci. Nanotechnol.*, 2017, **17**, 1579–1585.

23 M. He, J. Ge, Z. Lin, X. Feng, X. Wang, H. Lu, Y. Yang and F. Qiu, *Energy Environ. Sci.*, 2012, **5**, 8351.

24 K. Z. Xing, M. Fahlman, X. W. Chen, O. Inganäs and W. R. Salaneck, *Synth. Met.*, 1997, **89**, 161–165.

25 V. V. Pavlishchuk and A. W. Addison, *Inorganica Chim. Acta*, 2000, **298**, 97–102.

26 S. Dongmin Kang and G. Jeffrey Snyder, *Nat. Mater.*, 2016, **16**, 252–257.

27 O. Bubnova, Z. U. Khan, H. Wang, S. Braun, D. R. Evans, M. Fabretto, P. Hojati-Talemi, D. Dagnelund, J.-B. Arlin, Y. H. Geerts, S. Desbief, D. W. Breiby, J. W. Andreasen, R. Lazzaroni, W. M. Chen, I. Zozoulenko, M. Fahlman, P. J. Murphy, M. Berggren and X. Crispin, *Nat. Mater.*, 2014, **13**, 190–4.

28 B. Russ, A. Glaudell, J. J. Urban, M. L. Chabinyc and R. A. Segalman, *Nat. Rev. Mater.*, 2016, **1**, 16050.

Conclusions and Perspectives

In the broader framework of organic material thermoelectric application, the work of this PhD project was focused on the study of poly(3,4-ethylenedioxythiophene) or PEDOT features. Since the increase of thermoelectric performances resulted necessarily related with a better comprehension of charge transport mechanisms, this work aimed to understand the relation among the modification introduced into the system and the resulting charge transport features.

First, PEDOT final morphology was found to be dependent on the polymerization technique used, on the oxidant used, and on the solvent used. The combination of these three polymerization parameters can be therefore optimized to tune the polymeric film final quality. According to the results we obtained, WCP technique, combined with less hindering counterion and solvent molecules, allows to achieve the best results.

The study on chemical dedoping of PEDOT:Tf allowed to reach a maximum in thermoelectric power factor after a few seconds of exposure to a reducing agent. This result, similar to what has already been obtained for PEDOT:Tos obtained in different conditions, can lead to the conclusion that, even in presence morphological differences, PEDOT reactivity with amines remains substantially the same.

Second, the inclusion of a copolymer, containing two non-conjugated portions at the ends of PEDOT chains, was investigated. The copolymer structure resulted to deeply affect the PEDOT charge transport properties. A percolative behaviour of electrical conductivity and Seebeck coefficient was found when the concentration of the insulating portion is varied. Even though copolymer development involves a dramatic increase of the system complexity, they represent a great opportunity to permanently tune PEDOT features, obtaining completely novel materials.

Third, embedding inorganic nanoparticles into PEDOT was found to be detrimental for the polymer morphology in both the case of spherical nanoparticles of Mn_3O_4 and the case of lamellar nanoparticles of CuO. In the first case, such a phenomenon was investigated by means of humidity effect on electrical conductivity, which showed how differently nanocomposite can act with respect to the pristine polymeric matrix.

Nevertheless, the investigation of CuO nanocomposite samples at different oxidation levels, reached through electrochemical treatment, proved the retention of PEDOT charge transport behaviour. The resulting idea to impact only on morphology of the ICP, without affecting its

doping level or its charge carrier concentration, can be appealing for specific tuning of material properties.

The scenario emerging from the work done shows that many different paths may be pursued to tune PEDOT charge transport properties and, therefore, its thermoelectric features. Even though a first grasp of the effects owed to the different modification has been reached in this thesis, a deeper comprehension is still needed to obtain a full control over the emerging features. The future line of this research should aim at a more comprehensive view, including all possible tuneable parameters and modifications, together with their combinations. Such an extensive work could allow a more precise comprehension of PEDOT based systems, opening the route for the major breakthrough needed to compete with inorganic thermoelectric performances.

List of Publications and Conferences

Publications

- **D. Galliani**, L. Mascheroni, M. Sassi, R. Turrisi, R. Lorenzi, A. Scaccabarozzi, N. Stingelin and L. Beverina, "Thermochromic Latent-Pigment-Based Time-Temperature Indicators for Perishable Goods", *Adv. Opt. Mater.*, 2015, **3**, 1164–1168.

- **D. Galliani**, S. Battiston and D. Narducci, "Tuning PEDOT:Tos thermoelectric properties through nanoparticle inclusion" *J. Nanosci. Nanotechnol.*, 2017, **17**, 1579–1585.

- **D. Galliani**, S. Battiston, Ruffo R., Trabattoni S., D.Narducci, "Modulation of charge transport properties in poly(3,4-ethylenedioxythiophene) nanocomposites for thermoelectric applications" *J. Phys. D: Appl. Phys.*, 2018, **51** (3).

- R. Brooke, **D. Galliani**, K. Wijeratne, J. F. Franco-Gonzalés, I. Zozulenko, X. Crispin, "Vapor phase polymerized poly(3,4-ethylenedioxythiophene)-trifluoromethanesulfonate as transparent conductor material", *(Manuscript).*

Conferences

- **D. Galliani**, S. Battiston and D. Narducci, "Tuning PEDOT:Tos thermoelectric properties through nanoparticle inclusion" *Giornate della Termoelettricità 2016, Pisa* – **oral contribution** (Awarded as Best Talk)

- **D. Galliani**, L. Beverina, D. Narducci, "Conjugated Polymer Nanocomposite: Towards a Novel Material for Thermal Energy Microharversting" *European Material Research Society (EMRS) Spring Meeting 2016, Lille (France)*- **oral contribution**

- **D. Galliani**, R. Ruffo, D. Narducci "Thermoelectric properties of PEDOT nanocomposites with electrochemically tuned oxidation state" *European Conference on Thermoelectrics (ECT) 2016, Lisbon (Portugal)*- **oral contribution**

- **D. Galliani**, A. Piro, S. Battiston, D. Narducci "Partially conjugated copolymers: a novel tool to tune organic material thermoelectric properties" *Giornate della Termoelettricità 2017, Turin* – **oral contribution**

- **D. Galliani**, R. Brooke, U. Ail, Z. Ullah Khan, X. Crispin "Thermoelectric properties of vapour phase polymerized poly(3,4-ethylenedioxythiophene)-trifluoromethanesulfonate (VPP PEDOT:Tf): a study on a highly performing conductive polymer" *Workshop "Thermoelectric Materials: from Theoretical Design to Industrial Application" 2017, Cork (Ireland)* - **poster**

- **D. Galliani**, R. Brooke, U. Ail, Z. Ullah Khan, X. Crispin, D. Narducci "Understanding thermoelectric performance affecting parameters in poly(3,4-ethylendioxy)thiophene (PEDOT)" *European Conference on Thermoelectrics (ECT) 2017, Padua*- **oral contribution**